DOT/FAA/AR-00/10

Office of Aviation Research
Washington, D.C. 20591

Statistical Loads Data for B-767-200ER Aircraft in Commercial Operations

March 2000

Final Report

U.S. Department of Transportation
Federal Aviation Administration

NOTICE

This document is disseminated under the sponsorship of the U.S. Department of Transportation in the interest of information exchange. The United States Government assumes no liability for the contents or use thereof. The United States Government does not endorse products or manufacturers. Trade or manufacturer's names appear herein solely because they are considered essential to the objective of this report. This document does not constitute FAA certification policy. Consult your local FAA aircraft certification office as to its use.

This report is available at the Federal Aviation Administration William J. Hughes Technical Center's Full-Text Technical Reports page: www.actlibrary.tc.faa.gov in Adobe Acrobat portable document format (PDF).

Technical Report Documentation Page

1. Report No.	2. Government Accession No.	3. Recipient's Catalog No.
DOT/FAA/AR-00/10		

4. Title and Subtitle	5. Report Date
STATISTICAL LOADS DATA FOR B-767-200ER AIRCRAFT IN COMMERCIAL OPERATIONS	March 2000
	6. Performing Organization Code

7. Author(s)	8. Performing Organization Report No.
Daniel O. Tipps, John W. Rustenburg, and Donald A Skinn,	URD-TR 99-00072

9. Performing Organization Name and Address	10. Work Unit No. (TRAIS)
University of Dayton Research Institute Structural Integrity Division 300 College Park Dayton, OH 45469-0120	RPD-510-1998-00032
	11. Contract or Grant No.
	DTFA03-98-F-IA002

12. Sponsoring Agency Name and Address	13. Type of Report and Period Covered
U.S. Department of Transportation Federal Aviation Administration Office of Aviation Research Washington, DC 20591	Final Report
	14. Sponsoring Agency Code
	ANM-110

15. Supplementary Notes

The Federal Aviation Administration William J. Hughes Technical Center COTR was Thomas DeFiore.

16. Abstract

The University of Dayton is supporting Federal Aviation Administration (FAA) research on the structural integrity requirements for the US commercial transport airplane fleet. The primary objective of this research is to support the FAA Airborne Data Monitoring Systems Research Program by developing new and improved methods and criteria for processing and presenting large commercial transport airplane flight and ground loads usage data. The scope of activities performed involved (1) defining the service related factors which affect the operational life of commercial aircraft; (2) designing an efficient software system to reduce, store, and process large quantities of optical quick access recorder data; and (3) providing processed data in formats that will enable the FAA to reassess existing certification criteria. Equally important, these new data will also enable the FAA, the aircraft manufacturers, and the airlines to better understand and control those factors which influence the structural integrity of commercial transport aircraft. Presented herein are analyses and statistical summaries of data collected from 1285 flights representing 9164 flight hours of 10 typical B-767-200ER aircraft during operational usage recorded by a single airline. The data include statistical information on accelerations, speeds, altitudes, flight duration and distance, gross weights, speed brake/spoiler cycles, thrust reverser usage, and gust velocities encountered.

17. Key Words	18. Distribution Statement
Optical quick access recorder, Flight profiles, Flight loads, Ground loads, Miscellaneous loads, Statistical loads data	This document is available to the public through the National Technical Information Service (NTIS), Springfield, Virginia 22161.

19. Security Classif. (of this report)	20. Security Classif. (of this page)	21. No. of Pages	22. Price
Unclassified	Unclassified	83	N/A

PREFACE

The Flight Systems Integrity Group of the Structural Integrity Division of the University of Dayton Research Institute (URDI) performed this work under Federal Aviation Administration (FAA) Grant No. 96-G-020 entitled "Aircraft Operational Usage for Service Life Management and Design Criteria Development." The Program Manager for the FAA was Mr. Thomas DeFiore of the FAA William J. Hughes Technical Center at Atlantic City International Airport, New Jersey, and the Program Technical Advisor was Mr. Terence Barnes of the FAA Aircraft Certification Office. Mr. Daniel Tipps was the Principal Investigator for the University of Dayton and provided oversight direction for this effort. Mr. Donald Skinn developed the data reduction algorithms, established data reduction criteria, and performed the data reduction. Mr. John Rustenburg created the graphical presentations, compiled and performed the data analysis, and formatted the report.

TABLE OF CONTENTS

LIST OF FIGURES

LIST OF TABLES

LIST OF SYMBOLS AND ABBREVIATIONS

$\overline{A}$	aircraft PSD gust response factor
a	speed of sound (ft/sec)
$\overline{c}$	wing mean geometric chord (ft)
$\overline{C}$	aircraft discrete gust response factor
C_{L_α}	aircraft lift curve slope per radian
$C_{L_{max}}$	maximum lift coefficient
CAS	calibrated air speed
c.g.	center of gravity
EAS	equivalent airspeed
F(PSD)	continuous gust alleviation factor
g	gravity constant, 32.17 ft/sec^2
H_p	pressure altitude, (ft)
K_g	discrete gust alleviation factor, $0.88\ \mu/(5.3 + \mu)$
KCAS	knots calibrated air speed
KEAS	knots equivalent air speed
KIAS	knots indicated air speed
kts	knots
L	turbulence scale length (ft)
n	load factor (g)
N	number of occurrences for U_σ (PSD gust procedure)
nm	nautical mile
n_x	longitudinal load factor (g)
n_y	lateral load factor (g)
n_z	normal load factor (g)
N_0	number of zero crossings per nautical mile (PSD gust procedure)
q	dynamic pressure (lbs/ft^2)
S	wing area (ft^2)
TAS	true airspeed
U_{de}	derived gust velocity (ft/sec, EAS)
U_σ	continuous turbulence gust intensity (ft/sec, TAS)

V_B	design speed for maximum gust
V_C	design cruise speed
V_D	design dive speed
V_e	equivalent airspeed
V_T	true airspeed
W	gross weight (lbs)
Δm	incremental acceleration due to a turning maneuver
Δn_z	incremental normal load factor, n_z - 1
$\Delta n_{z_{man}}$	incremental maneuver load factor
$\Delta n_{z_{gust}}$	incremental gust load factor
μ	airplane mass ratio, $\frac{2(W/S)}{\rho g \bar{c} C_{L_\alpha}}$
μ_p	statistical mean of p (parameter on plots)
ρ	air density, slugs/ft^3 (at altitude)
ρ_0	standard sea level air density, 0.0023769 slugs/ft^3
σ_p	standard deviation of p (parameter on plots)
φ	bank angle (degrees)

EXECUTIVE SUMMARY

The University of Dayton is supporting Federal Aviation Administration (FAA) research on the structural integrity requirements for the US commercial transport airplane fleet. The primary objective of this research is to support the FAA Airborne Data Monitoring Systems Research Program by developing new and improved methods and criteria for processing and presenting large commercial transport airplane flight and ground loads usage data. The scope of activities performed involved (1) defining the service related factors which affect the operational life of commercial aircraft; (2) designing an efficient software system to reduce, store, and process large quantities of optical quick access recorder data; and (3) providing processed data in formats that will enable the FAA to reassess existing certification criteria. Equally important, these new data will also enable the FAA, the aircraft manufacturers, and the airlines to better understand and control those factors which influence the structural integrity of commercial transport aircraft. Presented herein are analyses and statistical summaries of data collected from 1285 flights representing 9164 flight hours of 10 typical B-767-200ER aircraft during operational usage recorded by a single airline. The data include statistical information on accelerations, speeds, altitudes, flight duration and distance, gross weights, speed brake/spoiler cycles, thrust reverser usage, and gust velocities encountered.

1. INTRODUCTION.

The Federal Aviation Administration (FAA) has an ongoing Airborne Data Monitoring Systems Research Program to collect, process, and evaluate statistical flight and ground loads data from transport aircraft used in normal commercial airline operations. The objectives of this program are (a) to acquire, evaluate, and utilize typical operational in-service data for comparison with the prior data used in the design and qualification testing of civil transport aircraft and (b) to provide a basis to improve the structural criteria and methods of design, evaluation, and substantiation of future airplanes. Since the inception of the FAA's Airborne Data Monitoring Systems Research Program, the scope of the program has steadily increased to include data collection on additional aircraft, different aircraft models, and additional operators. The University of Dayton has supported the FAA's efforts and has responsibility for the data analysis and processing tasks and report preparation. In consultation with airplane manufacturers and operators, the University has enhanced and improved the data processing capabilities to reduce, analyze, and report additional aircraft usage and statistical external loads data from the digital flight loads recorders in a form that will fulfill the requests of the aircraft manufacturers, the airlines, and the FAA. The report presents data obtained from 10 airplanes over 1285 flights and 9164 hours of airline operations for the B-767-200ER aircraft of a single operator.

2. AIRCRAFT DESCRIPTION.

Table 1 presents certain operational characteristics and major physical dimensions of the 10 Boeing 767-200ER aircraft which were equipped with optical-quick access recorders. Figure 1 shows front, top, and side views of the aircraft.

TABLE 1. BOEING 767-200ER AIRCRAFT CHARACTERISTICS

Maximum Taxi Weight	352,200lb
Maximum Takeoff Weight	351,000 lb
Maximum Landing Weight	278,000 lb
Maximum Zero-Fuel Weight	253,000 lb
Maximum Operating Empty Weight	183,300 lb
Fuel Capacity	137,100 lb @ 6.7 lb/ U.S. gallons
2 GE CF6-80 C2 Engines	@ 52,500 lbs static thrust @ sea level each
Wing Span	156.33 ft
Wing Reference Area	3050 ft^2
Wing MAC	19.54 ft
Wing Sweep	35 degrees
Length	159 ft 2 in
Height	52 ft 0 in
Tread	30 ft 6 in
Wheel Base	64 ft 7 in

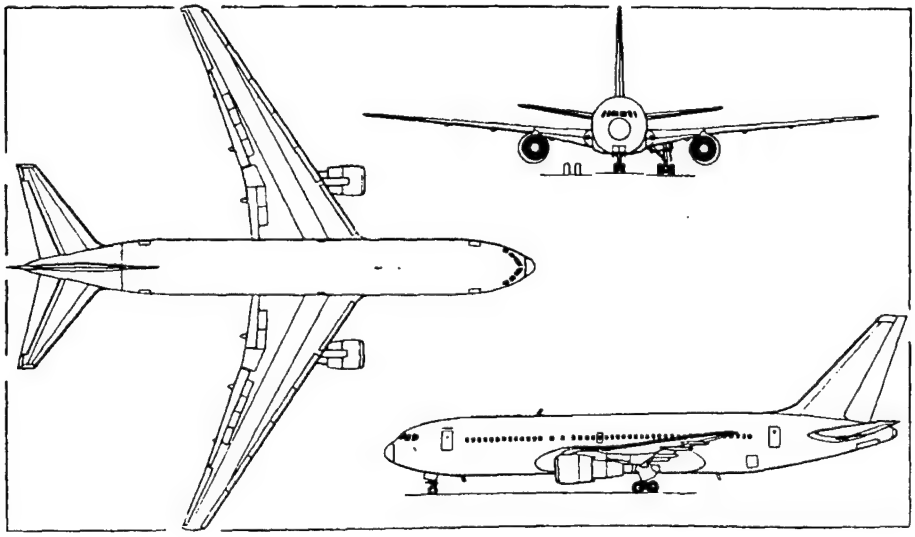

FIGURE 1. BOEING 767-200ER THREE-VIEW DRAWING

3. AIRLINE DATA COLLECTION AND EDITING SYSTEMS.

The airline data collection and editing system consists of two major components: (1) the data collection system installed on board the aircraft and (2) the ground data editing station. A schematic overview of the system is given in figure 2. The requirements for the data acquisition and processing are defined in reference 1. The collection and editing systems are discussed below.

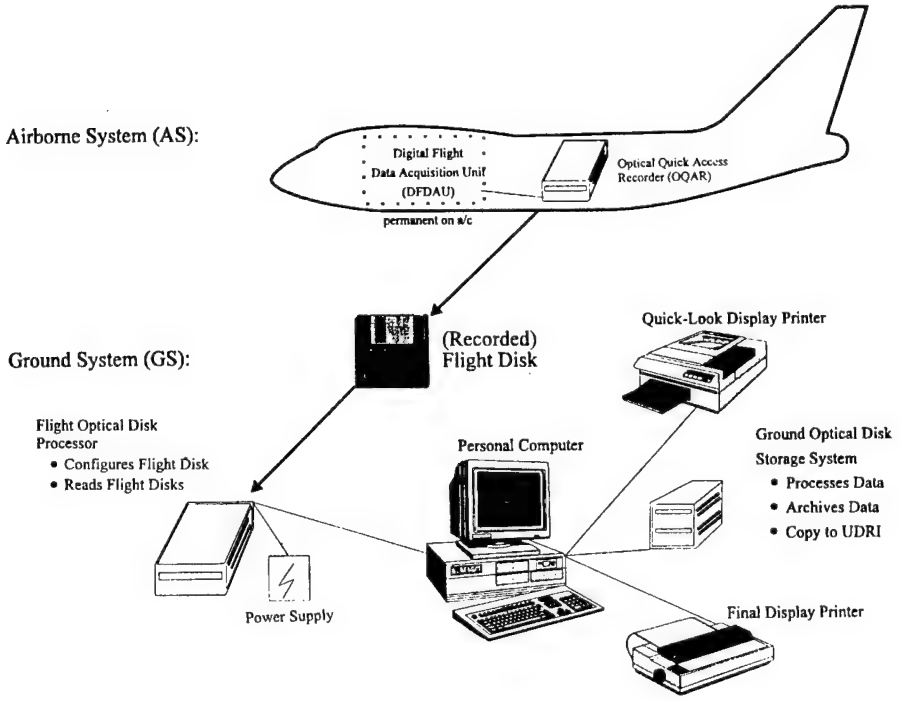

FIGURE 2. AIRLINE RECORDING AND EDITING SYSTEM

3.1 DATA COLLECTION SYSTEM.

The on-board data collection system consists of a Digital Flight Data Acquisition Unit (DFDAU), a Digital Flight Data Recorder (DFDR), and an Optical Quick-Access Recorder (OQAR). The DFDAU collects sensor signals and sends parallel data signals to both the DFDR and the OQAR. The OQAR is equipped with an optical disk which can store up to 300 hours of flight data, whereas the DFDR uses a 25-hour loop tape. The optical disk is periodically removed from the OQAR and forwarded to the ground processing station.

3.2 DATA EDITING SYSTEM.

The airline ground data editing station consists of a Pentium computer, a magneto-optical (MO) disk drive, and flight data editing software. The software performs a number of functions during the process of transferring the raw flight data into DOS file format onto the hard disk. The most important of these functions include a data integrity check and removal of flight sensitive information. Data considered sensitive are those which can be used to readily identify a specific flight. The desensitized data are forwarded to the University of Dayton Research Institute (UDRI) for flight loads processing and analysis. Table 2 presents the recorded data parameters provided by the airline to UDRI.

TABLE 2. RECORDED PARAMETERS PROVIDED TO UDRI

Parameter	Sample Rate
Normal Acceleration	8 per second
Lateral Acceleration	4 per second
Longitudinal Acceleration	4 per second
Aileron Position	1 per second
Elevator Position	1 per second
Rudder Position	2 per second
Pilot Trim Position	1 per second
Flap Handle Position	1 per second
Speed Brake Position	1 per second
N_1 Engine - Left	1 per second
N_1 Engine - Right	1 per second
Throttle #1 Position	1 per second
Throttle #2 Position	1 per second
Thrust Reverser Position	Discrete
Squat Switch (main gear)	4 per second
Calibrated Airspeed	1 per second
Ground Speed	1 per second
Mach Number	1 per 2 seconds
Pressure Altitude	1 per second
Gross Weight	1 per 64 seconds
Bank Angle	1 per second
Pitch Angle	1 per second
Magnetic Heading	1 per second
Total Air Temperature	1 per second
Radio Altitude	1 per second

4. UNIVERSITY OF DAYTON RESEARCH INSTITUTE DATA PROCESSING.

The data parameters of table 2 are provided by the airline to UDRI for each recorded flight. The data are provided on magneto-optical disks containing binary files for multiple flights for different airplanes. These data are processed by UDRI to extract the parameters required for statistical flight loads presentation. This section describes the reduction of the data and the derivation of required parameters.

4.1 DATA REDUCTION.

Each file provided by the airline contains multiple flights for each airplane. These files are first separated into individual flight files and subsequently into individual time history files for each flight. The time history files are compressed and stored on the same 230-MB magneto-optical (MO) disks for later recall by the flight loads processing software.

These data are edited and verified as the time histories are being prepared. Messages alert the user that obviously erroneous data have been removed and that questionable data have been retained but need to be manually reviewed prior to their acceptance. Table 3 lists the limits against which the data are compared.

TABLE 3. PARAMETER EDITING VALUES

Item		Min	Max
1.	Gross Weight	75,000 lbs	500,500 lbs
2.	Pressure Altitude (Hp)	-5,000 ft	50,000 ft
3.	Calibrated Airspeed	20 kts	600 kts
4.	Normal Acceleration	-2.0 g	+4.0 g
5.	Lateral Acceleration	-1.0 g	+1.0 g
6.	Longitudinal Acceleration	-1.0 g	+1.0 g
7.	Flap Handle Position	0°	60°
8.	Elevator Position	-40°	+40°
9.	Aileron Position	-40°	+40°
10.	Rudder Position	-40°	+40°
11.	Trim Position	-30°	+30°
12.	Speed Brake Handle Position	-1°	70°
13.	Throttles 1 and 2	All	All
14.	Engine N_1 and N_2	All	All
15.	Thrust Reverser Position	0	1
16.	Squat Switch (main gear)	0	1
17.	Pitch Attitude	-30°	+30°
18.	Bank Attitude	-70°	+70°
19.	Mach Number	0	1
20.	Ground Speed	4 kts	800 kts

Important characteristics about each set of flights received from the airline are recorded in a relational database. Airline identifier, aircraft tail number, and disk identifier of the disk received from the airline are in the data. Each flight is assigned a unique flight sequence number. The flight sequence number assigned to the first flight of the set and the number of flights in the set are also entered. Also recorded is the disk identifier of the MO disk, which contains the compressed time history files of all flights in the set.

4.2 RECORDED PARAMETERS.

Not all parameters listed in table 2 are used for statistical analysis and data presentation. The parameters used in the data reduction and for which time history files are created and compressed on the MO disk are listed in table 4. These parameters are used by the summarization software for statistical analysis and data presentation.

TABLE 4. RECORDED PARAMETERS USED IN DATA REDUCTION

Flight Parameter	Sample Rate
Gross Weight	1 per 64 seconds
Pressure Altitude	1 per second
Calibrated Airspeed	1 per second
Normal Acceleration (n_z)	8 per second
Lateral Acceleration (n_y)	4 per second
Longitudinal Acceleration (n_x)	4 per second
Flap Handle Position	1 per second
Speed Brake Handle Position	1 per second
Thrust Reverser Position	Discrete
Squat Switch (main gear)	Discrete
Pitch Angle	2 per second
Bank Angle	1 per second
Mach Number	1 per 2 seconds
Ground Speed	1 per second
Magnetic Heading	1 per second
N_1 Engine - Left	1 per second

4.3 COMPUTED PARAMETERS.

Derived gust velocity, U_{de}, and continuous gust intensity, U_σ, are important statistical load parameters which are derived from measured normal accelerations. This derivation of gust velocity U_{de} and continuous gust intensity U_σ from measured normal accelerations requires knowledge of atmospheric density, equivalent airspeed, and dynamic pressure. These values are calculated using equations that express the rate of change of density as a function of altitude based on the International Standard Atmosphere.

4.3.1 Atmospheric Density.

For altitudes below 36,089 feet, the density ρ is expressed as a function of altitude by

$$\rho = \rho_0 (1 - 6.876 \times 10^{-6} \times H_p)^{4.256} \quad (1)$$

where ρ_0 is air density at sea level (0.0023769 slugs/ft^3) and H_p is pressure altitude (ft). Pressure altitude is a recorded parameter.

4.3.2 Equivalent Airspeed.

Equivalent air speed (V_e) is a function of true air speed (V_T) and the square root of the ratio of air density at altitude (ρ) to air density at sea level (ρ_0)

$$V_e = V_T \sqrt{\frac{\rho}{\rho_0}} \quad (2)$$

True airspeed is derived from Mach number (M) and speed of sound (a):

$$V_T = Ma. \quad (3)$$

Mach number is a dimensionless, recorded parameter. The speed of sound (a) is a function of pressure altitude (H_p) and the speed of sound at sea level and is

$$a = a_0 \sqrt{(1 - 6.876 \times 10^{-6} \times H_p)} \quad (4)$$

Substituting equations 1 and 4 into equation 2 gives

$$V_e = M \times a_0 \times (1 - 6.876 \times 10^{-6} \times H_p)^{0.5} \times (1 - 6.876 \times 10^{-6} \times H_p)^{2.128} \quad (5)$$

and

$$V_e = M \times a_0 \times (1 - 6.876 \times 10^{-6} \times H_p)^{2.626} \quad (6)$$

where the speed of sound at sea level a_0 is 1116.4 fps or 661.5 knots.

4.3.3 Dynamic Pressure (q).

The dynamic pressure (q) is calculated from the air density and velocity

$$q = \frac{1}{2} \rho V^2 \quad (7)$$

where

ρ = air density at altitude (slugs/ft^3)
V = true air speed (ft/sec)

4.3.4 Derived Gust Velocity (U_{de}).

The derived gust velocity, U_{de}, is computed from the peak values of gust incremental normal acceleration as

$$U_{de} = \frac{\Delta n_z}{\overline{C}} \tag{8}$$

where Δn_z is gust peak incremental normal acceleration and $\overline{C}$ is the aircraft response factor considering the plunge-only degree of freedom and is calculated from

$$\overline{C} = \frac{\rho_0 V_e C_{L_\alpha} S}{2W} K_g \tag{9}$$

where

ρ_0 = 0.002377 slugs/ft^3, standard sea level air density
V_e = equivalent airspeed (ft/sec)
C_{L_α} = aircraft lift-curve slope per radian
S = wing reference area (ft^2)
W = gross weight (lbs)
K_g = $\dfrac{0.88\mu}{5.3+\mu}$ = gust alleviation factor

μ = $\dfrac{2W}{\rho g \bar{c} C_{L_\alpha} S}$

ρ = air density, slug/ft^3, at pressure altitude (Hp), from equation 1
g = 32.17 ft/sec^2
$\bar{c}$ = wing mean geometric chord (ft)

4.3.5 Continuous Gust Intensity (U_σ).

Power Spectral Density (PSD) functions provide a turbulence description in terms of the probability distribution of the root-mean-square (rms) gust velocities. The root-mean-square gust velocities or continuous gust intensities, U_σ, are computed from the peak gust value of normal acceleration using the power spectral density technique as described in reference 2. The procedure is

$$U_\sigma = \frac{\Delta n_z}{\overline{A}} \tag{10}$$

where Δn_z = gust peak incremental normal acceleration

$$\overline{A} = \text{aircraft PSD gust response factor} = \frac{\rho_0 V_e C_{L\alpha} S}{2W} \text{F(PSD) in } \frac{1}{ft/sec} \tag{11}$$

ρ_0 = 0.002377 slugs/ft^3, standard sea level air density
V_e = equivalent airspeed (ft/sec)
C_{L_α} = aircraft lift-curve slope per radian
S = wing reference area (ft^2)
W = gross weight (lbs)

$$F(PSD) = \frac{11.8}{\sqrt{\pi}}\left[\frac{\bar{c}}{2L}\right]^{\frac{1}{3}}\sqrt{\frac{\mu}{110+\mu}},\ dimensionless \tag{12}$$

$\bar{c}$ = wing mean geometric chord (ft)
L = turbulence scale length, 2500 ft

$$\mu = \frac{2W}{\rho g \bar{c} C_{L_\alpha} S},\ \text{dimensionless} \tag{13}$$

ρ = air density (slugs/ft^3)
g = 32.17 ft/sec^2

To determine the number of occurrences (N) for U_σ, calculate

$$N = \frac{N_0(o)_{ref}}{N_0(o)} = \frac{\pi\bar{c}}{203}\left[\frac{\rho}{\rho_0}\mu\right]^{0.46},\ \text{dimensionless} \tag{14}$$

where $\bar{c}$, ρ, ρ_0, and μ are defined above. Then each U_σ peak is counted as N counts at that U_σ value. This number of counts is used to determine the number of counts per nautical mile (nm)

or
$$\frac{\text{counts}}{nm} = \left(\frac{N}{\text{distance flown in counting interval}}\right) \tag{15}$$

Finally, the number of such counts is summed from the largest plus or minus value toward the smallest to produce the cumulative counts per nautical mile.

4.4 DATA REDUCTION CRITERIA.

To process the measured data into statistical flight loads format, specific data reduction criteria were established for each parameter. These criteria are discussed in this section.

4.4.1 Phases of Flight.

Each flight is divided into nine phases—four ground phases (taxi out, takeoff roll, landing roll with and without thrust reverser, and taxi in), and five airborne phases (departure, climb, cruise, descent, and approach). Figure 3 shows these nine phases of a typical flight. The phases of flight were not defined by the airline but had to be determined from the data. Table 5 lists the conditions for determining the starting times for each phase. It should be noted that an airborne phase can occur several times per flight because it is determined by the rate of climb and the

position of the flaps. When this occurs the flight loads data are combined and presented in a single flight phase. The UDRI software creates a file which chronologically lists the phases of flight and their corresponding starting times.

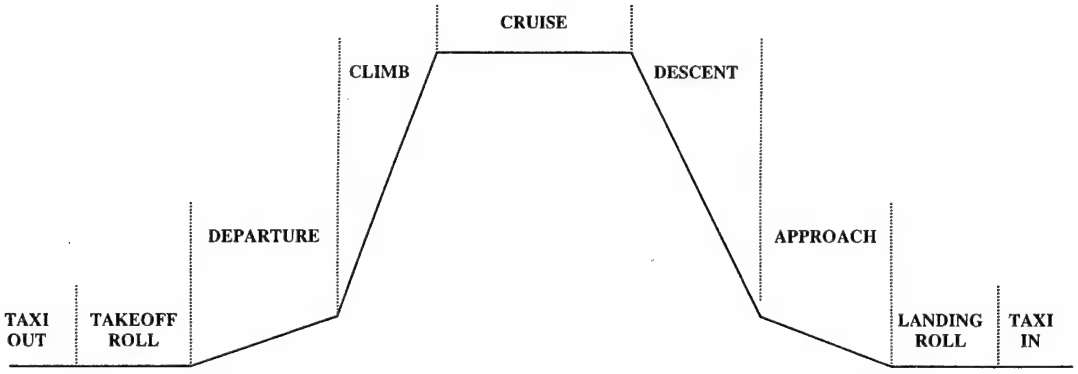

FIGURE 3. DESCRIPTION OF PHASES OF FLIGHT

TABLE 5. PHASE OF FLIGHT STARTING CRITERIA

Phase of Flight	Conditions at Start of Phase
Taxi Out	Initial Aircraft Movement
Takeoff Roll	Acceleration > 2 kts/sec for a minimum of 20 seconds
Departure	Time at liftoff; flaps extended (squat switch off)
Climb	Flaps retracted; rate of climb ≥ 250 ft/min. for at least 1 minute
Cruise	Flaps retracted; rate of climb ≤ 250 ft/min. for at least 1 minute
Descent	Flaps retracted; rate of descent ≥ 250 ft/min. for at least 1minute
Approach	Flaps extended; rate of descent ≥ 250 ft/min. for at least 1 minute
Landing Roll	Touchdown; (squat switch on)
Taxi In	Magnetic heading change greater than 13.5 degrees after touchdown or deviation from runway centerline greater than 100 feet

Should the above criteria fail the following additional secondary criteria are used.

The criteria for the start of the takeoff roll is defined as the earlier of (1) the time that the computed speed exceeds 45 knots or (2) the time that the longitudinal acceleration exceeds 0.15 g prior to liftoff.

The criterion for the start of taxi in is defined as the time when the aircraft turns off the active runway. Turnoff is detected by monitoring the magnetic heading for a change greater than 13.5 degrees from the landing magnetic heading. The time when the heading starts to change in the turnoff direction is then identified as the start of the turn or the beginning of the taxi-in phase. This method can fail to detect a shallow turnoff onto a taxiway. In this case an average landing roll of 32 seconds duration is assumed and the turnoff is marked as 32 seconds after touchdown.

The criteria for determining the pitch angle at takeoff has been defined as the angle occurring just prior to the airplane becoming airborne.

4.4.2 Flight Distance.

The flight distance can be obtained either by determining the stage length of the flight or by integrating the range with respect to changes in aircraft velocity as a function of time.

The stage length is defined as the distance from departure airport to destination airport and is determined as the great circle distance in nautical miles between the point of liftoff (departure) and the point of touchdown (destination). Appendix B describes the calculation of great circle distance. The time histories of longitude and latitude are matched against the UDRI-generated phase-of-flight file to determine the geographical location of the aircraft at the point of liftoff and the point of touchdown.

The integrated flight distance D is obtained by the numerical integration from the time at liftoff (t_0) to the time of touchdown (t_n), and V_T is the average true velocity during Δt.

$$D = \sum_{t_0}^{t_n} \Delta t \cdot V_T \tag{16}$$

4.4.3 Sign Convention.

Acceleration data are recorded in three directions: normal (z), lateral (y), and longitudinal (x). As shown in figure 4, the positive z direction is up; the positive y direction is airplane starboard; and the positive x direction is forward.

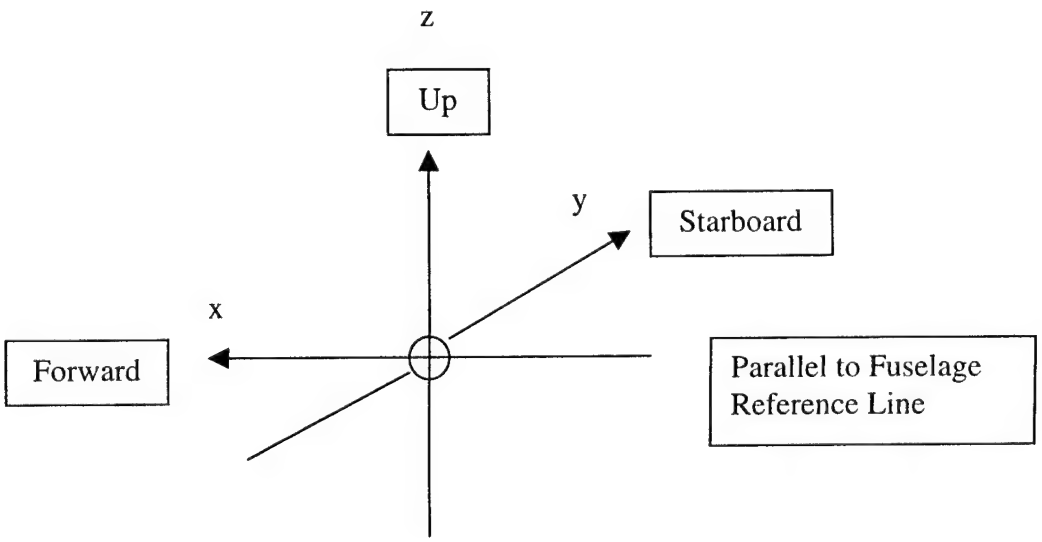

FIGURE 4. SIGN CONVENTION FOR AIRPLANE ACCELERATIONS

4.4.4 Peak-Valley Selection.

The peak-between-means method presented in reference 2 was used to select the peaks and valleys in the acceleration data. This method is consistent with past practices and pertains to all accelerations (n_x, n_y, Δn_z, $\Delta n_{z_{man}}$, $\Delta n_{z_{gust}}$). Figure 5 depicts an example of the peak-between-mean criteria. This method counts upward events as positive and downward events as negative. Only one peak or one valley is counted between two successive crossings of the mean. A threshold zone is used in the data reduction to ignore irrelevant loads variations around the mean. For the normal accelerations Δn_z, $\Delta n_{z_{gust}}$, and $\Delta n_{z_{man}}$, the threshold zone is ±0.05 g; for lateral acceleration n_y, the threshold zone is ±0.005 g; and for longitudinal accelerations n_x, the threshold zone is ±0.0025 g.

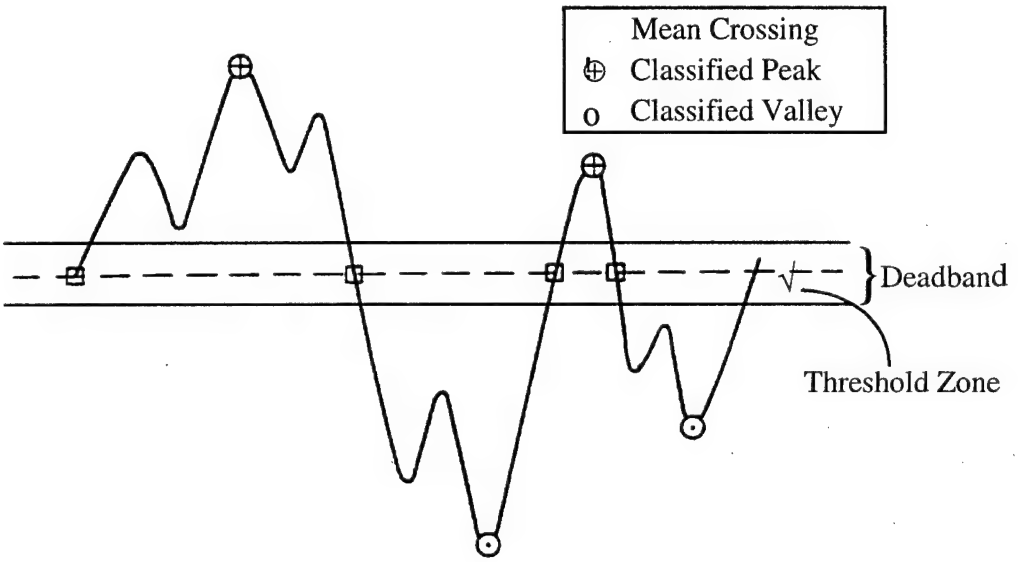

FIGURE 5. THE PEAK-BETWEEN-MEANS CLASSIFICATION CRITERIA

A peak is generated only when the acceleration data cross into or through the deadband. Two situations must be considered: the position of the current acceleration value relative to the deadband and the position of the previous acceleration value relative to the deadband. In the peak-between-means counting algorithm, the previous acceleration value is that value in a consecutive set of values all of which lie either above the deadband or below the deadband. The previous value is established as a peak when the current value has crossed into or through the deadband. Figures 6a and 6b demonstrate the concept of current and previous acceleration values. In figure 6a the current acceleration value passes into the deadband, whereas in figure 6b the current value passes through the deadband.

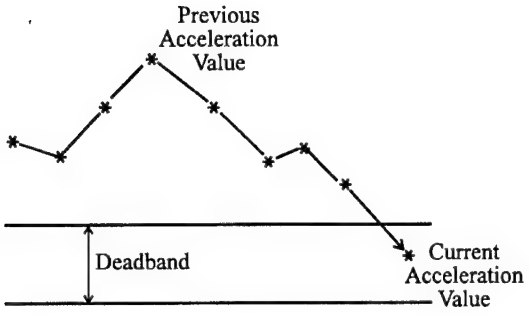

FIGURE 6a. CURRENT ACCELERATION VALUE PASSES INTO DEADBAND

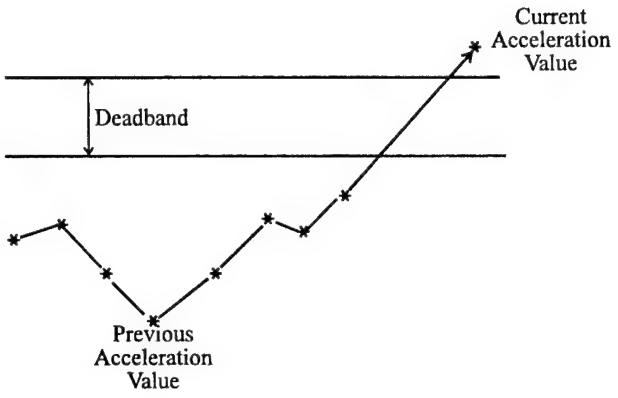

FIGURE 6b. CURRENT ACCELERATION VALUE PASSES THROUGH DEADBAND

Italicized text in table 6 summarizes the action(s) taken when the various possibilities occur. Note that when a previous acceleration value is retained as a potential peak, its coincident time is also retained.

TABLE 6. PEAK CLASSIFICATION CRITERIA

Previous Acceleration Value Relative to Deadband	Current Acceleration Value Relative to Deadband		
	Below	Within	Above
Above Previous value is potential positive peak	Current acceleration passes through deadband. *Previous value classified as a positive peak.* *Current value retained as a potential negative peak.*	Current acceleration passes into deadband. *Previous value classified as a positive peak.* *Acceleration value flagged as being in deadband.*	Current acceleration is on same side of deadband as previous. *If current value > previous value, retain current value as potential positive peak and release previous.*
Within At start of processing or a peak was established but current acceleration value has not since gone outside of deadband	Current acceleration passes downward out of deadband. *Current value is retained as a potential negative peak.*	*No Action Required*	Current acceleration passes upward out of deadband. *Current value retained as potential positive peak.*
Below Previous value is potential negative peak	Current acceleration is on same side of deadband as previous. *If current value < previous value, retain current value as potential negative peak and release previous value.*	Current acceleration passes into deadband. *Previous value is established as a negative peak.* *Acceleration value flagged as being in deadband.*	Current acceleration passes through deadband. *Previous value is classified as a negative peak.* *Current value retained as potential positive peak.*

4.4.5 Separation of Maneuver and Gust Load Factors.

The incremental acceleration measured at the center of gravity (c.g.) of the aircraft may be the result of either maneuvers or gusts. In order to derive gust and maneuver statistics, the maneuver-induced acceleration and gust response accelerations must be separated from the total acceleration

history. Reference 3 reported the results of a UDRI study to evaluate methods of separating maneuver and gust load factors from measured acceleration time histories. As a result of this study UDRI recommended and the FAA accepted that a cycle duration rule be used to separate gusts and maneuvers. A cycle duration of 2.0 seconds was recommended for use with B-737 and MD-82/83 aircraft. Review of the B-767-200 response characteristics has shown that this cycle duration value is also appropriate for the B-767-200 data. In order to avoid the inclusion of peaks and valleys associated with nonsignificant small load variations, a threshold zone of Δn_z = ±0.05 g was established. An algorithm was then developed to extract the acceleration peaks and valleys.

For each flight the maximum and minimum total accelerations were determined from just after liftoff to just before touchdown. For the in-flight phases, the Δn_z cumulative occurrences were determined as cumulative counts per nautical mile and cumulative counts per 1000 hours using the peak-between-means counting method of reference 2 as explained in section 4.4.3. The measurements of Δn_z, $\Delta n_{z_{gust}}$, and $\Delta n_{z_{man}}$ are maintained as three unique data streams. The Δn_z, $\Delta n_{z_{gust}}$, and $\Delta n_{z_{man}}$ data are plotted as cumulative occurrences of a given acceleration increment per nautical mile and per 1000 flight hours. The incremental normal load factor Δn_z is the airplane limit load factor minus 1.0 g. As a result of the threshold zone, only accelerations greater than ±0.05 g (measured from a 1.0-g base) are counted for data presentation. The recorded normal acceleration (n_z) values included the 1-g flight condition. The 1-g condition was removed from each n_z reading which was then recorded as Δn_z. In order to avoid the inclusion of peaks and valleys associated with nonsignificant small load variations, a threshold zone of Δn_z = ±0.05 g was established. An algorithm was then developed to extract the acceleration peaks and valleys.

Once calculated, the measurements of Δn_z, $\Delta n_{z_{gust}}$, and $\Delta n_{z_{man}}$ are maintained as three unique data streams. The $\Delta n_{z_{gust}}$ and $\Delta n_{z_{man}}$ data are plotted as cumulative occurrences of incremental accelerations per nautical mile and per 1000 flight hours. Separate plots are provided for each phase of flight and all phases combined. The Δn_z value is the recorded incremental normal load factor (airplane limit load factor minus 1.0 g). As a result of the threshold zone, only accelerations greater than ±0.05 g (measured from a 1.0-g base) are counted for data presentation.

4.4.6 Flap Detents.

When flaps are extended, the effective deflection is considered to be that of the applicable detent, as indicated in table 7. The flap deflection ranges and placard speeds reflect the flap design and cockpit placards.

TABLE 7. FLAP DETENTS (B-767-200)

Flap Detent	Minimum Flap Setting	Maximum Flap Setting	Handbook Airspeed Placards (KIAS)
1	> 0	≤ 0.5	240
5	> 0.5	≤ 5	220
10	> 5	≤ 10	210
15	> 10	≤ 15	195
25	> 15	≤ 25	190
30	> 25	≤ 30	162
40	> 30		162

5. DATA PRESENTATION.

Table 8 lists the statistical data presentation formats for which data were processed and included in appendix A.

Figures A-1 through A-80 present the processed data. It will be noted that the data presented in these figures are not always based on an identical number of flights. During data reduction it was found that the acceleration measurements in certain flights exhibited random errors and were unreliable. When this occurred, those flights were eliminated from the statistical data for any parameters associated, directly or indirectly, with the unreliable acceleration measurements. As a result, not all figures are based on data from identical numbers of flights, hours, or nautical miles.

5.1 AIRCRAFT OPERATIONAL USAGE DATA.

The aircraft usage data include flight profile statistics such as weights, altitudes, speeds, and flight distance information. This information is useful in the derivation of typical flight profiles and in defining ground-air-ground cycles for structural durability and damage tolerance analyses, future design criteria, and for use in the analysis of airline operating economics. Aircraft usage data are presented in figures A-1 through A-12.

TABLE 8. STATISTICAL DATA FORMATS

Data Description	Figure
AIRCRAFT USAGE DATA	
WEIGHT DATA	
Cumulative Probability of Takeoff Gross Weight	A-1
Cumulative Probability of Takeoff Fuel Weight	A-2
Cumulative Probability of Landing Gross Weight	A-3
Takeoff Fuel Weight vs Flight Distance	A-4
Correlation of Takeoff Gross Weight and Flight Distance, Percent of Flights	A-5
Correlation of Gross Weight at Liftoff and Touchdown, Percent of Flights	A-6
ALTITUDE DATA	
Correlation of Maximum Altitude and Flight Distance, Percent of Flights	A-7
Percent of Total Distance in Altitude Bands	A-8
Coincident Altitude at Maximum Mach Number, All Flight Phases	A-9
Coincident Altitude at Maximum Indicated Airspeed, All Flight Phases	A-10
FLIGHT DISTANCES	
Cumulative Probability of Great Circle Flight Distance	A-11
Cumulative Probability of Integrated Flight Distance	A-12
GROUND LOADS DATA	
LATERAL LOAD FACTOR, n_y	
Cumulative Frequency of Maximum Side Load Factor During Ground Turns	A-13
LONGITUDINAL LOAD FACTOR, n_x	
Cumulative Frequency of Longitudinal Load Factor During Ground Taxi	A-14
Cumulative Frequency of Longitudinal Load Factor During Landing Roll	A-15
Cumulative Probability of Maximum Longitudinal Load Factor During Takeoff	A-16
Cumulative Probability of Minimum Longitudinal Load Factor During Landing	A-17
VERTICAL LOAD FACTOR, n_z	
Cumulative Frequency of Incremental Vertical Load Factor During Taxi Operations	A-18
Cumulative Frequency of Incremental Vertical Load Factor During Takeoff Roll	A-19
Cumulative Frequency of Incremental Vertical Load Factor During Landing Roll	A-20
Cumulative Probability of Minimum and Maximum Incremental Vertical Load Factor at Touchdown and Spoiler Deployment	A-21
Coincident Vertical Load Factor and Touchdown Gross Weight	A-22
GROUND SPEED DATA	
Cumulative Probability of Ground Speed During Taxi	A-23
Cumulative Probability of Airspeed at Liftoff and Touchdown	A-24
FLARE DATA	
Cumulative Probability of Airspeed at Flare	A-25
PITCH/ROTATION DATA	
Cumulative Probability of Pitch Angle at Liftoff and Touchdown	A-26
Cumulative Probability of Maximum Pitch Rate at Takeoff Rotation	A-27
Cumulative Probability of Pitch Angle at Touchdown Peak Vertical Load Factor	A-28

TABLE 8. STATISTICAL DATA FORMATS (Continued)

Data Description	Figure
FLIGHT LOADS DATA	
GUST LOADS DATA	
Cumulative Occurrences of Incremental Vertical Gust Load Factor per 1000 Hours by Flight Phase	A-29
Cumulative Occurrences of Incremental Vertical Gust Load Factor per 1000 Hours, Combined Flight Phases	A-30
Cumulative Occurrences of Incremental Vertical Gust Load Factor per Nautical Mile by Flight Phase	A-31
Cumulative Occurrences of Incremental Vertical Gust Load Factor per Nautical Mile, Combined Flight Phases	A-32
Cumulative Occurrences of Derived Gust Velocity per Nautical Mile, < 500 Feet	A-33
Cumulative Occurrences of Derived Gust Velocity per Nautical Mile, 500-1,500 Feet	A-34
Cumulative Occurrences of Derived Gust Velocity per Nautical Mile, 1,500-4,500 Feet	A-35
Cumulative Occurrences of Derived Gust Velocity per Nautical Mile, 4,500-9,500 Feet	A-36
Cumulative Occurrences of Derived Gust Velocity per Nautical Mile, 9,500-19,500 Feet	A-37
Cumulative Occurrences of Derived Gust Velocity per Nautical Mile, 19,500-29,500 Feet	A-38
Cumulative Occurrences of Derived Gust Velocity per Nautical Mile, 29,500-39,500 Feet	A-39
Cumulative Occurrences of Derived Gust Velocity per Nautical Mile,39,500-49,500 Feet	A-40
Cumulative Occurrences of Derived Gust Velocity per Nautical Mile, Flaps Extended	A-41
Cumulative Occurrences of Derived Gust Velocity per Nautical Mile, Flaps Retracted	A-42
Cumulative Occurrences of Continuous Gust Intensity per Nautical Mile, Flaps Extended	A-43
Cumulative Occurrences of Continuous Gust Intensity per Nautical Mile, Flaps Retracted	A-44
MANEUVER LOADS DATA	
Cumulative Occurrences of Incremental Maneuver Load Factor per 1000 Hours During Departure by Altitude	A-45
Cumulative Occurrences of Incremental Maneuver Load Factor per 1000 Hours During Climb by Altitude	A-46
Cumulative Occurrences of Incremental Maneuver Load Factor per 1000 Hours During Cruise by Altitude	A-47
Cumulative Occurrences of Incremental Maneuver Load Factor per 1000 Hours During Descent by Altitude	A-48
Cumulative Occurrences of Incremental Maneuver Load Factor per 1000 Hours During Approach by Altitude	A-49
Cumulative Occurrences of Incremental Maneuver Load Factor per Nautical Mile During Departure by Altitude	A-50
Cumulative Occurrences of Incremental Maneuver Load Factor per Nautical Mile During Climb by Altitude	A-51
Cumulative Occurrences of Incremental Maneuver Load Factor per Nautical Mile During Cruise by Altitude	A-52
Cumulative Occurrences of Incremental Maneuver Load Factor per Nautical Mile During Descent by Altitude	A-53
Cumulative Occurrences of Incremental Maneuver Load Factor per Nautical Mile During Approach by Altitude	A-54
Cumulative Occurrences of Incremental Maneuver Load Factor per 1000 Hours by Flight Phase	A-55
Cumulative Occurrences of Incremental Maneuver Load Factor per 1000 Hours, Combined Flight Phases	A-56
Cumulative Occurrences of Incremental Maneuver Load Factor per Nautical Mile by Flight Phase	A-57
Cumulative Occurrences of Incremental Maneuver Load Factor per Nautical Mile, Combined Flight Phases	A-58

TABLE 8. STATISTICAL DATA FORMATS (Continued)

Data Description	Figure
COMBINED MANEUVER AND GUST LOADS DATA	
Cumulative Occurrences of Combined Maneuver and Gust Incremental Vertical Load Factor per 1000 Hours by Flight Phase	A-59
Cumulative Occurrences of Incremental Vertical Load Factor per 1000 Hours, Combined Flight Phases	A-60
Cumulative Occurrences of Incremental Vertical Load Factor per Nautical Mile by Flight Phase	A-61
Cumulative Occurrences of Incremental Vertical Load Factor per Nautical Mile, Combined Flight Phases	A-62
Cumulative Occurrences of Lateral Load Factor per 1000 Hours, Combined Flight Phases	A-63
Coincident Maneuver Load Factor and Speed Versus V-n Diagram for Flaps Retracted	A-64
Coincident Maneuver Load Factor and Speed Versus V-n Diagram for Flaps Extended	A-65
Coincident Gust Load Factor and Speed Versus V-n Diagram for Flaps Retracted	A-66
Coincident Gust Load Factor and Speed Versus V-n Diagram for Flaps Extended	A-67
MISCELLANEOUS OPERATIONAL DATA	
FLAP USAGE DATA	
Cumulative Probability of Maximum Airspeed in Flap Detent During Departure	A-68
Cumulative Probability of Maximum Airspeed in Flap Detent During Approach	A-69
Percent of Time in Flap Detent During Departure	A-70
Percent of Time in Flap Detent During Approach	A-71
SPEED BRAKE/FLIGHT SPOILER DATA	
Cumulative Probability of Maximum Speed During Speed Brake Deployment	A-72
Cumulative Frequency of Speed at Speed Brake Deployment	A-73
Cumulative Frequency of Altitude at Speed Brake Deployment	A-74
Cumulative Probability of Maximum Deployment Angle During Speed Brake Deployment, Flaps Retracted	A-75
Cumulative Flight Hours for Coincident Speed Brake Deflection and Flap Handle Position	A-76
THRUST REVERSER DATA	
Cumulative Probability of Time With Thrust Reversers Deployed	A-77
Cumulative Probability of Speed at Thrust Reverser Deployment and Stowage	A-78
PROPULSION SYSTEM DATA	
Cumulative Probability of Percent of N_1 at Takeoff	A-79
Cumulative Probability of Percent of N_1	A-80

5.1.1 Weight Data.

The cumulative probabilities of takeoff gross weight, takeoff fuel weight, and landing weight are presented in figures A-1 through A-3 respectively. The correlation between fuel weight at takeoff and the flight distance is presented in figure A-4. A similar correlation for takeoff gross weight and flight distance is shown in tabular form as a percentage of flights in figure A-5. The flight distances in figures A-4 and A-5 are based on the great circle distance between departure and arrival points.

Figure A-6 provides the correlation between the takeoff gross weight and the landing gross weight. The figure shows two distinct distributions, one for liftoff gross weights below approximately 280,000 pounds, and a second one for liftoff gross weights above approximately 280,000 pounds. The correlation shows that for most flights with takeoff weights less than 280,000 pounds the landing weight is within 10,000 to 20,000 pounds of the takeoff weight. For

the higher takeoff weights above 280,000 pounds the variation in landing weights is greater and may vary from 60,000 to 100,000 pounds below liftoff weight. Not unexpectedly the highest variations occur at the higher liftoff weights.

5.1.2 Altitude Data.

Measured operational altitudes and their correlation to flight distance and maximum speed are presented. Figure A-7 shows the correlation between the maximum altitude attained in flight and the flight distance flown in percent of flights. The data show that for shorter flights of less than 500 nautical miles, the maximum altitude does not exceed 40,000 feet with the most flights occurring between 30,000-35,000 feet. For flights above 500 nautical miles the maximum altitude will always be above 30,000 feet, with the vast majority of flights occurring at altitudes between 35,000 and 40,000 feet. It should be noted that the B-767-200ER data showed that no flights occurred in the flight distance range from 750-1,750 nautical miles, hence this distance range is not shown in figure A-7.

Figure A-8 presents the percent of total flight distance spent in various altitude bands as a function of flight distance. The flight distances in figure A-7 reflect the stage lengths; whereas the flight distances in figure A-8 are based on the numerical integration approach mentioned in paragraph 4.4.2. Since the stage lengths reflect the straight line distance between departure and arrival points, this distance will almost always be less than the integrated distance. The integrated distance includes the effects of flying enroute navigation fixes from departure to destination that deviate from the straight line and the effects of tail or head winds encountered during the flight. Based on the integrated flight distance no flight distances in the range from 1,000-1,500 nautical miles were observed, hence this distance range is not shown in figure A-8. This is consistent with the data shown in figure A-4. The combined information in figures A-7 and A-8 provide a comprehensive picture of the flight profile distribution.

Figures A-9 and A-10 show the maximum Mach number or the maximum calibrated airspeed reached during the flight with respect to maximum airspeed limits as defined in the aircraft flight manual. It is not known if these speeds represent the actual structural design speeds M_{MO} or V_{MO}. The maximum Mach number or airspeed data points represent the one speed that most closely approached the speed limit in a given flight during any of the flight phases. As an example, in one flight the maximum speed with respect to the limit might have been attained in the climb phase, while in another flight the maximum speed with respect to the limit speed might have occurred in the cruise phase. It should be noted that maximum Mach number and maximum indicated airspeed do not necessarily occur simultaneously. Data points outside the operational flight limits must be interpreted with some caution. The speed limit is provided in terms of indicated airspeed. The data points reflect the calibrated airspeed. Information on the differences between the indicated airspeed and calibrated airspeed due to instrument and static error or which are a function of airplane flight attitude, Mach number or flap position is not available.

5.1.3 Flight Distance Data.

Flight distance statistics useful in the generation of flight profiles are presented. The cumulative probability of flight distances flown is presented in figures A-11 and A-12. The great circle

distance reflects the ground distance between two points as obtained from the great circle distance calculation, but does not necessarily reflect the actual distance flown. Deviation from direct flight between departure and arrival points resulting from traffic control requirements will increase the actual distance flown by some unknown amount. To a much lesser extent, the climb and descent distances are slightly larger than the level flight distance. Head or tail winds also are unknown contributors. The integrated distance accounts for such variables. The figure provides a graphical presentation of the differences in flight distance obtained by the two approaches.

5.2 GROUND LOADS DATA.

The ground loads data include frequency and probability information on vertical, lateral, and longitudinal accelerations, speeds, and pitch rotation associated with takeoff, landing, and ground operations. These data are of primary importance to landing gear and landing gear backup structure and to a lesser extent to the wing, fuselage, and empennage.

5.2.1 Lateral Load Factor Data.

Lateral load factor statistics resulting from ground turning during taxi were derived and are presented. Figure A-13 shows the cumulative frequency of the maximum side load factor during ground turns. The information is presented for pre- and postflight taxi as well as left and right turns. The turning load factors during taxi in are shown to be more severe than those experienced during turning while taxiing out. This is likely the result of higher taxi in speed as shown later in figure A-23. There is no significant difference between the number of left and right turns. It is interesting to note that the probability of exceeding given side load factor levels during ground turning is lower for the B-767-200ER as presented in this report when compared with the same data for the B-737-400 and MD-82/83 aircraft reported in references 5 and 6.

5.2.2 Longitudinal Load Factor Data.

Longitudinal load factor statistics were derived for all phases of ground operation, including pre- and postflight taxi and takeoff and landing roll. Figures A-14 presents the cumulative frequency of longitudinal load factor during ground operations. The figure shows the data for pre- and postflight taxi. Figure A-15 shows the cumulative frequency of longitudinal load factor during the landing rollout with and without thrust reverser deployment. It appears that the additional braking from deployment of thrust reversers changes the longitudinal load factor spectra by approximately 0.1 g in the negative direction. The occurrence of positive longitudinal load factors may be due to variations in the overall retardation forces from thrust reversers, hydraulic brakes, and rolling friction. Figures A-16 and A-17 present the cumulative probability of the maximum and minimum longitudinal load factor measured during the takeoff and landing rolls respectively.

5.2.3 Vertical Load Factor Data.

Vertical load factor statistics during all phases of ground operation with and without thrust reverser are presented. Figure A-18 presents the cumulative frequency of incremental vertical load factor during pre- and postflight taxi. Figure A-19 presents the cumulative frequency of incremental vertical load factor during the takeoff roll, while figure A-20 presents the cumulative

frequency of incremental vertical load factor during the landing roll for operation with and without thrust reverser. As can be seen, there are large differences in the frequency of vertical load factor occurrences between the taxi-in and taxi-out phases. This is a major departure from what was observed on the B-737-400 and MD-82/83 aircraft as presented in references 5 and 6. These references show nearly identical frequency distributions of vertical accelerations for the taxi-out and taxi-in phases.

Figure A-21 presents the cumulative probability of the minimum and maximum incremental vertical load factors associated with touchdown and ground spoiler deployment. As can be seen, spoiler deployment increases the probability of encountering given levels of vertical acceleration. This is consistent with the B-737-400 data presented in reference 5, but opposite from the MD-82/83 data presented in reference 6.

Figure A-22 shows the coincident incremental vertical load factor and gross weight at touchdown for all flights. Six landing load factors occur at touchdown gross weights above the maximum landing gross weight of 278,000 pounds for the B-767-200ER as shown in table 1. It is noteworthy that the maximum landing gross weight for the B-767-200ER varies from 278,000 to 285,000 pounds depending on airplane/engine configuration. The basic B-767 airplane has a maximum landing gross weight that varies from 270,000 to 320,000 pounds depending on airplane/engine model. Although the actual airplane/engine configuration of the airplanes for which data was obtained is unknown, it may provide a clue to the higher landing gross weights observed. Detailed examination of the data for these landings did not surface any reasons to suspect the validity of the data.

5.2.4 Ground Speed Data.

The cumulative probabilities of ground speed for taxi in and taxi out operations are presented in figure A-23. The taxi in speeds are seen to be considerably higher than the taxi out speeds. There can be several reasons for this difference. First, the airplane may still be moving at a fairly high speed shortly after turning off the active runway. Departure from the active runway has been used as the criterion for start of taxi in. Second, movement of inbound traffic to the terminal after landing is generally accomplished faster than similar movement from the terminal to the takeoff position. Figure A-24 shows the cumulative probabilities of airspeed at liftoff and touchdown rotation. The liftoff speeds are approximately 30 knots higher than the touchdown speeds.

5.2.5 Flare Data.

Figure A-25 presents the cumulative probability of airspeed at flare. Since the actual instant of flare is difficult to determine with any great accuracy, the start of flare was assumed to occur 3 seconds prior to main gear squat switch closure.

5.2.6 Pitch/Rotation Data.

The cumulative probability of maximum pitch angle at takeoff and landing is presented in figure A-26. Figure A-27 presents the cumulative probability of maximum takeoff pitch rate at takeoff rotation. Figure A-28 presents the cumulative probability of pitch angle that occurs upon

encountering the maximum vertical load factor associated with touchdown. Comparison of the data in figures A-26 and A-28 shows close agreement between the cumulative probability of pitch angle at touchdown and at touchdown peak vertical load factor. This indicates that little change in pitch angle occurs between the time of initial touchdown and the time when the maximum vertical load factor occurs.

5.3 FLIGHT LOADS DATA.

The flight loads data include the statistical data that describe the gust and maneuver environment. The gust environment is presented in the form of cumulative occurrences of derived gust velocity, continuous gust intensity, and vertical load factor. The derived gust velocity and continuous gust intensity are computed values as described in section 4.3. Since the 1950s, it has been common practice to present flight loads data as cumulative occurrences. Data that were previously recorded on the B-737 and MD-82/83 are reported in references 4, 5, and 6 as cumulative occurrences per 1000 hours. To compare to data from different references, the normal acceleration data are plotted two ways, as cumulative occurrences per 1000 hours and as cumulative occurrences per nautical mile.

5.3.1 Gust Loads Data.

The gust data are presented in the form of incremental vertical accelerations, derived gust velocity U_{de}, and continuous gust intensities U_{σ}. The magnitudes of the derived gust velocities and continuous gust intensities were derived from the measured accelerations in accordance with the procedures presented in paragraphs 4.3.4 and 4.3.5. Figure A-29 presents the cumulative occurrences of incremental vertical gust load factor per 1000 hours. The data are presented by phase of flight. Figure A-30 shows cumulative occurrences of incremental vertical gust load factor for the total combined airborne phases per 1000 hours. Figure A-31 presents the cumulative occurrences of incremental vertical gust load factor per nautical mile by phase of flight, and figure A-32 shows the cumulative occurrences of incremental vertical gust load factor for the total combined airborne phases per nautical mile. In figures A-33 through A-40, the derived gust velocity U_{de} is plotted as cumulative counts per nautical mile for altitudes from sea level to 49,500 feet. The derived gust velocities are compared to the gust velocity distributions presented in reference 7. The gust velocity data from reference 7 have frequently been used in establishing structural design criteria for repeated gust loads. The gust experience at altitudes below 500 feet compares very well with the reference 7 predictions. The gusts experienced between 500 and 4,500 feet are more severe than would be predicted by the reference 7 approach. Above 9,500 feet reference 7 predicts increasingly more severe gust spectra than was obtained form the B-767-200ER data. Figures A-41 and A-42 present the derived gust velocity U_{de} as cumulative counts per nautical mile with flaps extended and retracted respectively. Figures A-43 and A-44 present the cumulative occurrences per nautical mile of the continuous gust intensities for the flaps extended and flaps retracted conditions respectively.

5.3.2 Maneuver Loads Data.

Figures A-45 through A-49 present the cumulative occurrences of incremental maneuver load factor per 1000 hours by altitude for each of the airborne flight phases, i.e., departure, climb, cruise, descent, and approach. Figures A-50 through A-54 present the cumulative occurrences of

incremental maneuver load factor by altitude per nautical mile in the airborne phases of flight. Figure A-55 presents the total cumulative occurrences of incremental maneuver load factor per 1000 hours for each phase of flight regardless of altitude. Figure A-56 presents the total cumulative occurrences of incremental maneuver load factor per 1000 hours for all flight phases combined. Figure A-57 presents the total cumulative occurrences of incremental maneuver load factor per nautical mile for each phase of flight regardless of altitude. Figure A-58 presents the total cumulative occurrences of incremental maneuver load factor per nautical mile for all flight phases combined.

5.3.3 Combined Maneuver and Gust Loads Data.

For the data presented in this section, the maneuver and gust load factors were not separated, but the total load factor occurrences regardless of the cause were used in the derivation of the figures. Figure A-59 shows the cumulative occurrences of total combined maneuver and gust normal load factor per 1000 hours by phases of flight, and figure A-60 shows the occurrences for all phases combined. Figures A-61 and A-62 show the data of figures A-59 and A-60 as occurrences per nautical mile. Figure A-63 presents the cumulative occurrences of lateral load factor for the combined phases of flight.

5.3.4 V-n Diagrams.

Federal Aviation Regulation (FAR) 25.333 requires that strength requirements be met at each combination of airspeed and load factor on and within the boundaries of the representative maneuvering and gust load envelopes (V-n diagrams). For purposes of displaying the coincident maneuver or gust accelerations, four representative V-n diagrams were developed from the FAR requirements. V-n diagrams are a function of altitude and gross weight. For illustration purposes a gross weight of 290,000 pounds and a sea level altitude were selected to develop representative V-n diagrams.

5.3.4.1 Maneuver V-n Diagram Derivation.

For the maneuver V-n diagram, the required limit load factors are specified in FAR 25.337. The positive limit maneuvering load factor (n) may not be less than 2.5, and the negative limit maneuvering load factor may not be less than -1.0 at speeds up to V_C, varying linearly with speed to zero at V_D. FAR 25.345 specifies that the positive limit maneuver load factor is 2.0 g when the flaps are extended. The stall curve on the left side of the envelopes is determined by the maximum lift coefficient. The curve was estimated by using the 1-g stall speed to estimate $C_{L_{max}}$.

5.3.4.2 Gust V-n Diagram Derivation.

For the gust V-n diagram, the required limit load factors for gusts result from gust velocities as specified in FAR 25.341. The FAR specifies positive (up) and negative (down) air gust design requirements for three different aircraft design speeds: maximum gust intensity (V_B), cruising speed (V_C), and dive speed (V_D). Between sea level and 20,000 feet, the gust requirement is constant, varying linearly to the value given for 50,000 feet. FAR 25.345 sets a requirement of

positive, negative, and head-on for 25-fps gusts when flaps are extended. These gust design requirements are shown in table 9.

TABLE 9. FAR REQUIREMENTS FOR DERIVED DISCRETE GUST VELOCITIES

Aircraft Design Speed	Gust Velocity	
	0-20,000 Feet Altitude	50,000 Feet Altitude
V_B	66 fps	38 fps
V_C	50 fps	25 fps
V_D	25 fps	12.5 fps
Flaps Extended	25 fps	—

5.3.4.3 Coincident Speed and Load Factor Data.

Figures A-64 through A-67 show the V-n diagrams for maneuver and for gust with flaps retracted and extended. Coincident acceleration and speed measurements are also plotted on the V-n diagrams. As can be seen in figure A-67, some gust accelerations occurred outside the gust V-n diagram for the flaps extended case. It must be kept in mind that the V-n diagram is for a specific gross weight-altitude combination and may well be within the V-n diagram for the actual gross weight-altitude combination that existed at the time the acceleration was measured. Furthermore, the V-n diagram reflects only one static strength requirement. The actual structure is designed by many different strength and rigidity design requirements including static strength, durability, and damage tolerance. The exceedance of a single design requirement may indicate a shortcoming in the design requirement but does not necessarily translate into a deficiency in the design strength.

5.4 MISCELLANEOUS OPERATIONAL DATA.

The miscellaneous operational data includes statistical usage information for flaps, speed brakes/spoilers, and thrust reverser operations. Although control information, such as aileron and rudder deflection, was available, it was not processed because it was deemed that the slow sampling rates for control deflection prevent the reduction of reliable statistical usage information for these components.

5.4.1 Flap Usage Data.

Flap usage statistics that characterize the sources of repeated loads on flap structure, backup structure, and other flap components were reduced from the measured data. Figure A-68 presents the cumulative probability of maximum airspeed encountered in various flap detents during the departure phase of the flights. The flap detents are defined in table 7. The cumulative probabilities for detents 20 and 25 are based on two occurrences each. The cumulative probability for detent 15 is based on three data occurrences. Because of the few data occurrences underlying these cumulative probabilities there is no statistical significance to these curves. Figure A-69 presents similar data for the approach phase of the flights. Figures A-70 and A-71 present the percent of time spent in various flap detents during the departure and approach

phases of flight, respectively. The figures are presented in semilog format to provide a visible indication of the very short exposure times. As shown in figure A-70, flap detent 5 was the detent used in almost all cases during departure.

5.4.2 Speed Brake/Spoiler Usage Data.

Information on speed brake or symmetrical spoiler deflections during flight was determined to be of major interest to both aircraft manufacturers and operators. Therefore, statistics on speed brake/spoiler usage as a function of speed, altitude, and deflection angle were derived from the measured data. To be counted as a deployment cycle the speed brake/spoiler had to deflect more than 7 degrees for a period of 3 seconds. Data on speed brake/spoiler operations occurring during the landing roll are available, but were not reduced into statistical format. Figure A-72 presents the cumulative occurrences of maximum speed encountered while the speed brakes were deployed, while figure A-73 presents the cumulative occurrences of speed at the moment of speed brake deployment. Figure A-74 presents the cumulative occurrences of altitude at the moment of speed brake deployment. As can be seen in figures A-73 and A-74, speed brake cycles occur on average more than once per flight. This is opposite to the spoiler experience on the B-737-400 as presented in reference 5, which shows that the speed brakes were deployed less than once per flight. Figure A-75 presents the cumulative probability of maximum deployment angle reached during the time that the speed brakes were deployed for the flaps retracted configuration. No speed brake cycles were counted for the conditions of flaps deflected in various detents. Figure A-76 provides information regarding the time spent in various coincident speed brake/flap settings.

5.4.3 Thrust Reverser Data.

Cumulative probabilities of duration and speed associated with thrust reverser operations were derived from the measured data. Figure A-77 presents the cumulative probability of total time that thrust reversers are deployed. Figure A-78 presents the cumulative probability of the speed at the time when the thrust reversers were deployed or stowed. Although normally the thrust reversers are deployed and stowed a single time for each landing, the measured data showed two cycles of thrust reverser operation on a few occasions. This accounts for the rare occurrence of thrust reverser deployment at speeds as low as 45 knots in figure A-78. The data processing did not evaluate the engine power lever angles existing at these specific low-speed thrust reverser deployments.

5.5 PROPULSION SYSTEM DATA.

The cumulative probability of engine fan speed N_1 associated with thrust reverser operations was derived from the measured N_1 engine parameter. Figure A-79 presents the cumulative probability of percent of engine fan speed N_1 at takeoff, while figure A-80 presents similar data for the landing roll at the instant of thrust reverser deployment and the maximum percent of fan speed N_1 encountered during the time that the thrust reverser is deployed.

6. CONCLUSIONS.

The data in figure A-67 shows that the measured gust load factors for the flaps extended configuration can occur outside the design V-n diagram. Identical data based on longer data collection periods for other large transport aircraft as shown in references 5 and 6 show many more occurrences outside the V-n diagram. This suggests that the present gust design requirements for the flaps extended configuration may need to be reviewed for adequacy. An assessment of the appropriateness of the continued use of U_{de} design values specified in FAR 25.345 for high-lift devices appears to be justified.

Derived gust velocity, U_{de}, values recorded from this effort show deviation from the data presented in reference 7. In general, for altitudes above 4,500 feet the B-767-200ER data show lower levels of occurrences for the upward and downward gusts than would be predicted by the data in reference 7. This is consistent with the data from the B-737-200 and MD-82/83 in references 5 and 6. In as much as reference 7 represented a rather preliminary effort to define atmospheric turbulence and the data from three different aircraft are relatively consistent, it is appropriate that the turbulence descriptions in reference 7 be used with caution. It is reasonable to expect that the gust intensity U_{σ} spectra would show a similar deviation from the spectra based on the requirements in Appendix G of the FAR. Comparison of gust intensity spectra with the requirements in the FAR is considered a desirable addition to the report. The FAR requirements for gust intensity spectra are specified in terms of turbulence field parameters P and b. Development of new values for the turbulence field parameters based on gust intensity data from the B-767-200ER combined with similar data from other aircraft such as the B-737-400 and MD-82/83 is considered very desirable.

Statistical information on flight control surface activity is a valuable input to the design requirements for these surfaces and their associated components. Flight control surface deflections are recorded at two samples per second (2 sps) and can easily be reduced to provide the desired information. Unfortunately, there are doubts about the adequacy of the sampling rates to provide reliable results. For this reason the flight control surface deflection data were not processed.

7. REFERENCES.

1. Crabill, Norman L., "FAA/NASA Prototype Flight Loads Program Systems Requirements, B737-400 Aircraft," Eagle Aerospace Inc., Contract NAS1-19659, unpublished report, November 1994.

2. de Jonge, B., "Reduction of Incremental Load Factor Acceleration Data to Gust Statistics," DOT/FAA/CT-94/57, August 1994.

3. Rustenburg, John W., Skinn, Donald, and Tipps, Daniel O., "An Evaluation of Methods to Separate Maneuver and Gust Load Factors From Measured Acceleration Time Histories," DOT/FAA/AR-99/14, April 1999.

4. "Flight Loads Data for a Boeing 737-400 in Commercial Operation," DOT/FAA/AR-95/21, April 1996.

5. "Flight Loads Data for a Boeing 737-400 in Commercial Operation," DOT/FAA/AR-98/28, August 1998.

6. "Flight Loads Data for a MD-82/83 in Commercial Operation," DOT/FAA/AR-98/65, February 1999.

7. Press, Harry and Steiner, Roy, "An Approach to the Problem of Estimating Severe and Repeated Gust Loads for Missile Operations," National Advisory Committee for Aeronautics Technical Note 4332, September 1958, Langley Aeronautical Laboratory, Langley Field, Va.

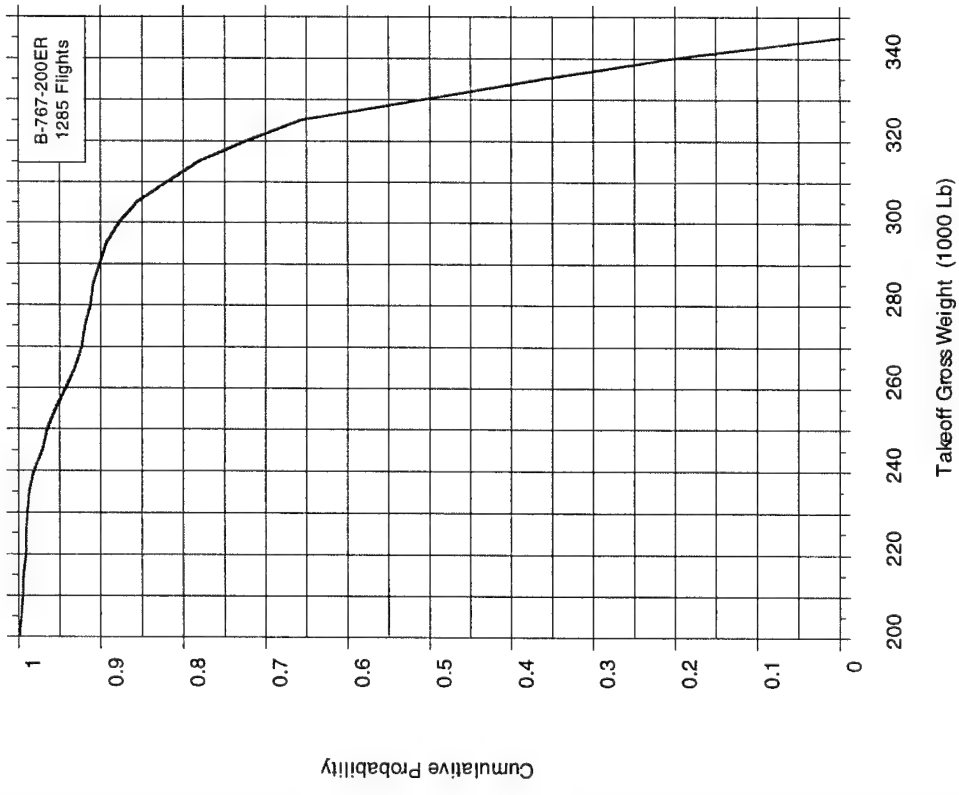

FIGURE A-1. CUMULATIVE PROBABILITY OF TAKEOFF GROSS WEIGHT

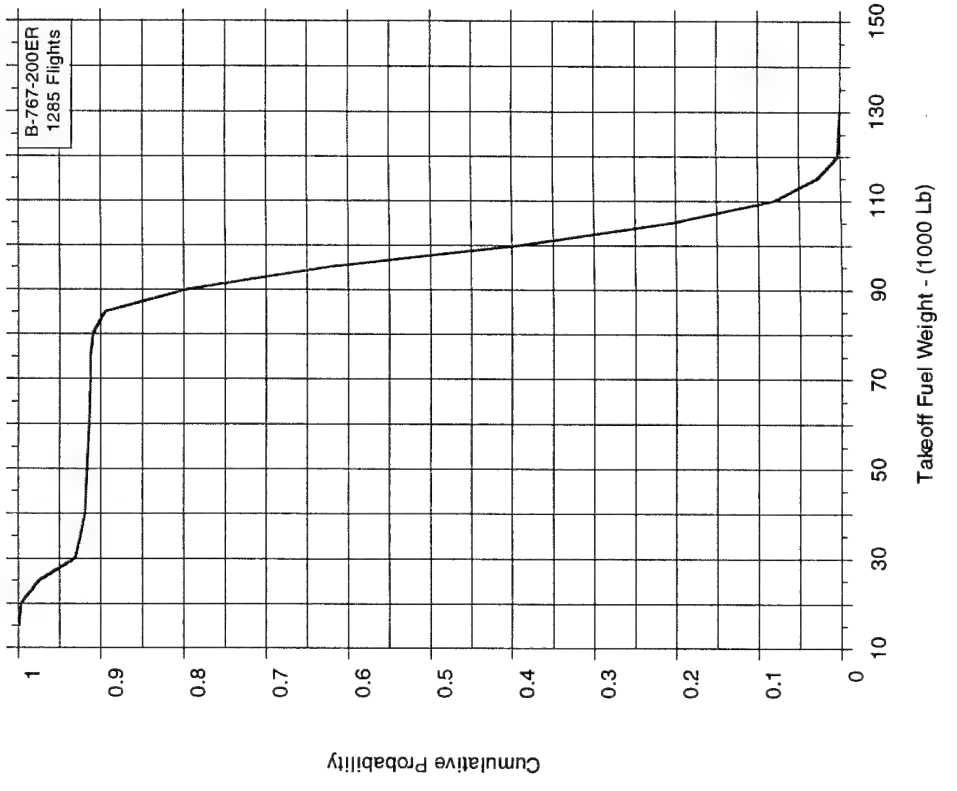

FIGURE A-2. CUMULATIVE PROBABILITY OF TAKEOFF FUEL WEIGHT

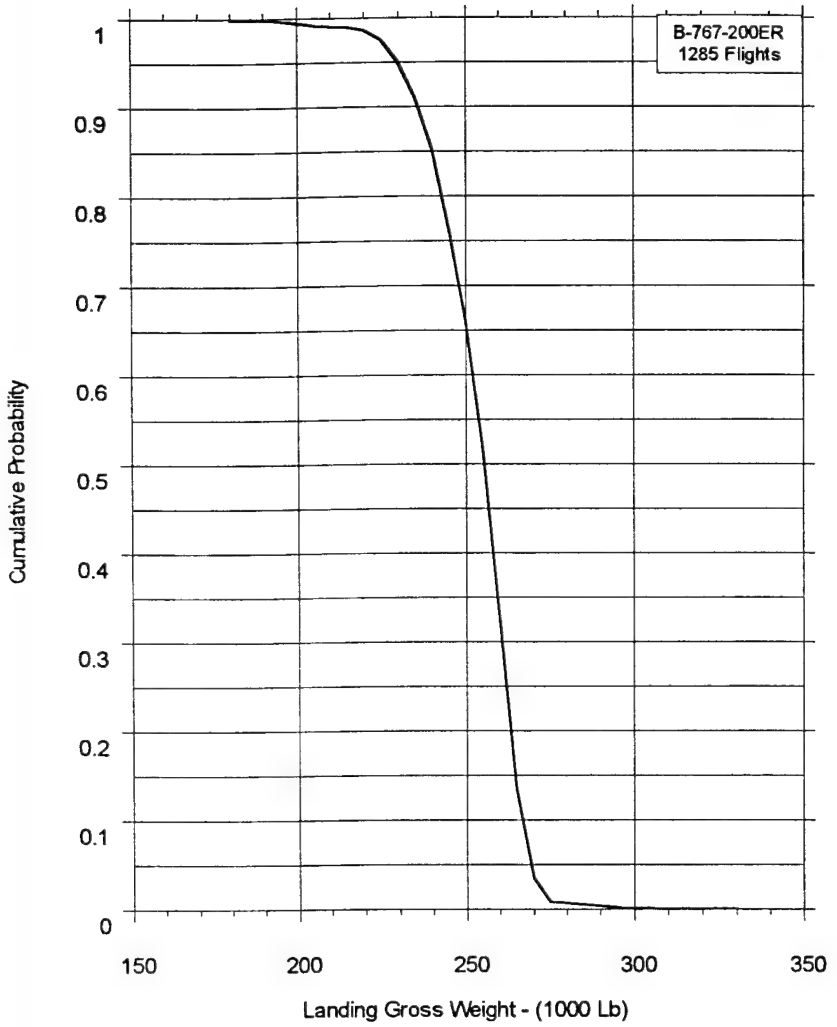

FIGURE A-3. CUMULATIVE PROBABILITY OF LANDING GROSS WEIGHT

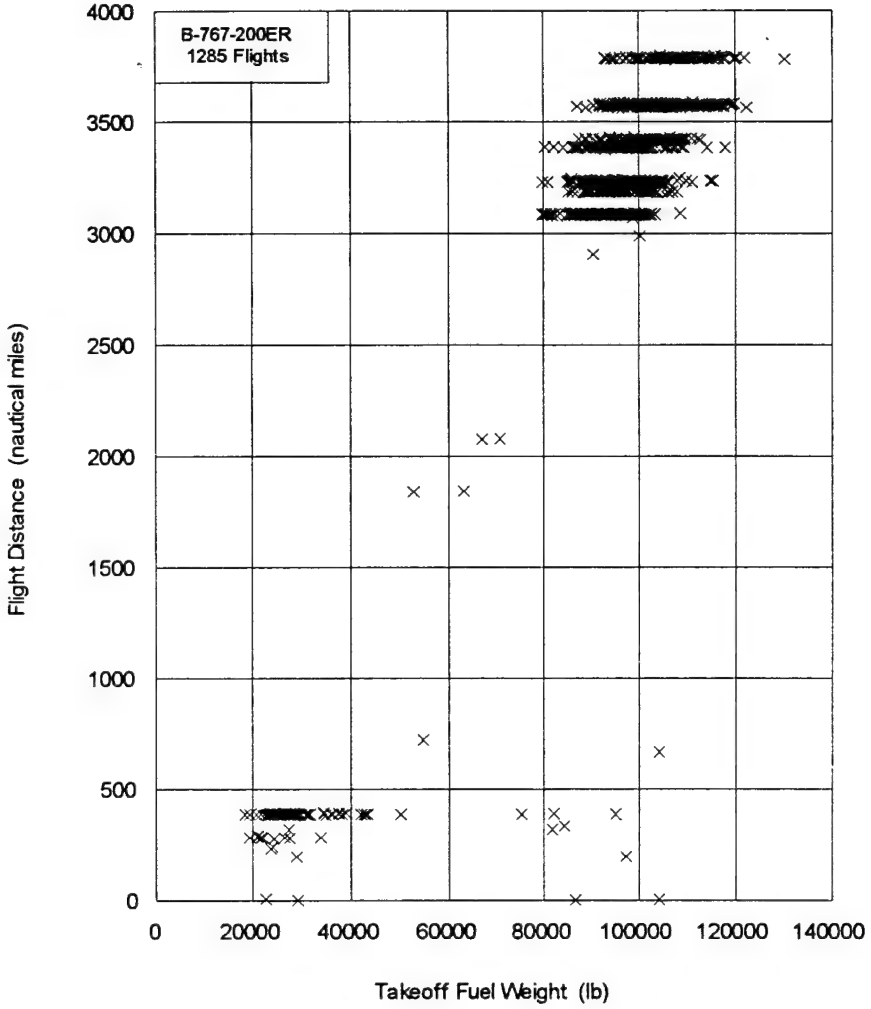

FIGURE A-4. CORRELATION OF TAKEOFF FUEL WEIGHT AND FLIGHT DISTANCE

Takeoff Gross Weight (lb)

Flight Distance (nautical miles) 1285 Flts	200-210	210-220	220-230	230-240	240-250	250-260	260-270	270-280	280-290	290-300	300-310	310-320	320-330	330-340	340-350
0-250	0.233			0.078			0.156							0.078	0.078
250-500	0.233	0.311	0.233	0.700	1.556	2.335	1.712	0.856	0.311						
500-750									0.078						0.078
1750-2000									0.078	0.078					
2000-2250										0.078	0.078				
2750-3000														0.156	
3000-3250								0.078	0.467	1.712	3.346	6.304	13.385	14.708	3.891
3250-3500									0.233	0.545	1.790	1.634	4.591	5.292	4.125
3500-3750									0.078		0.623	1.012	2.646	6.381	8.405
3750-4000												0.623	1.167	3.735	3.735
Total	0.467	0.311	0.233	0.778	1.556	2.335	1.868	0.934	1.245	2.412	5.837	9.572	21.790	30.350	20.311

FIGURE A-5. CORRELATION OF TAKEOFF GROSS WEIGHT AND FLIGHT DISTANCE, PERCENT OF FLIGHTS

Gross Weight at Liftoff (lb)

Gross Weight at Touchdown (lb) 1284 Flts	200-210	210-220	220-230	230-240	240-250	250-260	260-270	270-280	280-290	290-300	300-310	310-320	320-330	330-340	340-350
180-190	0.078														
190-200	0.389														
200-210		0.312													
210-220			0.234	0.078				0.078	0.078						
220-230				0.701	0.312				0.701	0.857	1.012	0.078			
230-240					1.246	0.467			0.078	1.402	2.862	2.336	1.090	0.234	
240-250						1.869	0.623				1.869	4.907	6.931	2.259	0.779
250-260							1.246	0.389		0.156	0.078	2.259	10.514	9.502	8.956
260-270								0.467	0.234				3.271	16.277	9.190
270-280									0.156					2.025	1.246
290-300															0.078
300-310														0.078	
Total	0.467	0.312	0.234	0.779	1.558	2.336	1.869	0.935	1.246	2.414	5.841	9.579	21.807	30.374	20.249

FIGURE A-6. CORRELATION OF GROSS WEIGHT AT LIFTOFF AND TOUCHDOWN, PERCENT OF FLIGHTS

Maximum Altitude (1000 feet)

Flight Distance (nautical miles)

1285 Flts	15-20	20-25	25-30	30-35	35-40	40-45	Total
0-250	0.156	0.078	0.156	0.078	0.156		0.623
250-500		0.078	1.868	4.436	1.868		8.249
500-750					0.156		0.156
1750-2000					0.078	0.078	0.156
2000-2250					0.156		0.156
2750-3000					0.156		0.156
3000-3250				0.311	41.946	1.634	43.891
3250-3500					16.965	1.245	18.210
3500-3750					18.288	0.856	19.144
3750-4000					8.405	0.856	9.261
Total	0.156	0.156	2.023	4.825	88.171	4.669	100

FIGURE A-7. CORRELATION OF MAXIMUM ALTITUDE AND FLIGHT DISTANCE, PERCENT OF FLIGHTS

Total Flight Distance (nautical miles)

Altitude Band (feet)

1285 Flts	0-500	500-1000	1500-2000	2000-2500	2500-3000	3000-3500	3500-4000	4000-4500	4500-5000
39500-44500			8.69		0.18	0.91	0.81	0.80	
29500-39500	25.91	34.16	77.62	90.10	91.45	90.53	90.34	91.42	93.39
19500-29500	38.44	37.62	5.18	3.13	3.29	4.02	4.66	3.77	2.97
9500-19500	21.49	17.58	5.07	4.22	2.99	2.62	2.50	2.33	1.87
4500-9500	8.81	6.35	2.06	1.34	1.14	1.16	1.05	1.07	1.14
1500-4500	4.08	3.53	1.02	0.90	0.74	0.59	0.50	0.48	0.45
500-1500	0.94	0.59	0.27	0.20	0.14	0.11	0.10	0.09	0.10
0-500	0.32	0.17	0.08	0.10	0.06	0.05	0.05	0.05	0.07
Total	100	100	100	100	100	100	100	100	100

FIGURE A-8. PERCENT OF TOTAL DISTANCE IN ALTITUDE BANDS

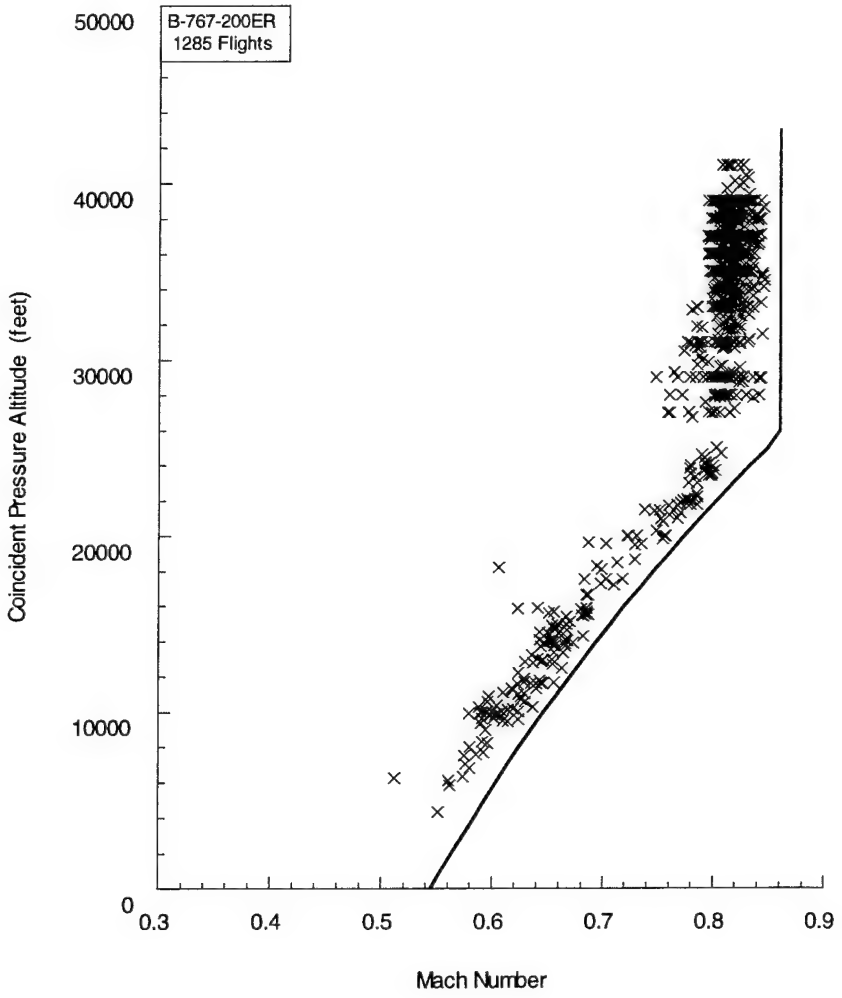

FIGURE A-9. COINCIDENT ALTITUDE AT MAXIMUM MACH NUMBER, ALL FLIGHT PHASES

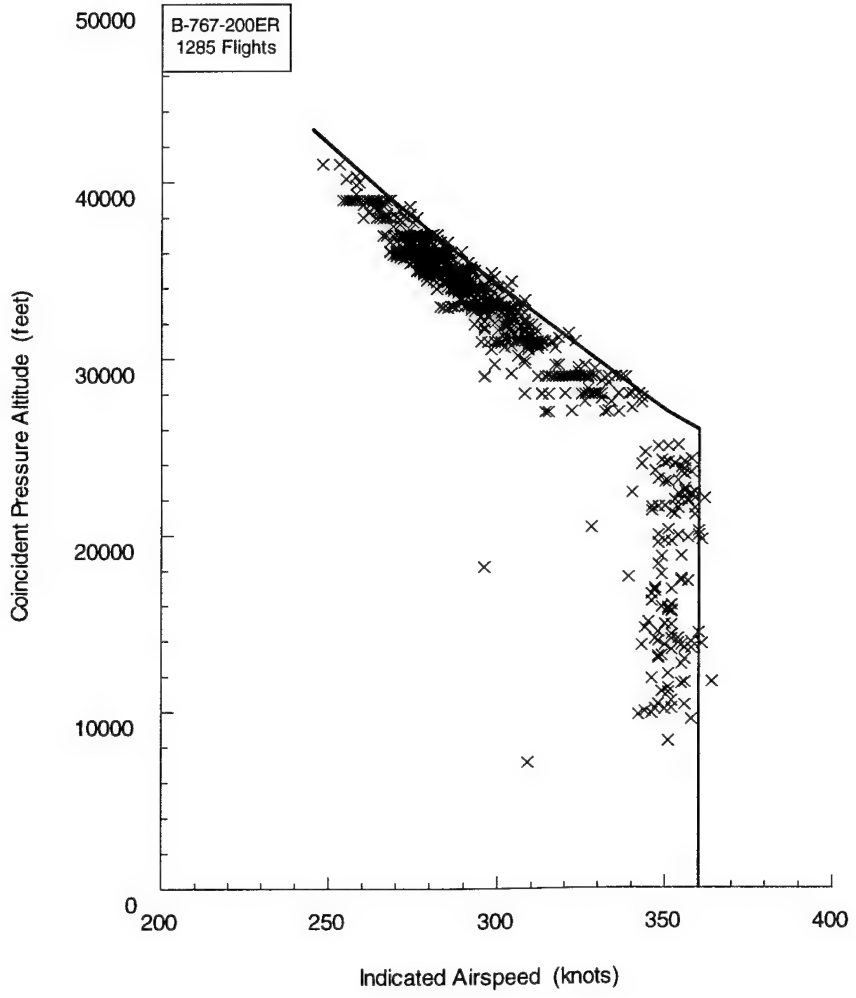

FIGURE A-10. COINCIDENT ALTITUDE AT MAXIMUM CALIBRATED AIRSPEED, ALL FLIGHT PHASES

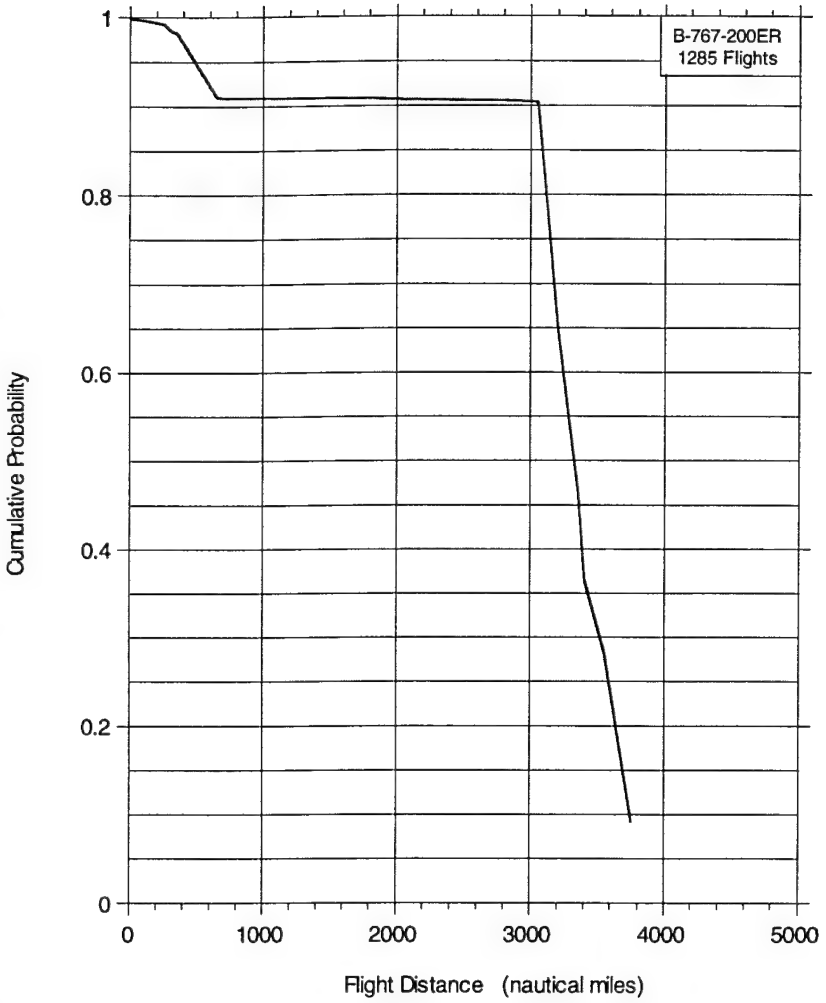

FIGURE A-11. CUMULATIVE PROBABILITY OF GREAT CIRCLE FLIGHT DISTANCE

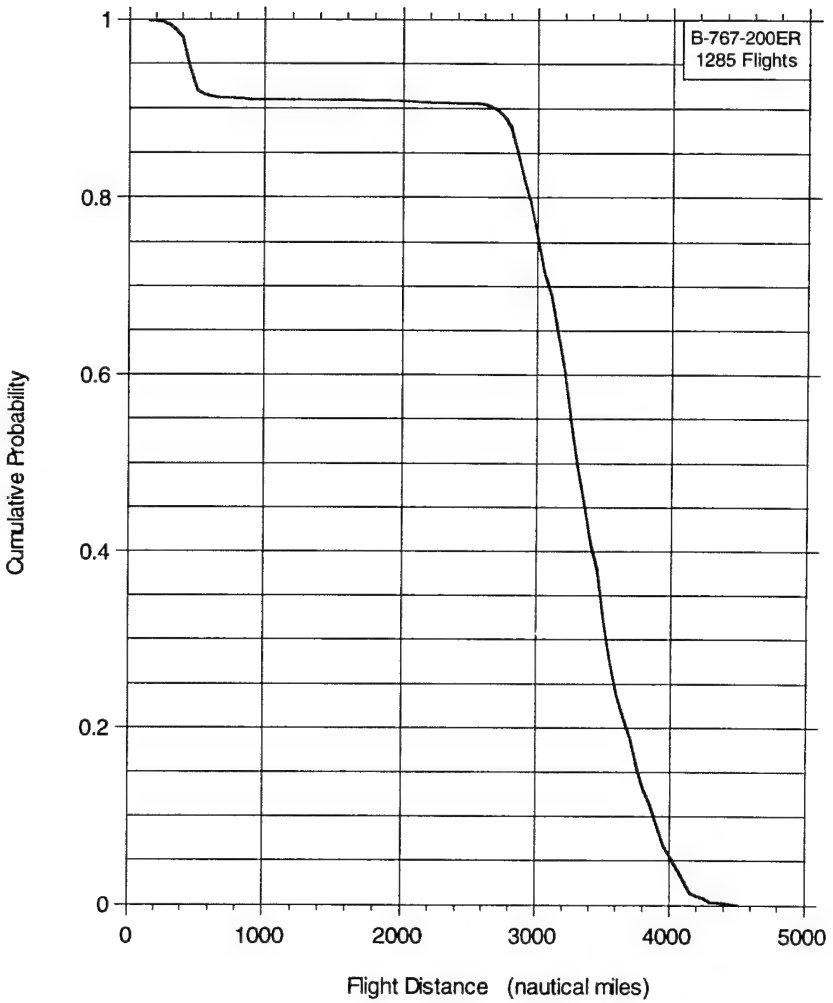

FIGURE A-12. CUMULATIVE PROBABILITY OF INTEGRATED FLIGHT DISTANCE

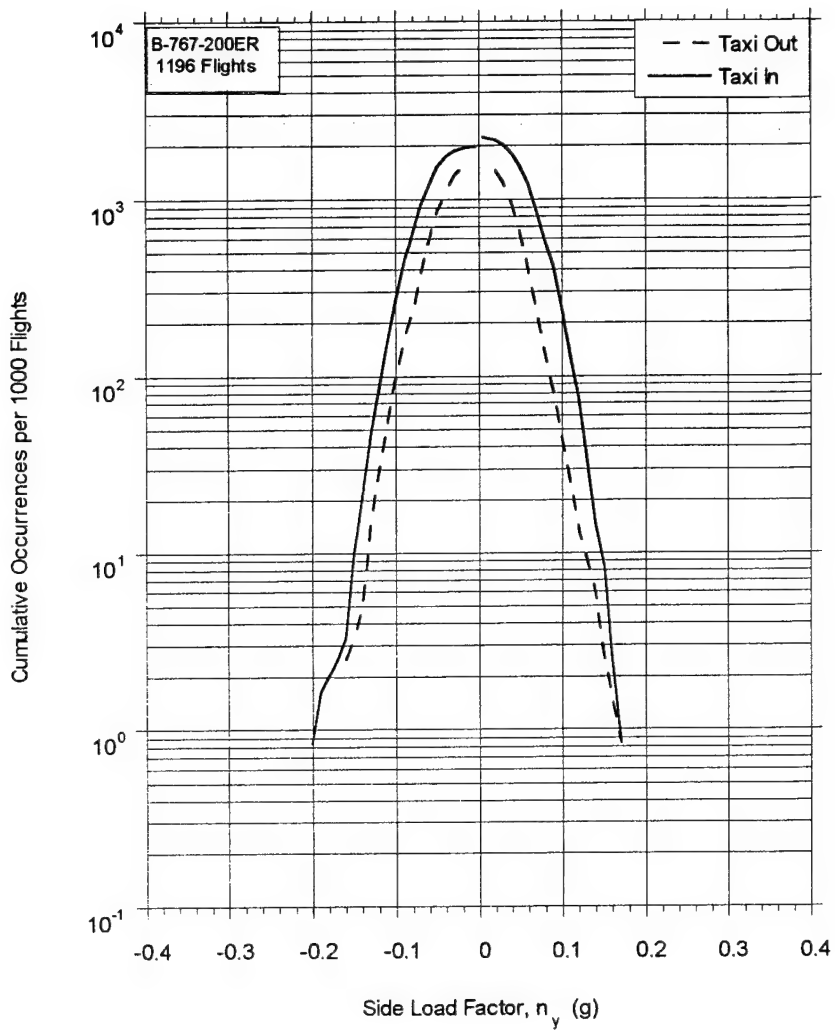

FIGURE A-13. CUMULATIVE FREQUENCY OF MAXIMUM SIDE LOAD FACTOR DURING GROUND TURNS

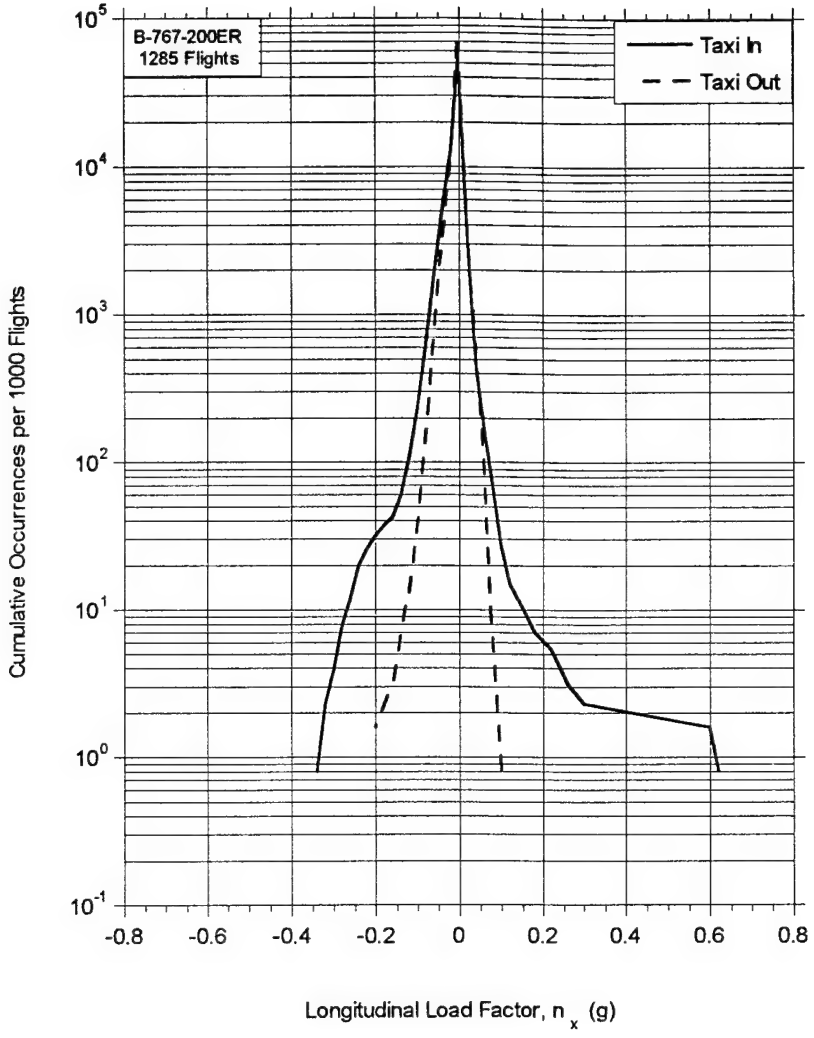

FIGURE A-14. CUMULATIVE FREQUENCY OF LONGITUDINAL LOAD FACTOR DURING GROUND TAXI

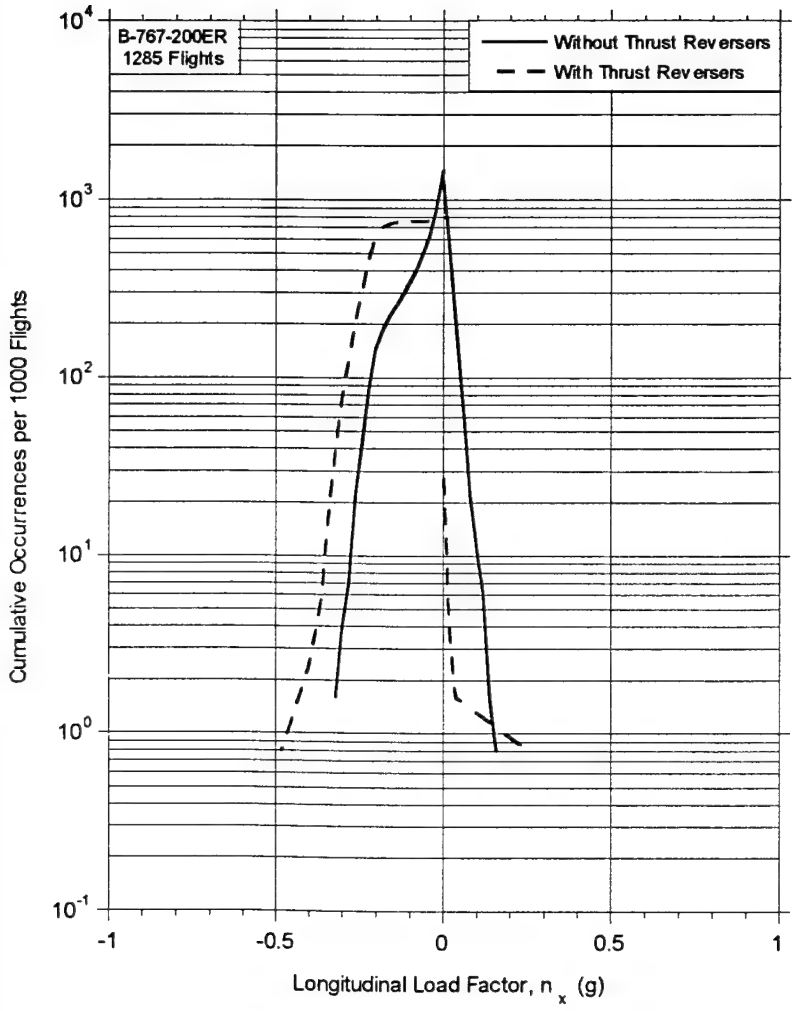

FIGURE A-15. CUMULATIVE FREQUENCY OF LONGITUDINAL LOAD FACTOR DURING LANDING ROLL

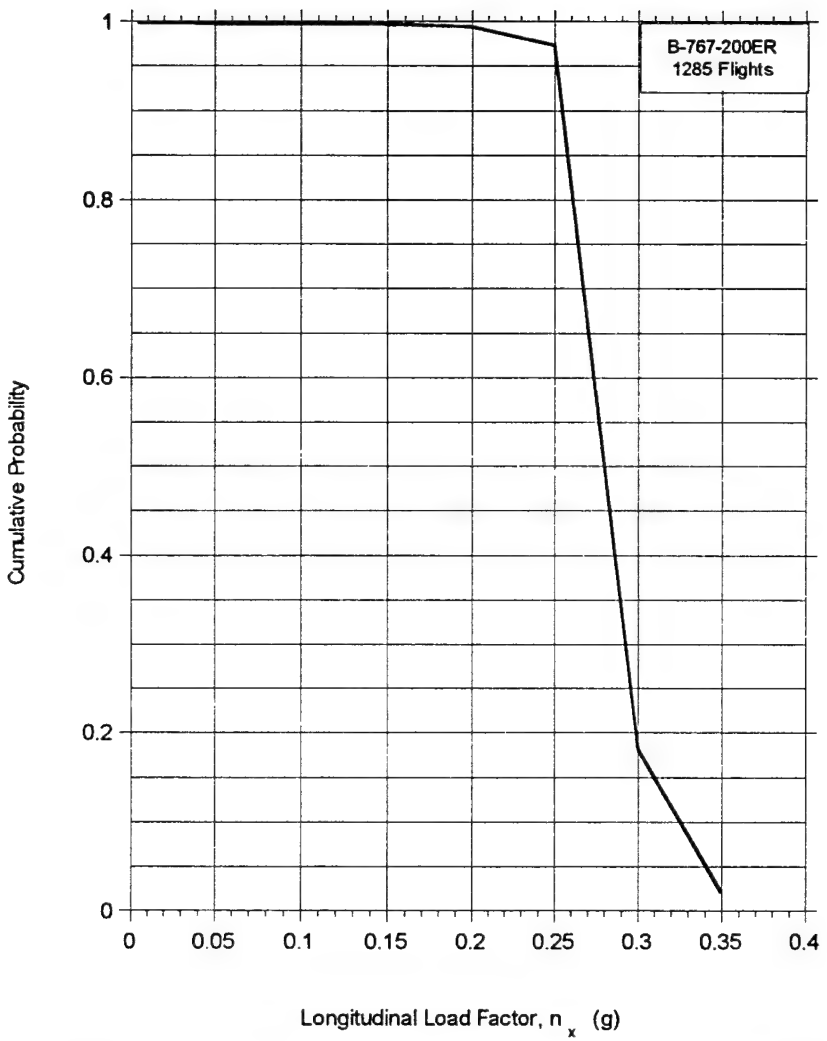

FIGURE A-16. CUMULATIVE PROBABILITY OF MAXIMUM LONGITUDINAL LOAD FACTOR DURING TAKEOFF

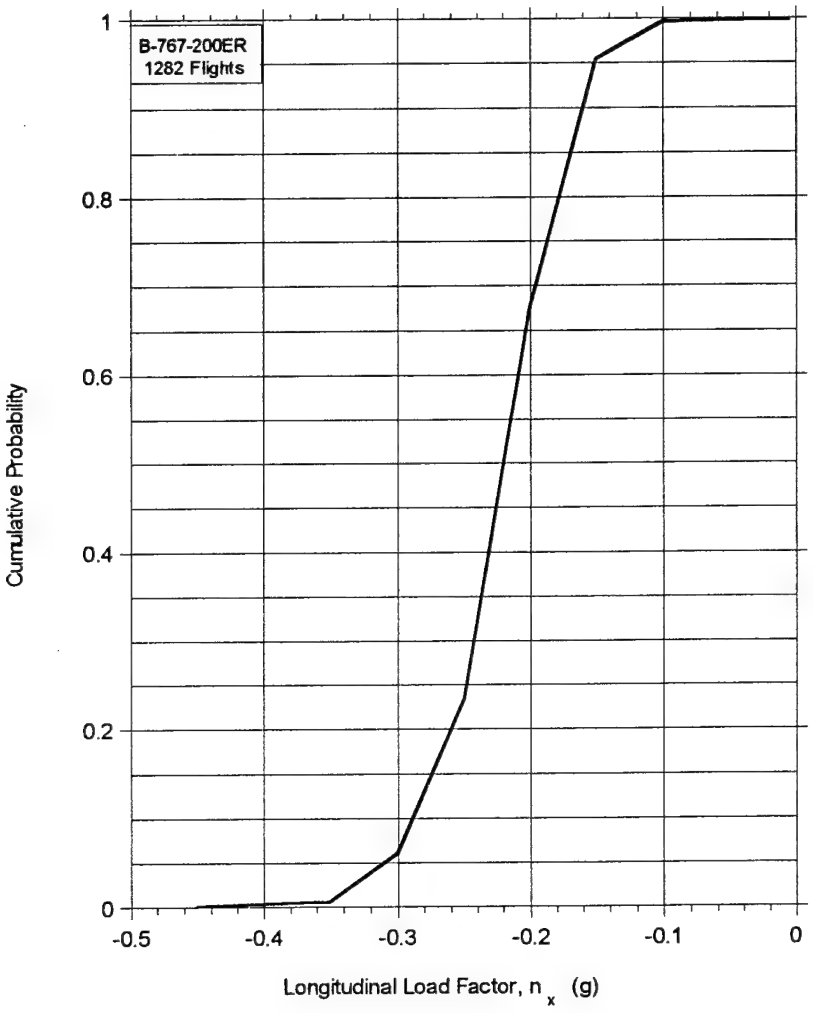

FIGURE A-17. CUMULATIVE PROBABILITY OF MINIMUM LONGITUDINAL LOAD FACTOR DURING LANDING

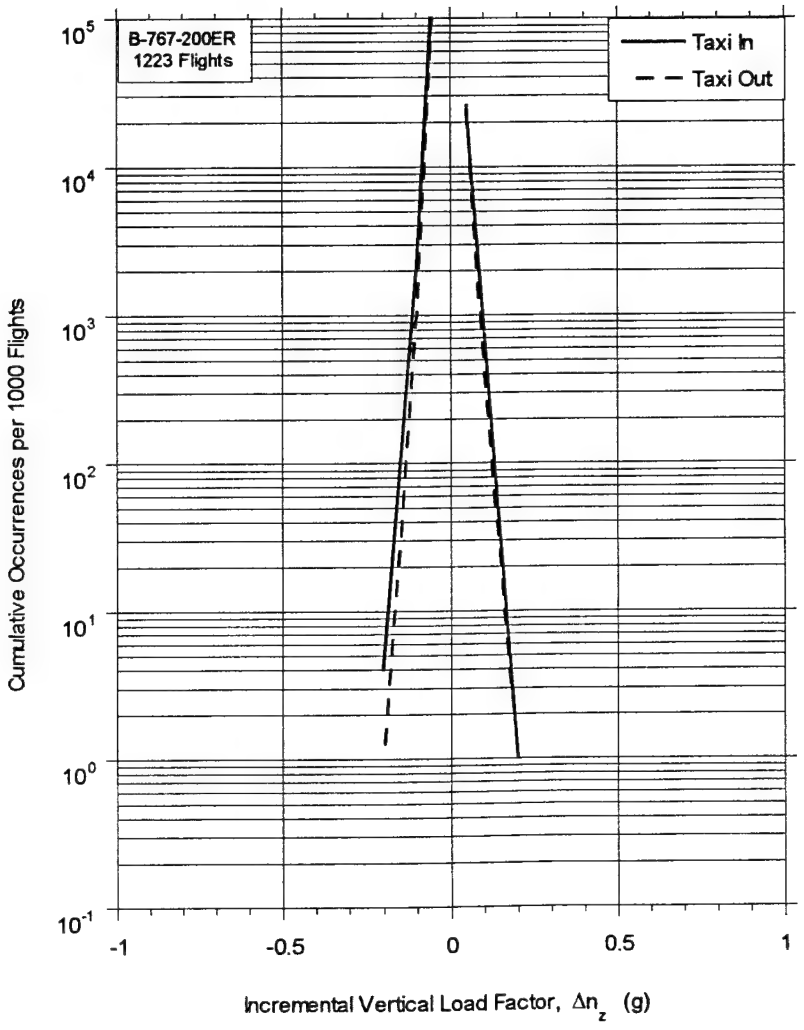

FIGURE A-18. CUMULATIVE FREQUENCY OF INCREMENTAL VERTICAL LOAD FACTOR DURING TAXI OPERATIONS

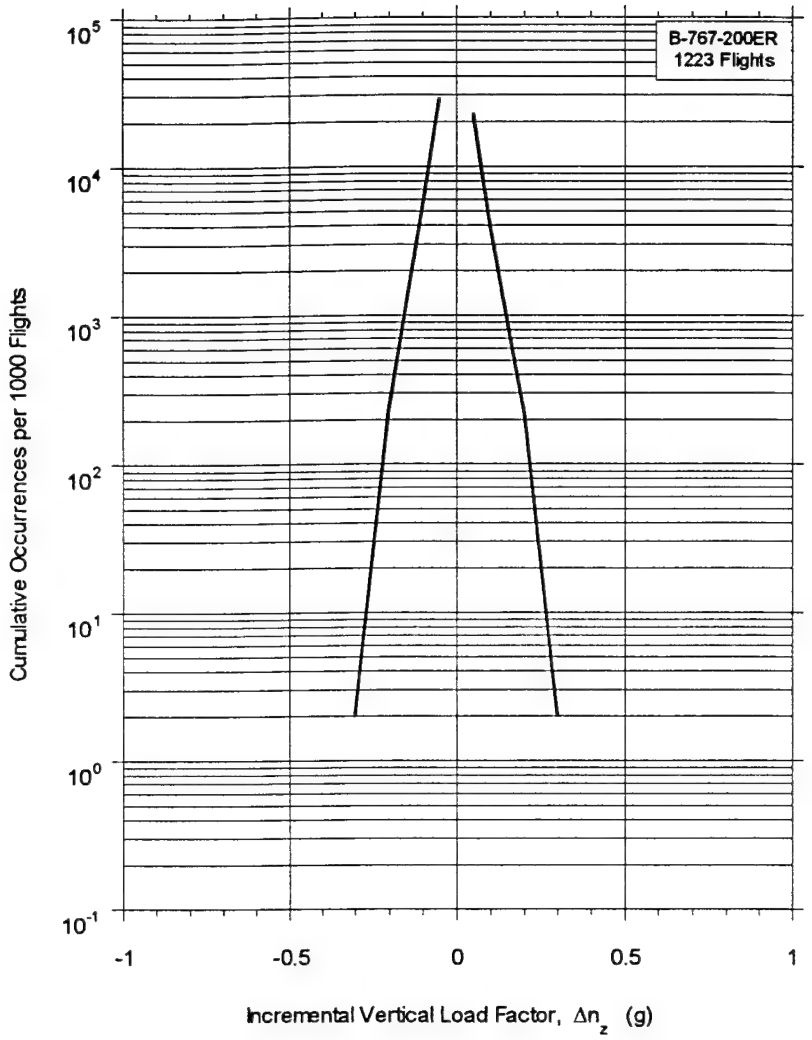

FIGURE A-19. CUMULATIVE FREQUENCY OF INCREMENTAL VERTICAL LOAD FACTOR DURING TAKEOFF ROLL

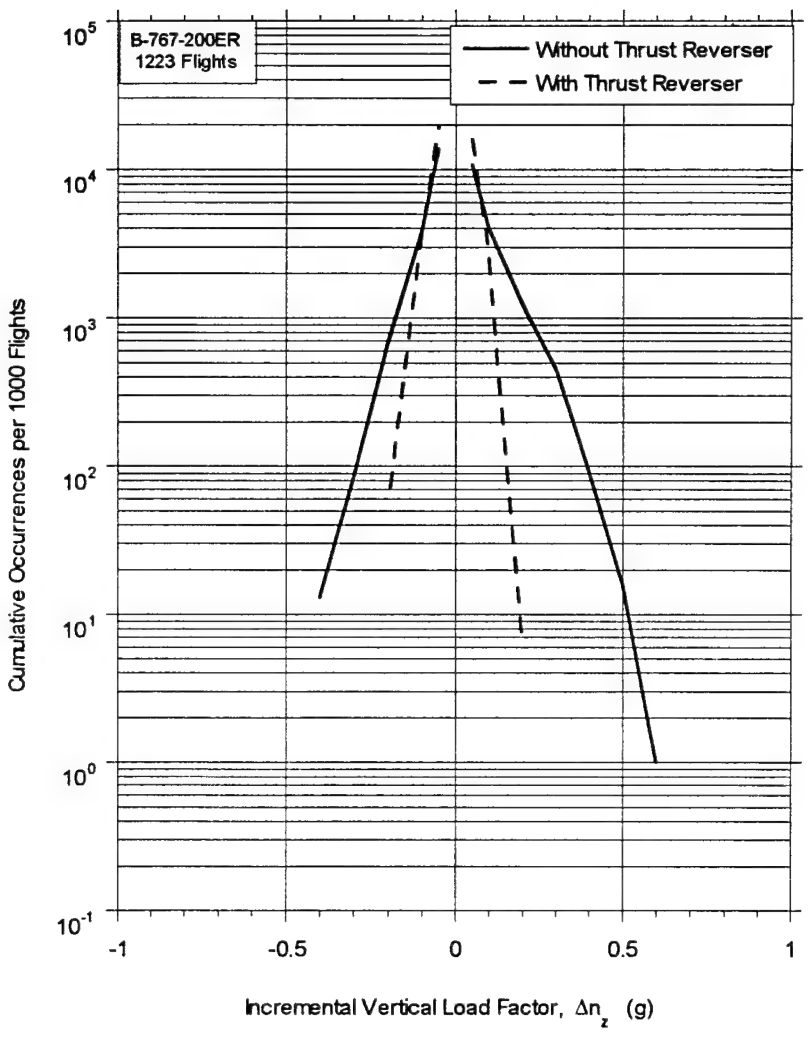

FIGURE A-20. CUMULATIVE FREQUENCY OF INCREMENTAL VERTICAL LOAD FACTOR DURING LANDING ROLL

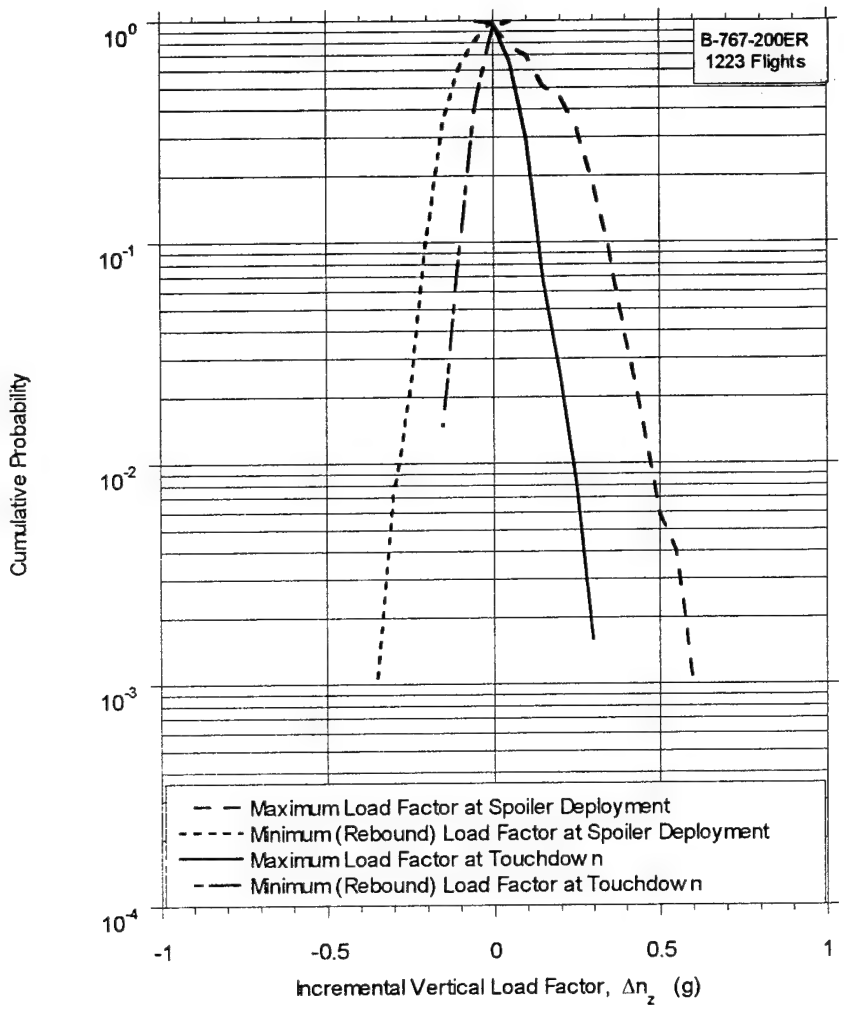

FIGURE A-21. CUMULATIVE PROBABILITY OF MINIMUM AND MAXIMUM INCREMENTAL VERTICAL LOAD FACTOR AT TOUCHDOWN AND SPOILER DEPLOYMENT

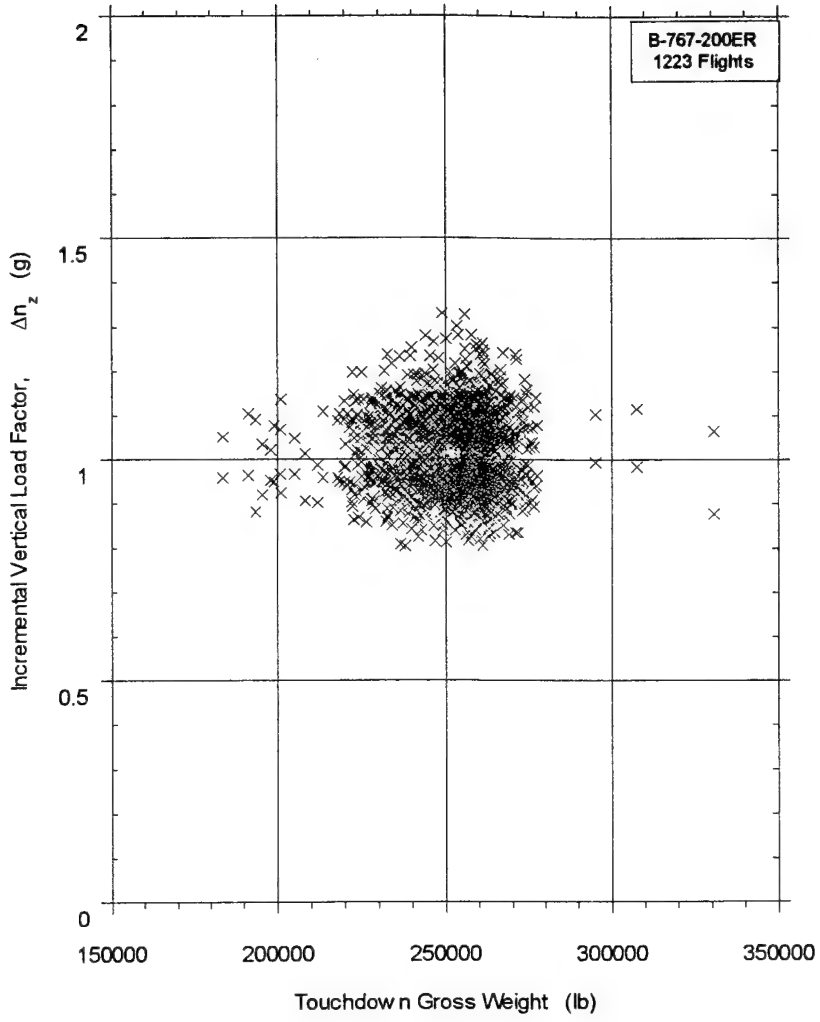

FIGURE A-22. COINCIDENT VERTICAL LOAD FACTOR AND TOUCHDOWN GROSS WEIGHT

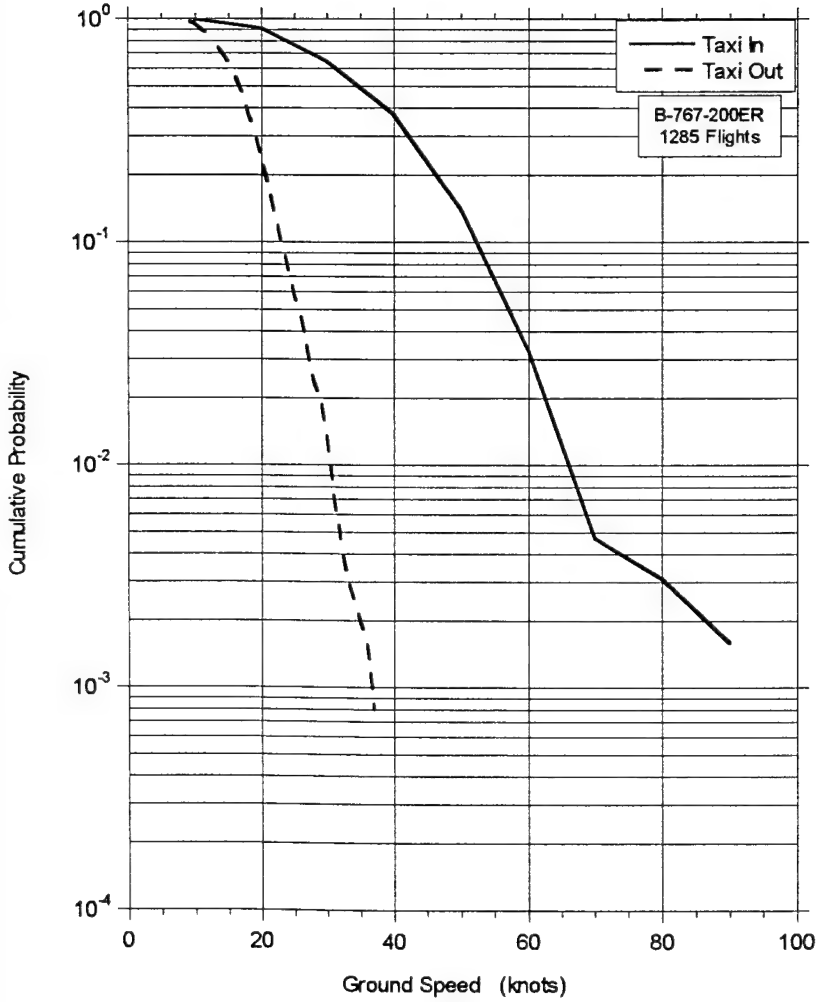

FIGURE A-23. CUMULATIVE PROBABILITY OF GROUND SPEED DURING TAXI

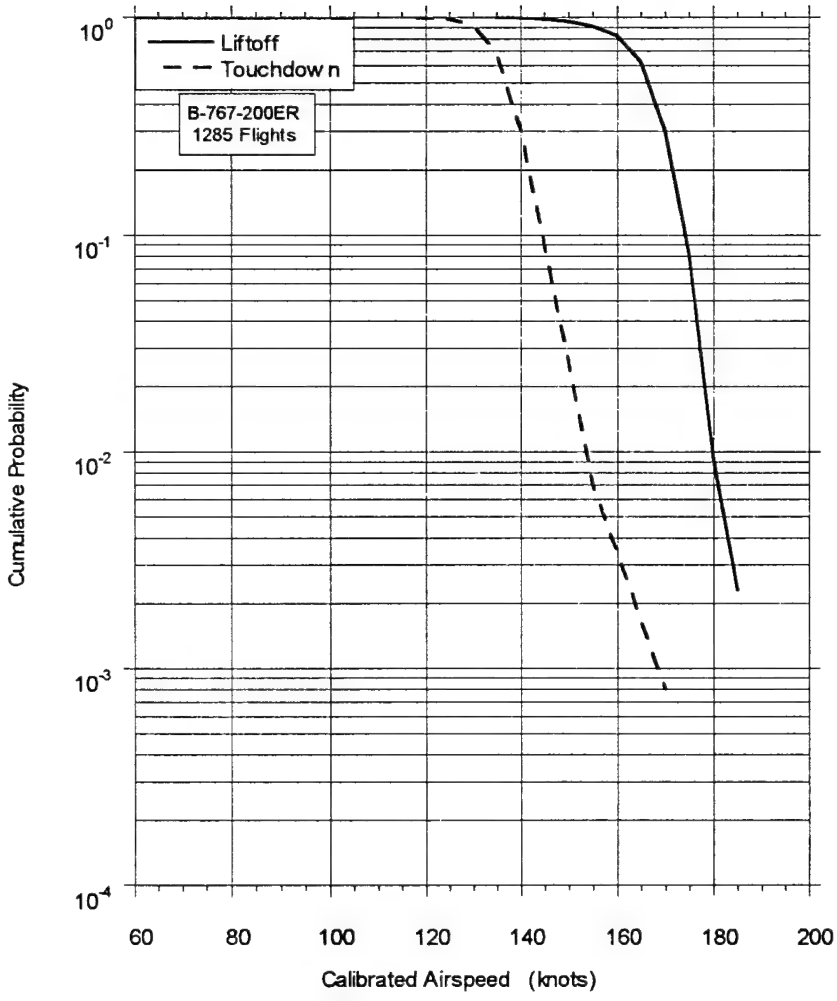

FIGURE A-24. CUMULATIVE PROBABILITY OF AIRSPEED AT LIFTOFF AND TOUCHDOWN

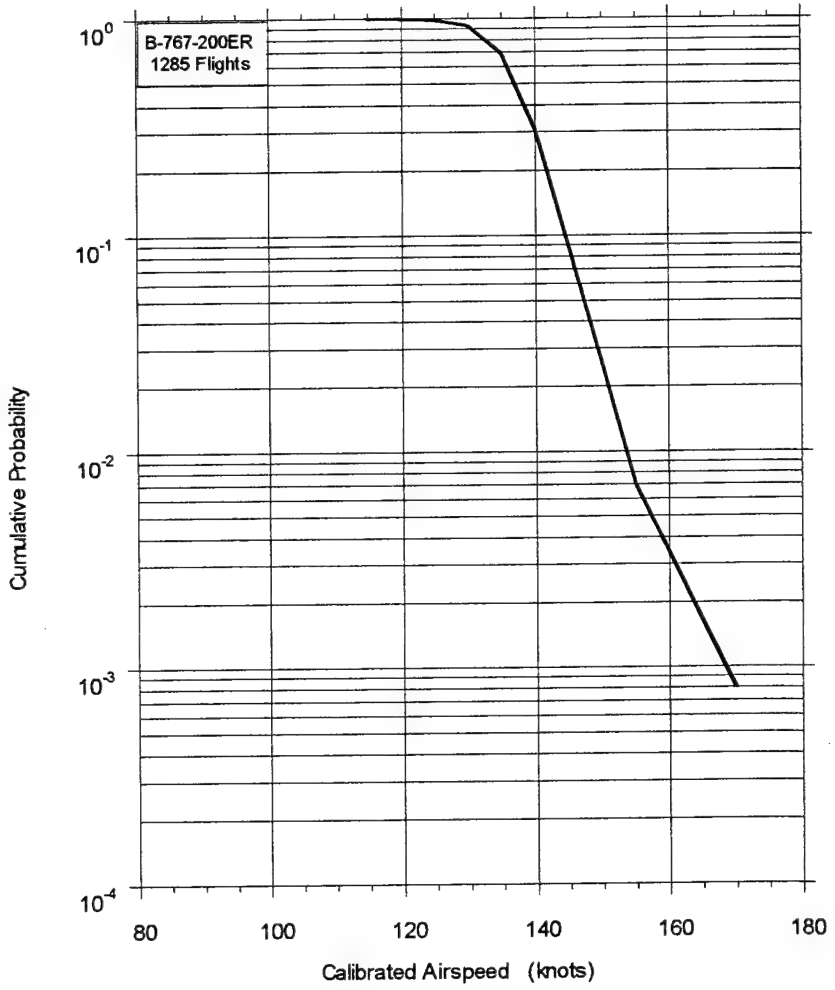

FIGURE A-25. CUMULATIVE PROBABILITY OF AIRSPEED AT FLARE

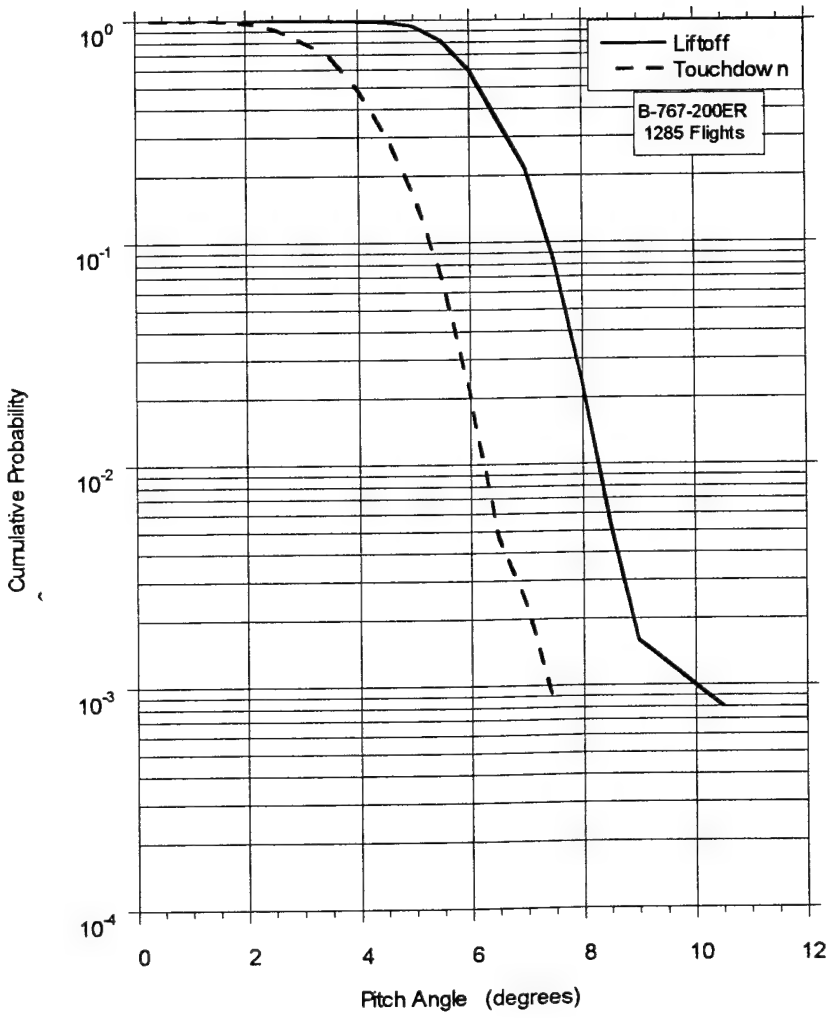

FIGURE A-26. CUMULATIVE PROBABILITY OF PITCH ANGLE AT LIFTOFF AND TOUCHDOWN

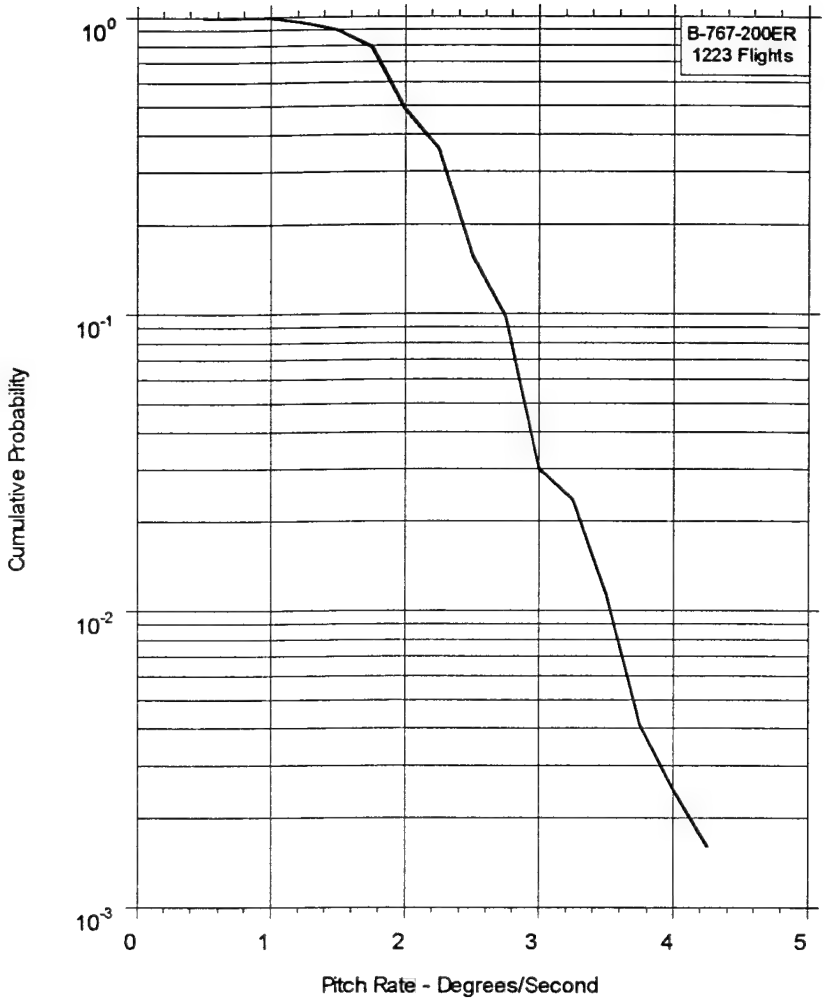

FIGURE A-27. CUMULATIVE PROBABILITY OF MAXIMUM PITCH RATE AT TAKEOFF ROTATION

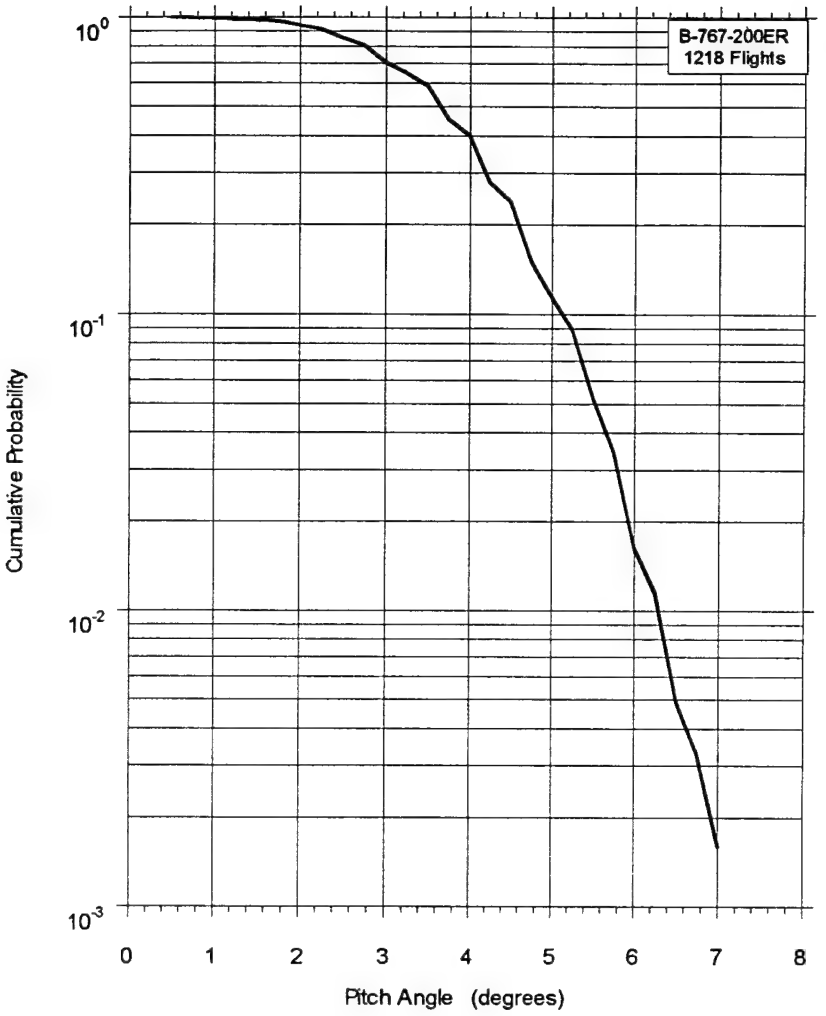

FIGURE A-28. CUMULATIVE PROBABILITY OF PITCH ANGLE AT TOUCHDOWN PEAK VERTICAL LOAD FACTOR

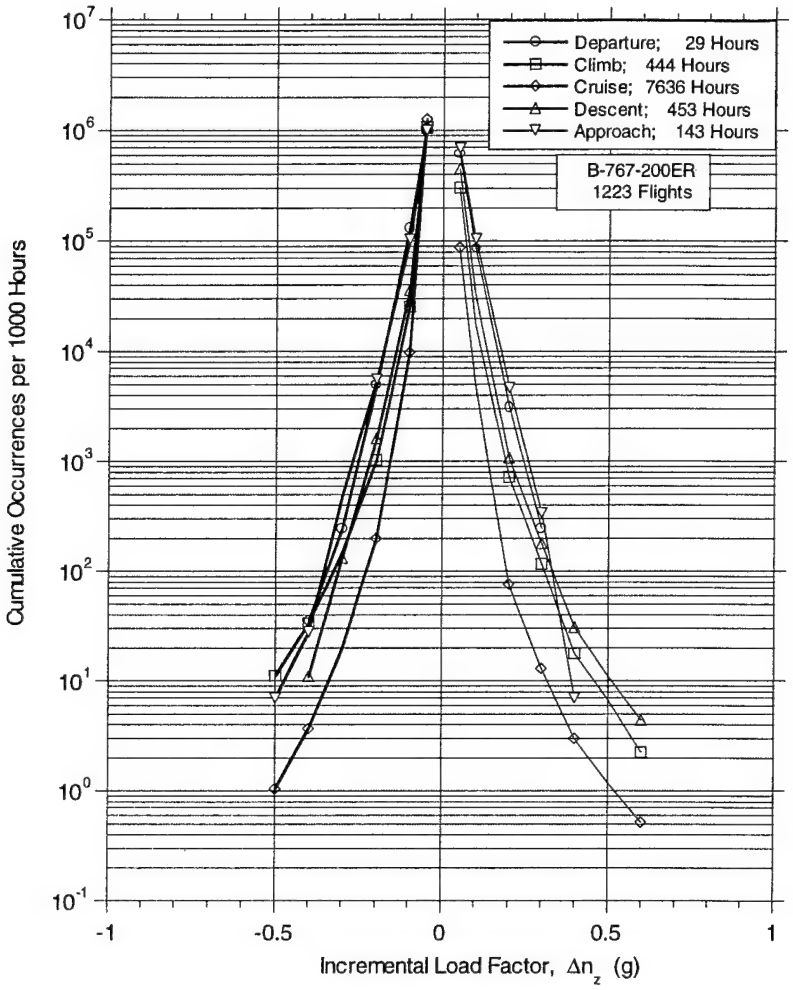

FIGURE A-29. CUMULATIVE OCCURRENCES OF INCREMENTAL VERTICAL GUST LOAD FACTOR PER 1000 HOURS BY FLIGHT PHASE

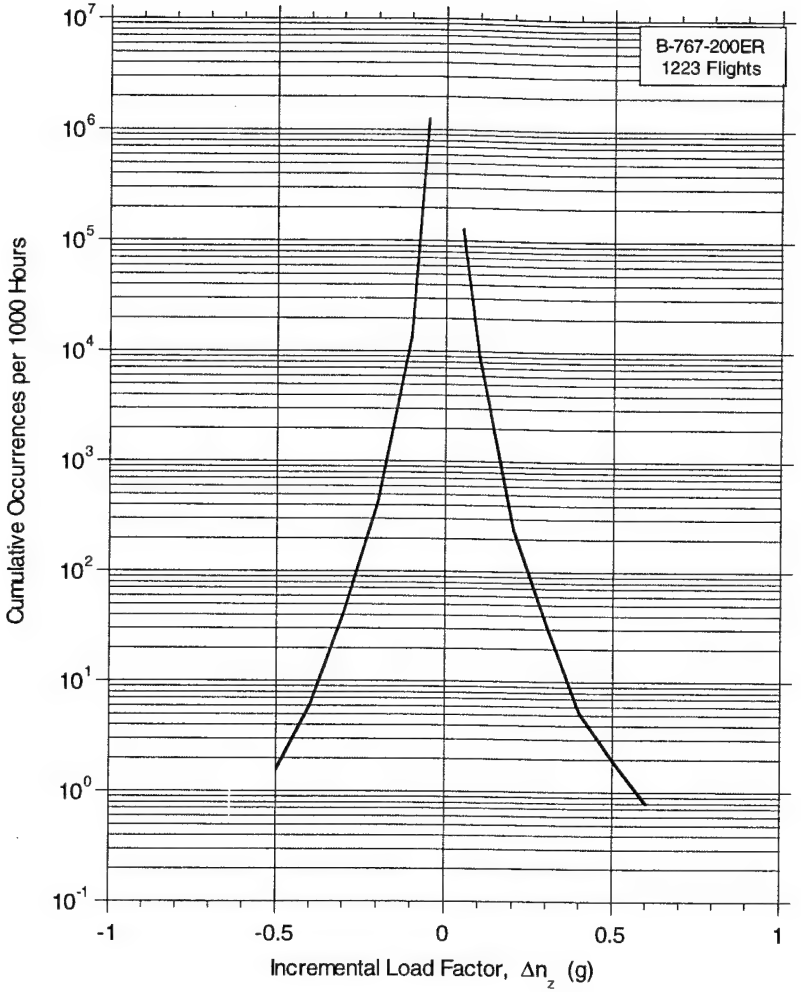

FIGURE A-30. CUMULATIVE OCCURRENCES OF INCREMENTAL VERTICAL GUST LOAD FACTOR PER 1000 HOURS, COMBINED FLIGHT PHASES

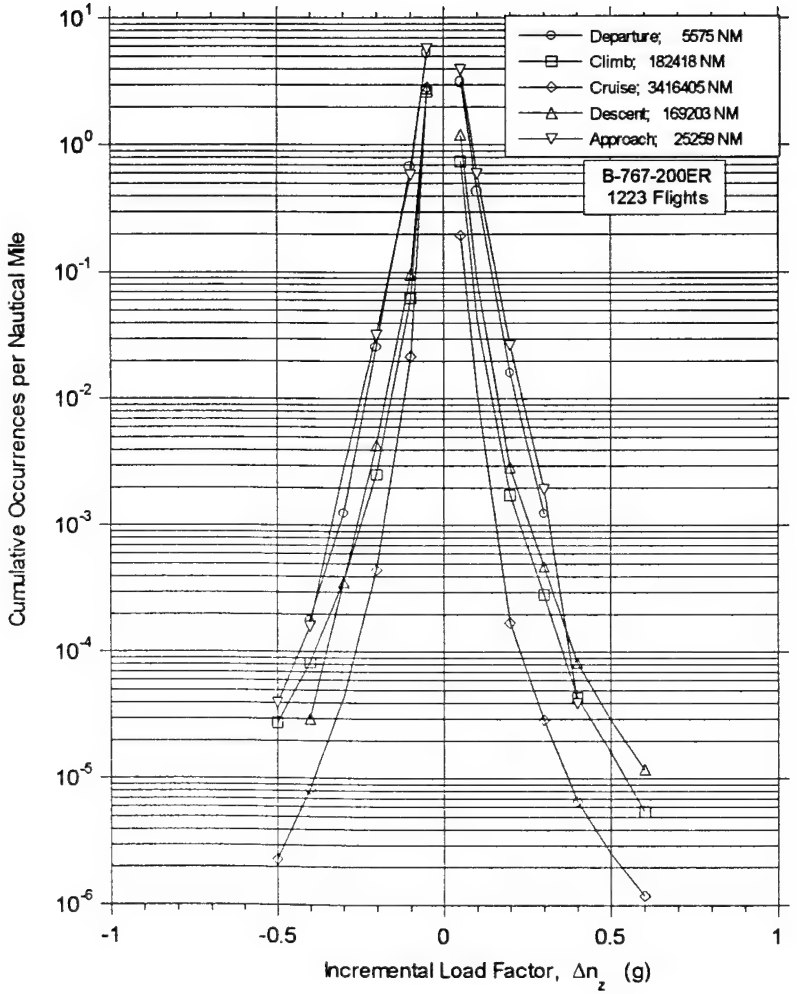

FIGURE A-31. CUMULATIVE OCCURRENCES OF INCREMENTAL VERTICAL GUST LOAD FACTOR PER NAUTICAL MILE BY FLIGHT PHASE

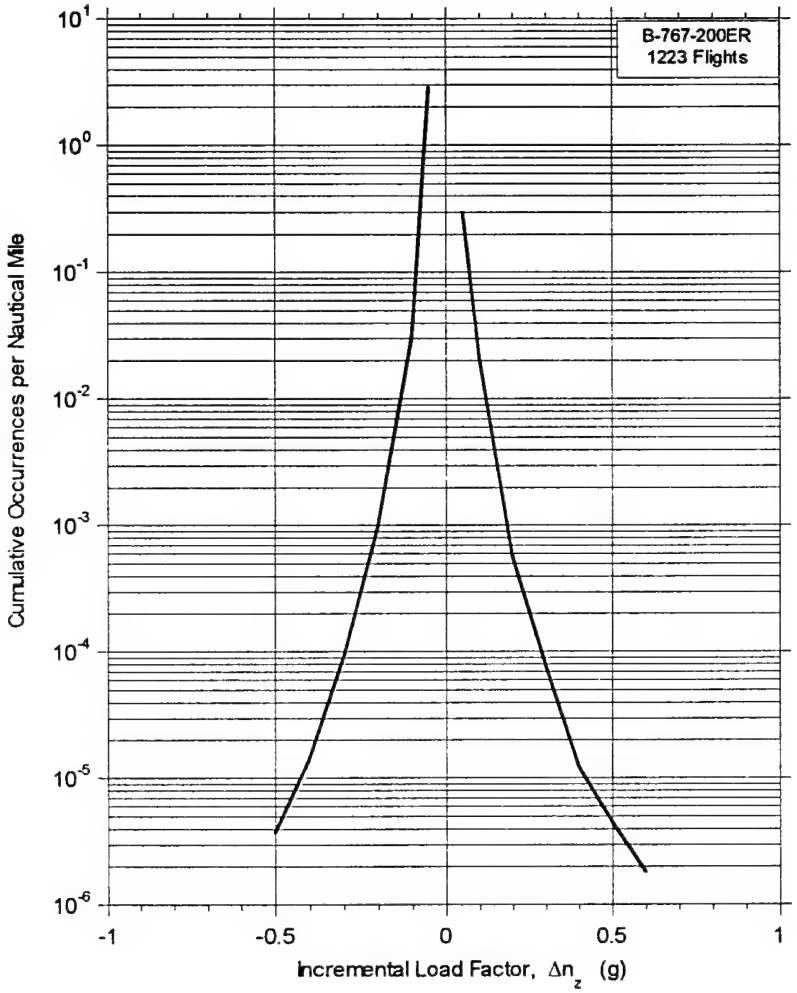

FIGURE A-32. CUMULATIVE OCCURRENCES OF INCREMENTAL VERTICAL GUST LOAD FACTOR PER NAUTICAL MILE, COMBINED FLIGHT PHASES

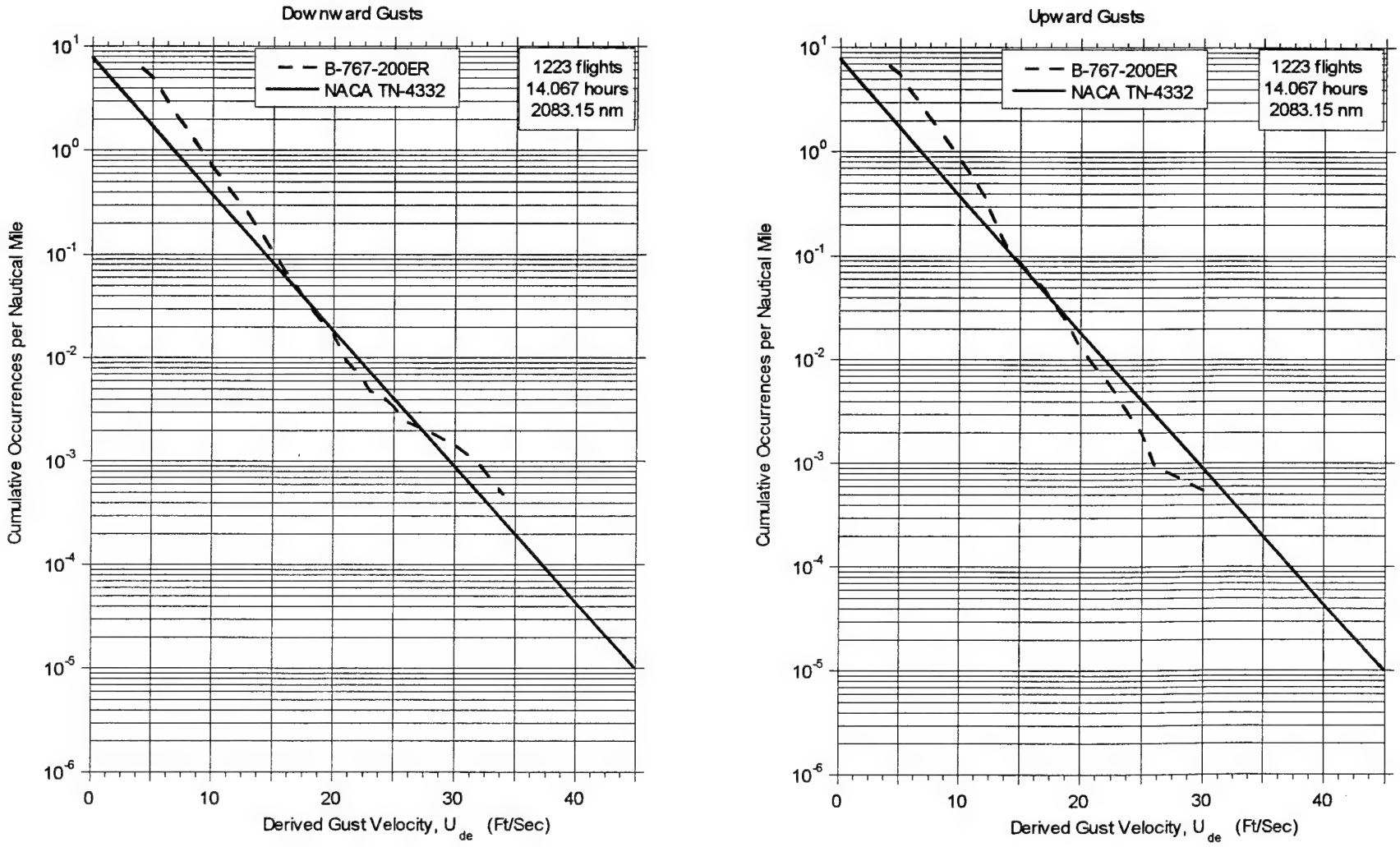

FIGURE A-33. CUMULATIVE OCCURRENCES OF DERIVED GUST VELOCITY PER NAUTICAL MILE, < 500 FEET

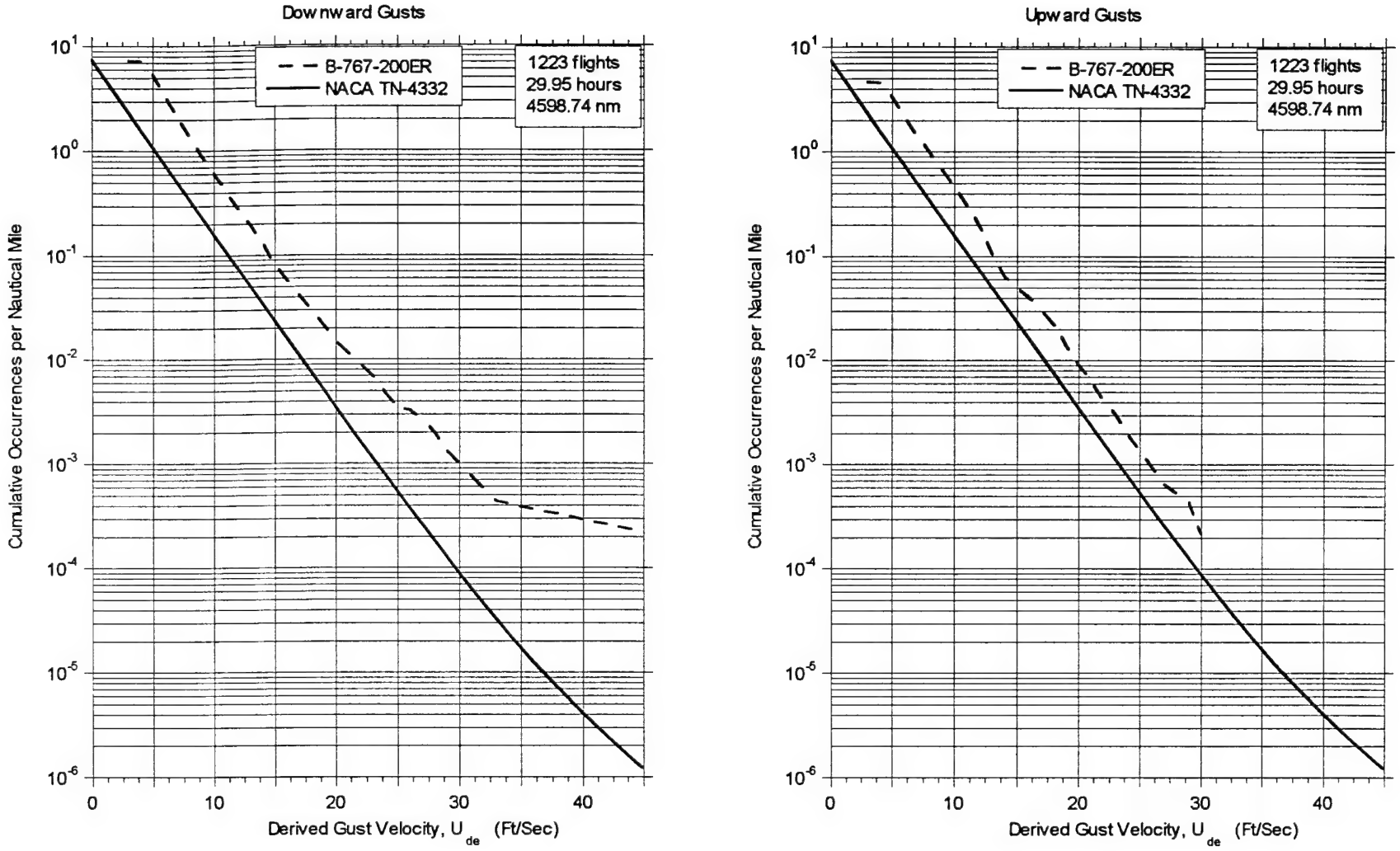

FIGURE A-34. CUMULATIVE OCCURRENCES OF DERIVED GUST VELOCITY PER NAUTICAL MILE, 500-1,500 FEET

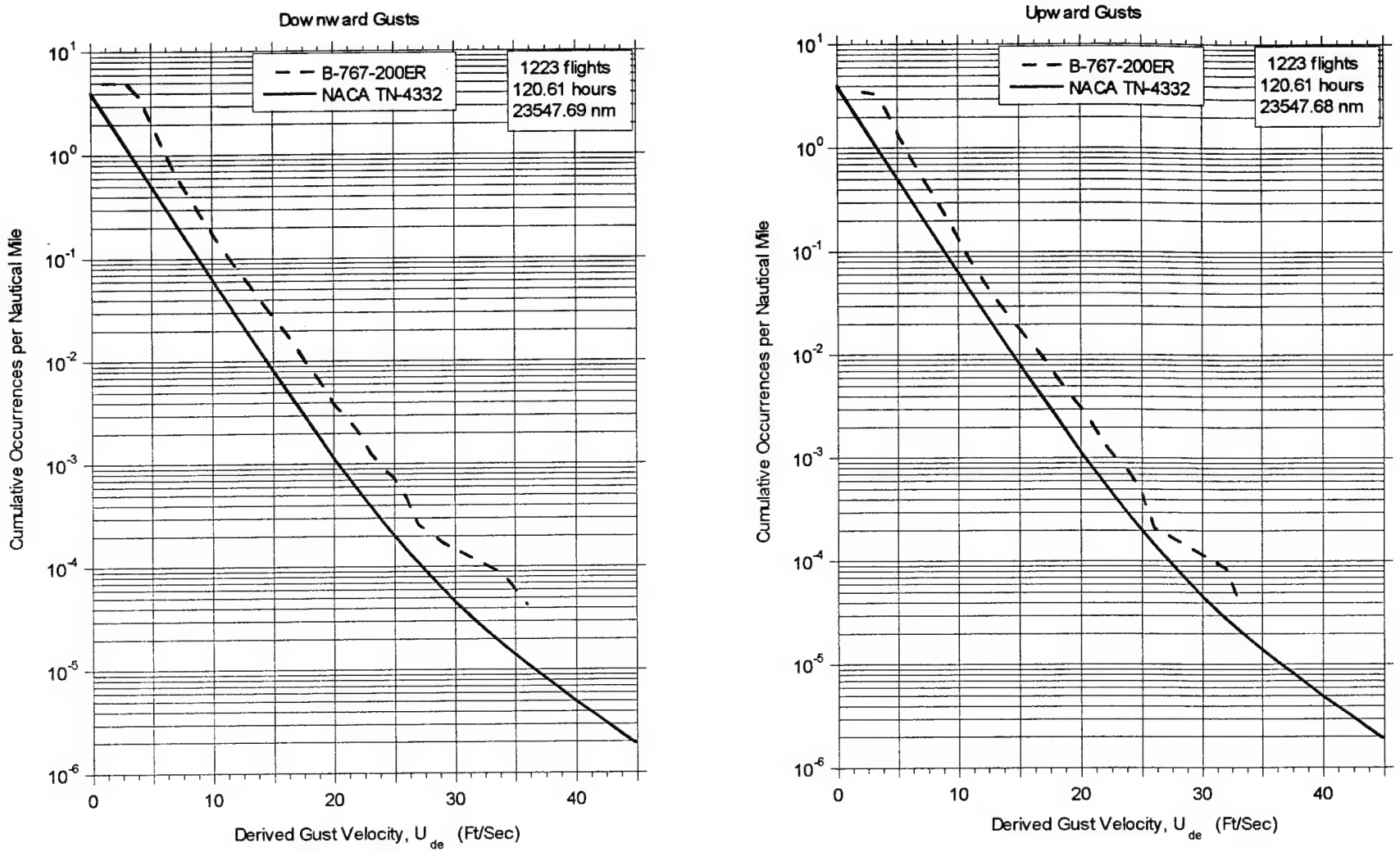

FIGURE A-35. CUMULATIVE OCCURRENCES OF DERIVED GUST VELOCITY PER NAUTICAL MILE, 1,500-4,500 FEET

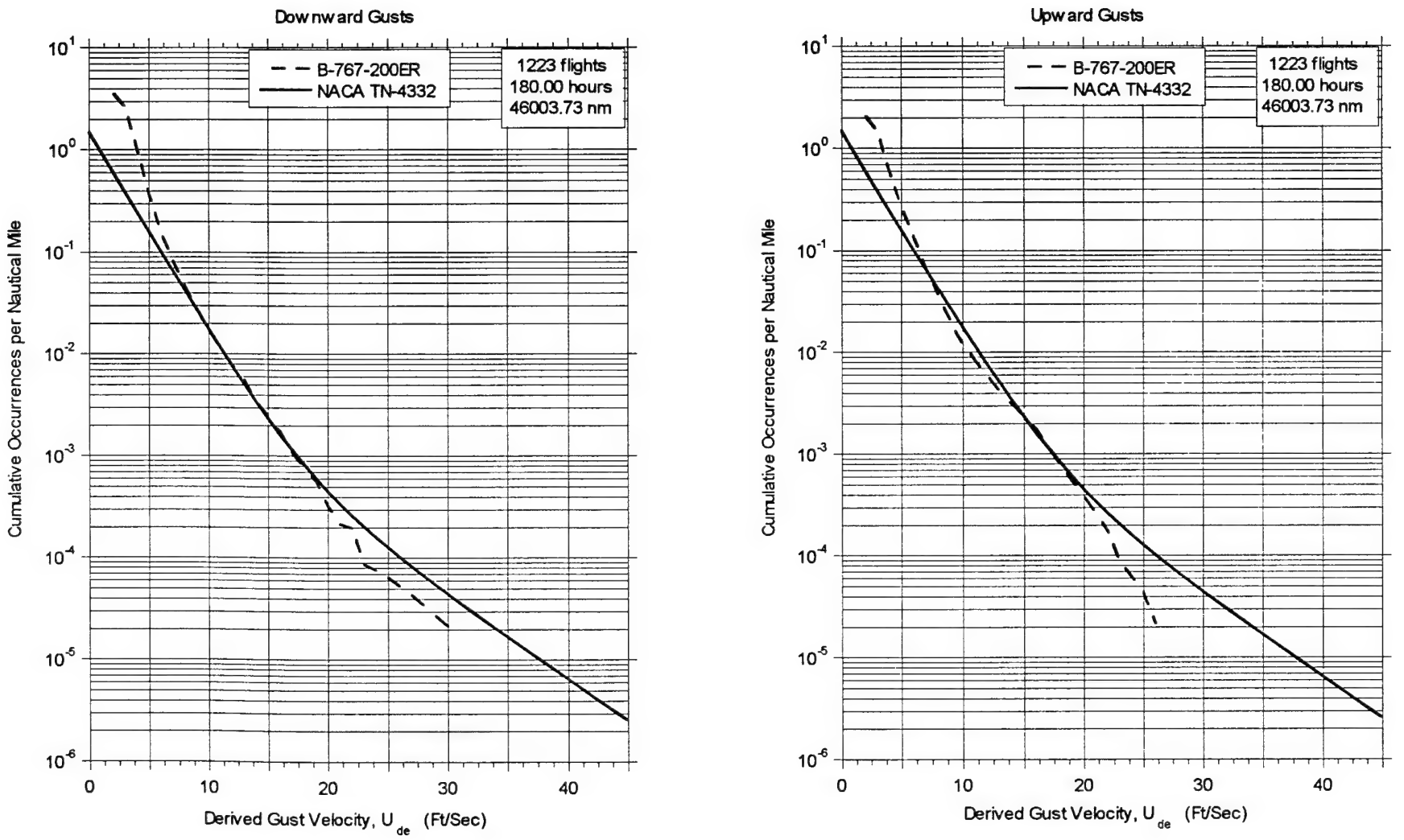

FIGURE A-36. CUMULATIVE OCCURRENCES OF DERIVED GUST VELOCITY PER NAUTICAL MILE, 4,500-9,500 FEET

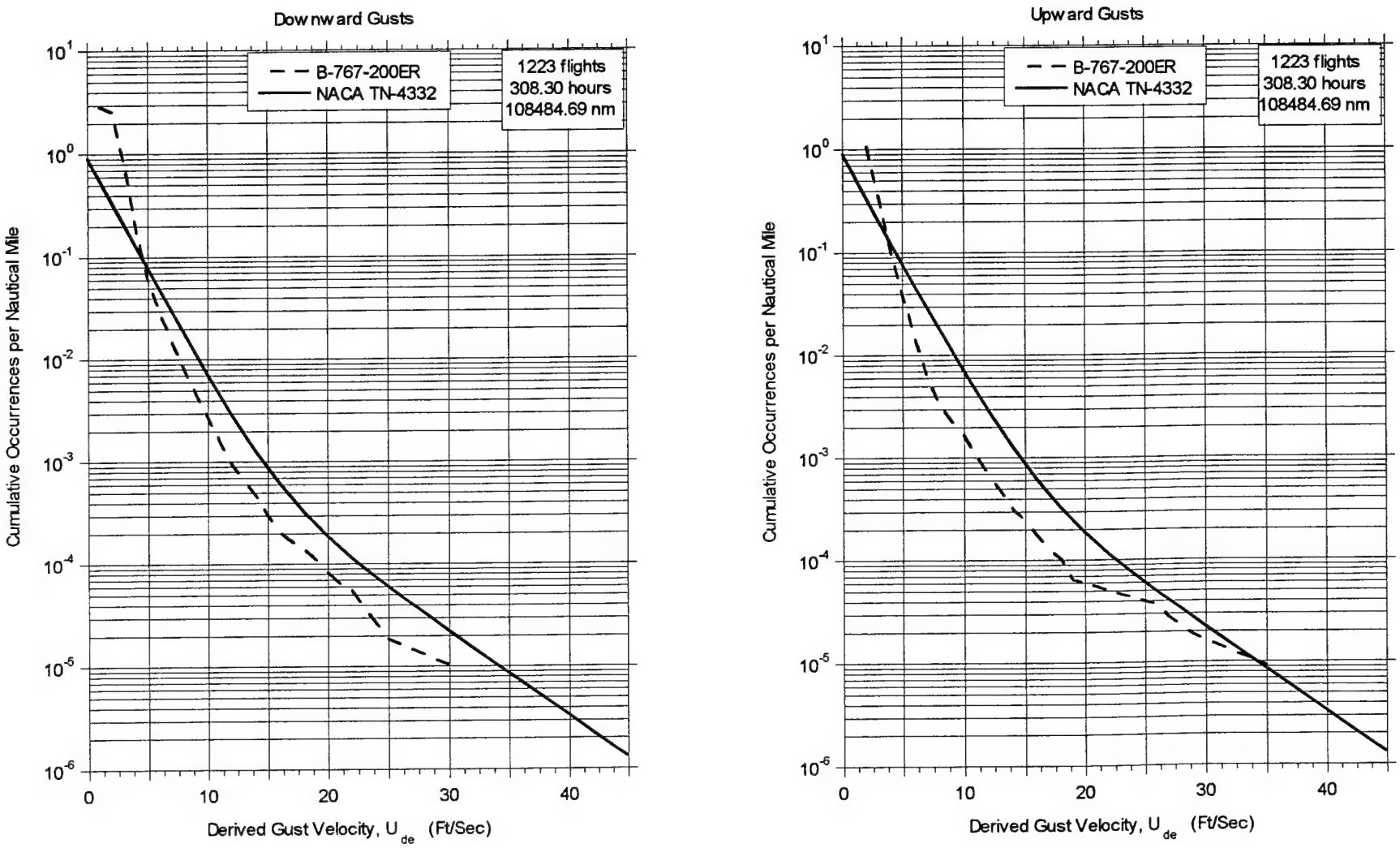

FIGURE A-37. CUMULATIVE OCCURRENCES OF DERIVED GUST VELOCITY PER NAUTICAL MILE, 9,500-19,500 FEET

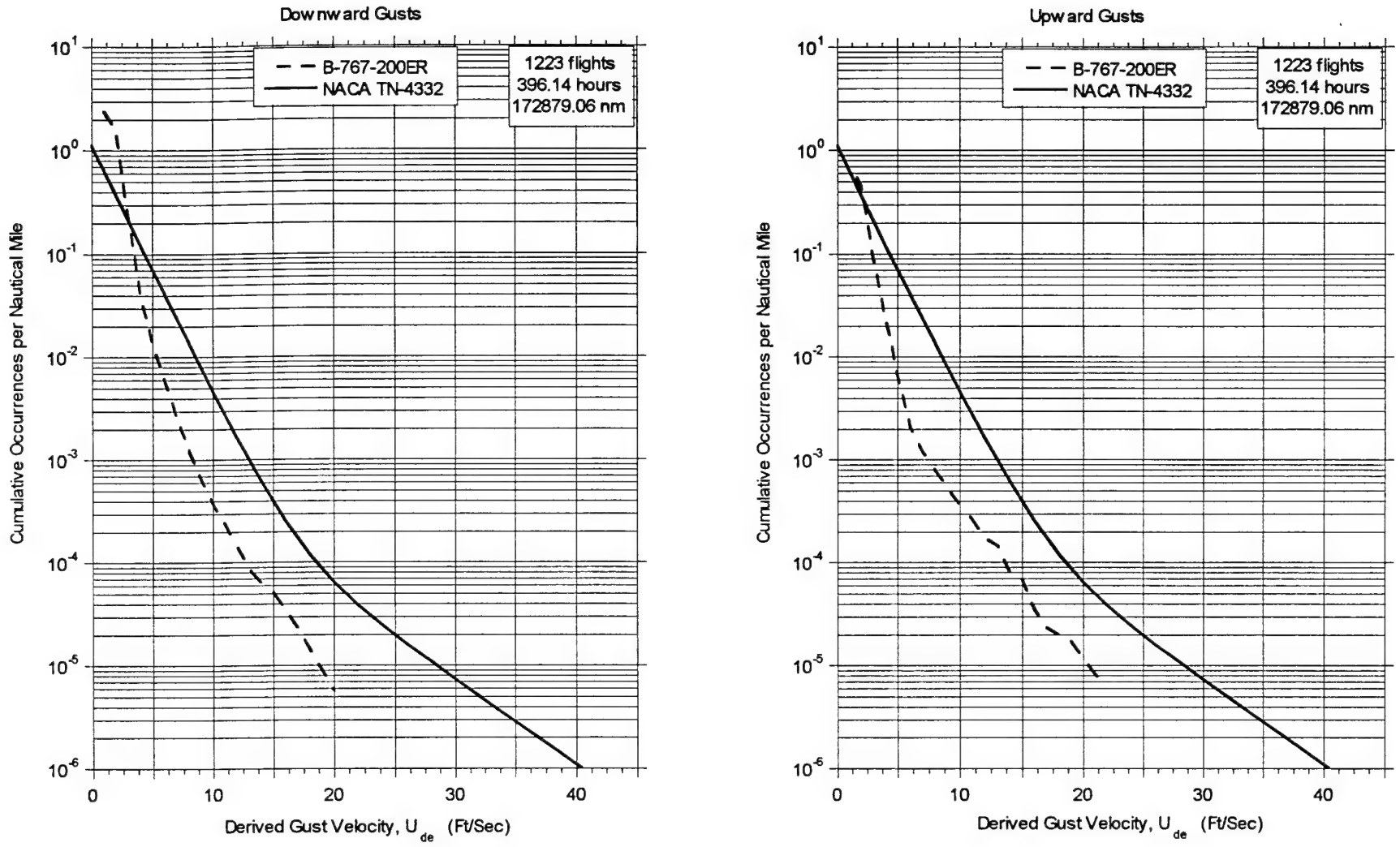

FIGURE A-38. CUMULATIVE OCCURRENCES OF DERIVED GUST VELOCITY PER NAUTICAL MILE, 19,500-29,500 FEET

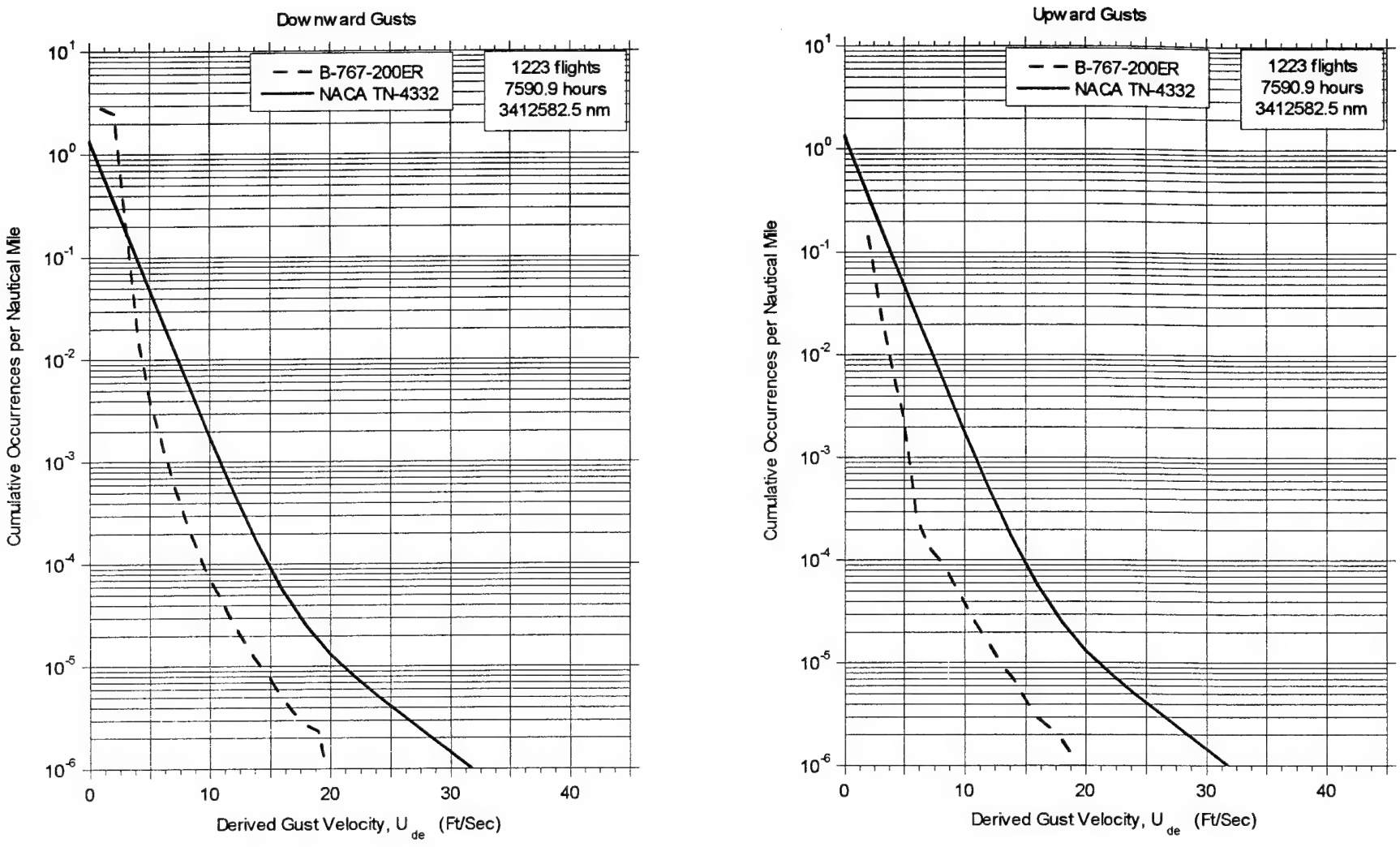

FIGURE A-39. CUMULATIVE OCCURRENCES OF DERIVED GUST VELOCITY PER NAUTICAL MILE, 29,500-39,500 FEET

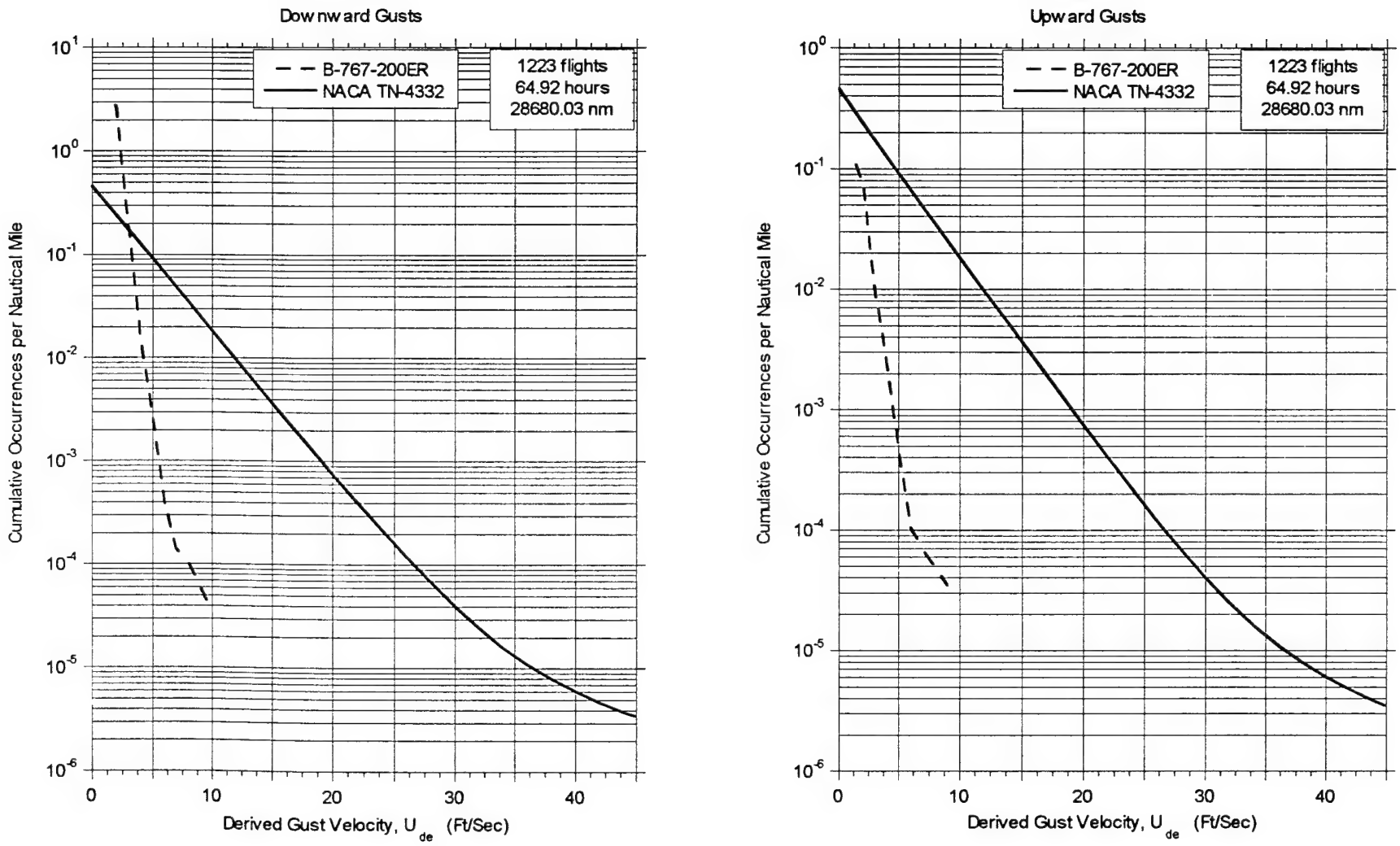

FIGURE A-40. CUMULATIVE OCCURRENCES OF DERIVED GUST VELOCITY PER NAUTICAL MILE, 39,500-49,500 FEET

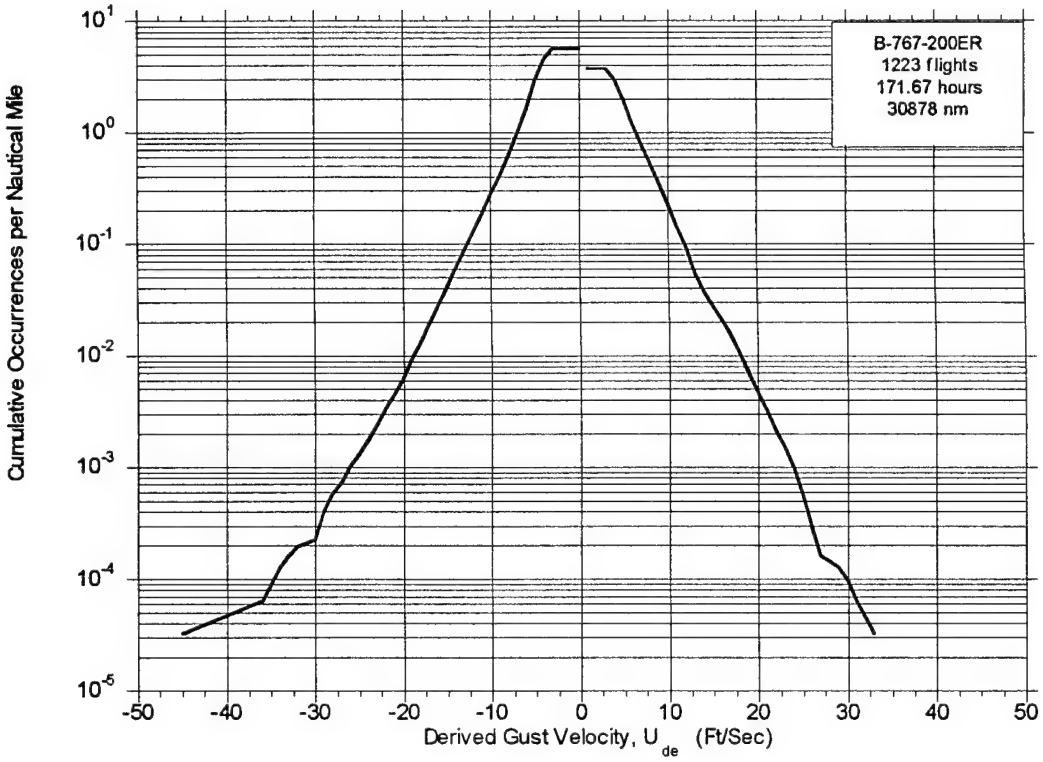

FIGURE A-41. CUMULATIVE OCCURRENCES OF DERIVED GUST VELOCITY PER NAUTICAL MILE, FLAPS EXTENDED

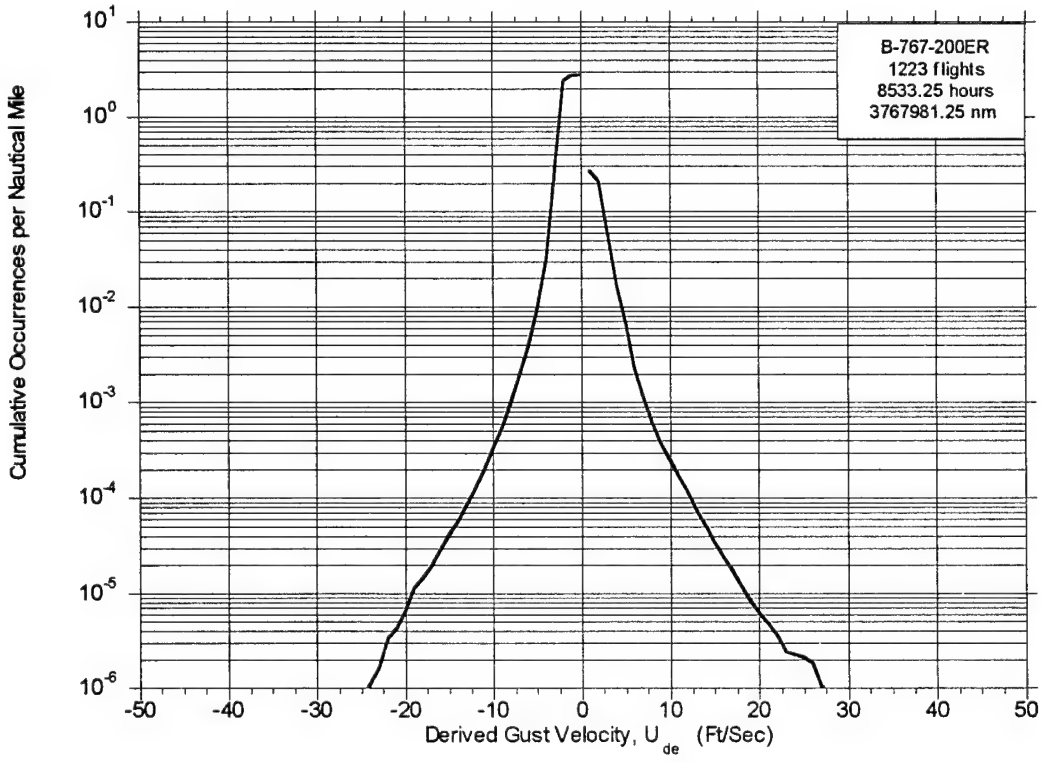

FIGURE A-42. CUMULATIVE OCCURRENCES OF DERIVED GUST VELOCITY PER NAUTICAL MILE, FLAPS RETRACTED

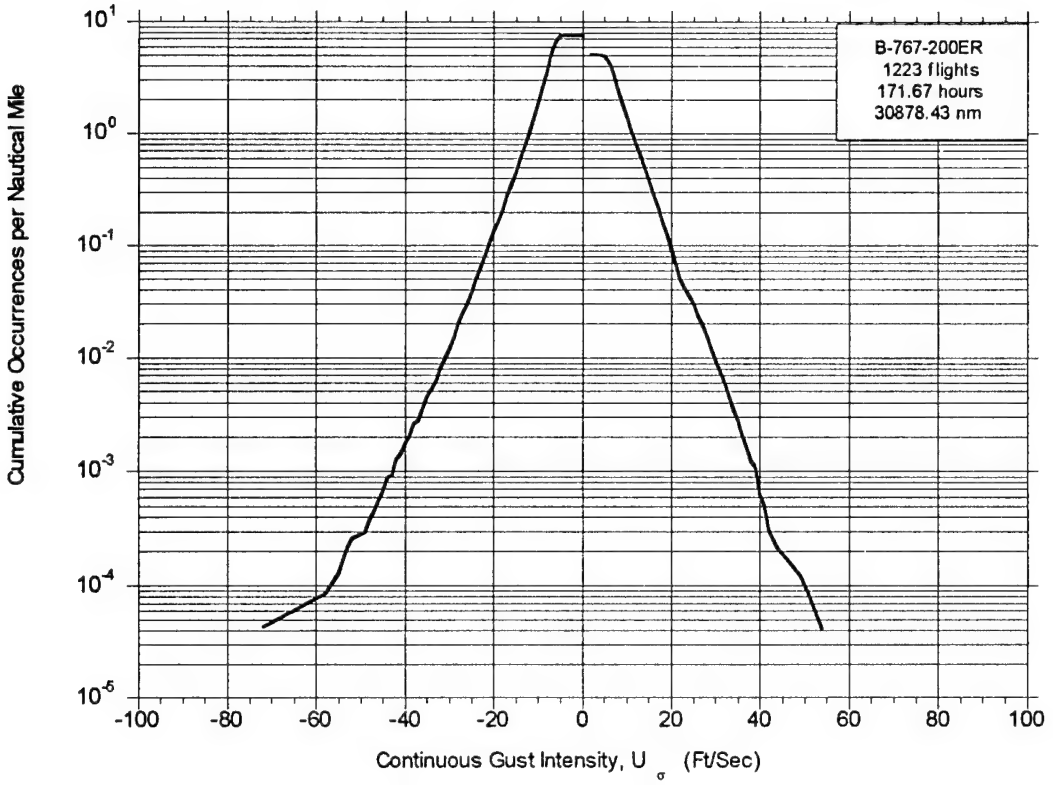

FIGURE A-43. CUMULATIVE OCCURRENCES OF CONTINUOUS GUST INTENSITY PER NAUTICAL MILE, FLAPS EXTENDED

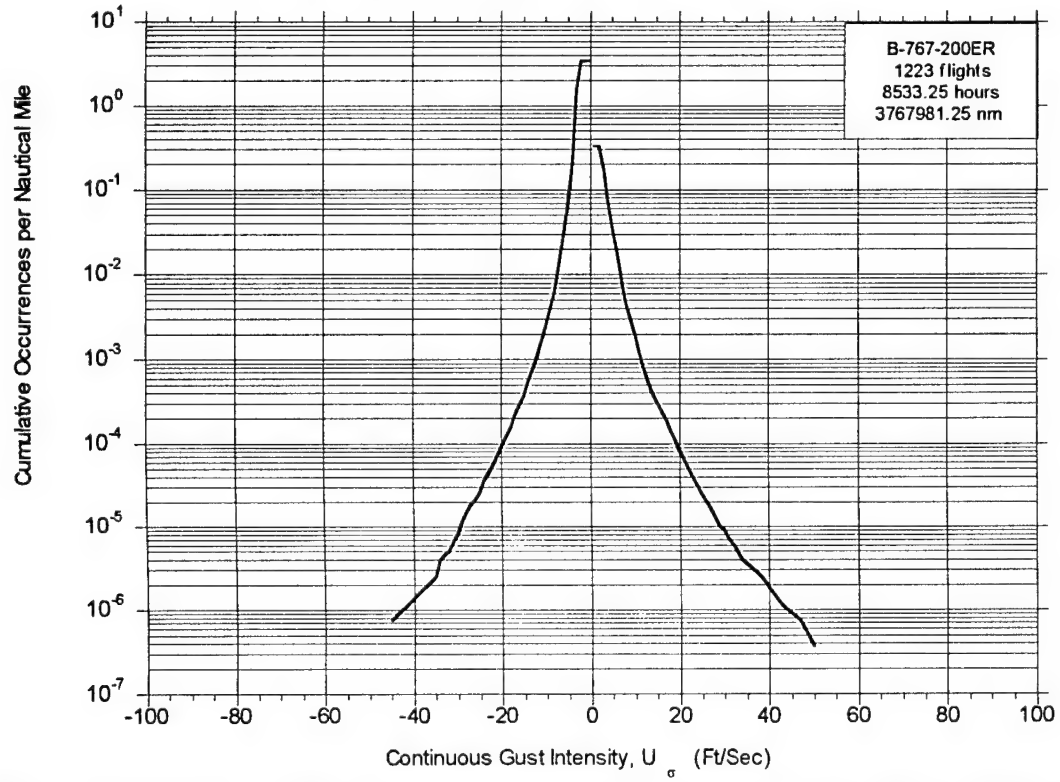

FIGURE A-44. CUMULATIVE OCCURRENCES OF CONTINUOUS GUST INTENSITY PER NAUTICAL MILE, FLAPS RETRACTED

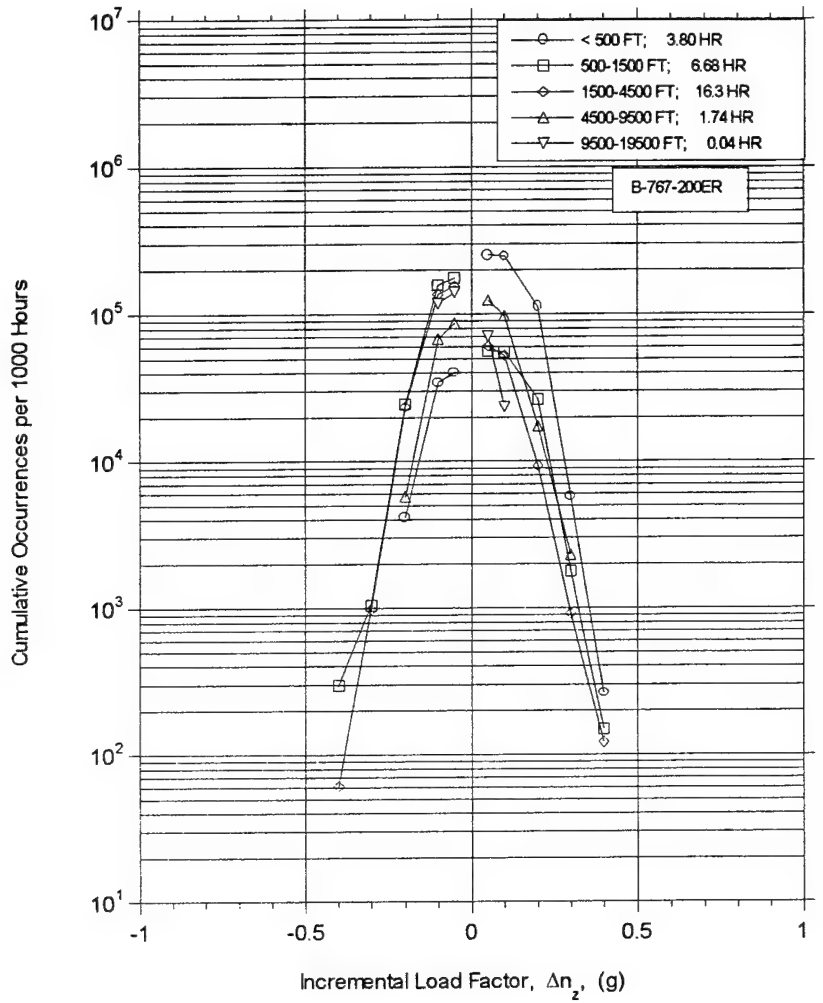

FIGURE A-45. CUMULATIVE OCCURRENCES OF INCREMENTAL MANEUVER LOAD FACTOR PER 1000 HOURS DURING DEPARTURE BY ALTITUDE

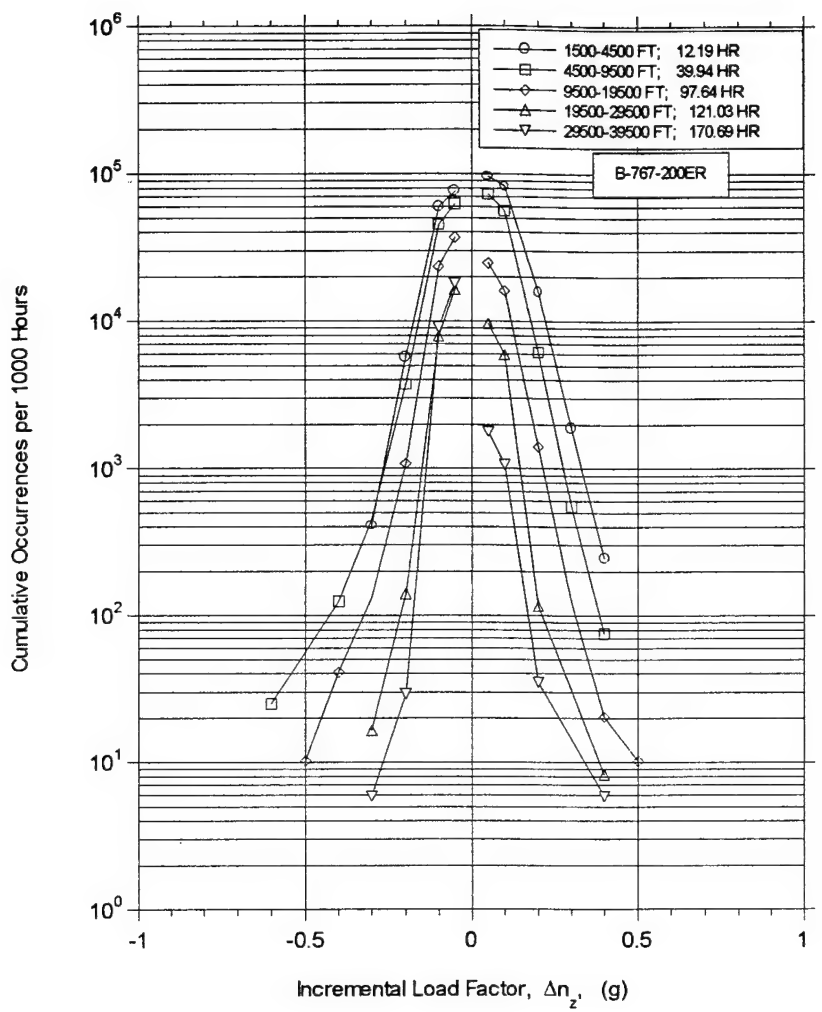

FIGURE A-46. CUMULATIVE OCCURRENCES OF INCREMENTAL MANEUVER LOAD FACTOR PER 1000 HOURS DURING CLIMB BY ALTITUDE

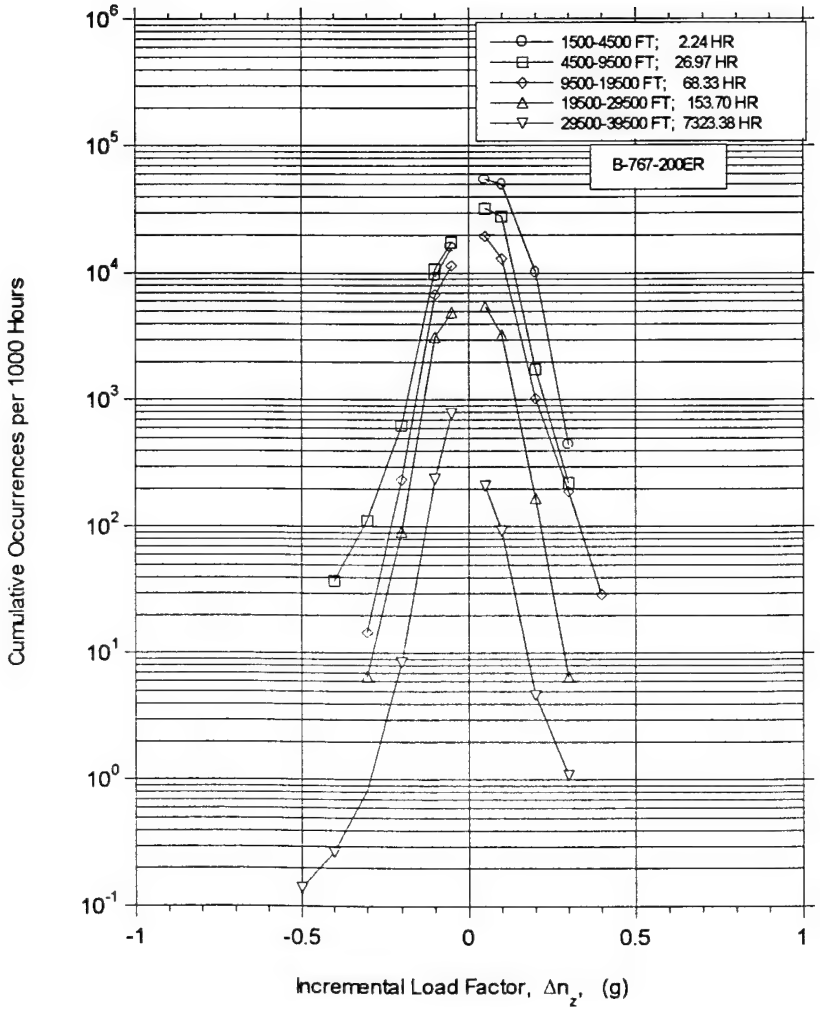

FIGURE A-47. CUMULATIVE OCCURRENCES OF INCREMENTAL MANEUVER LOAD FACTOR PER 1000 HOURS DURING CRUISE BY ALTITUDE

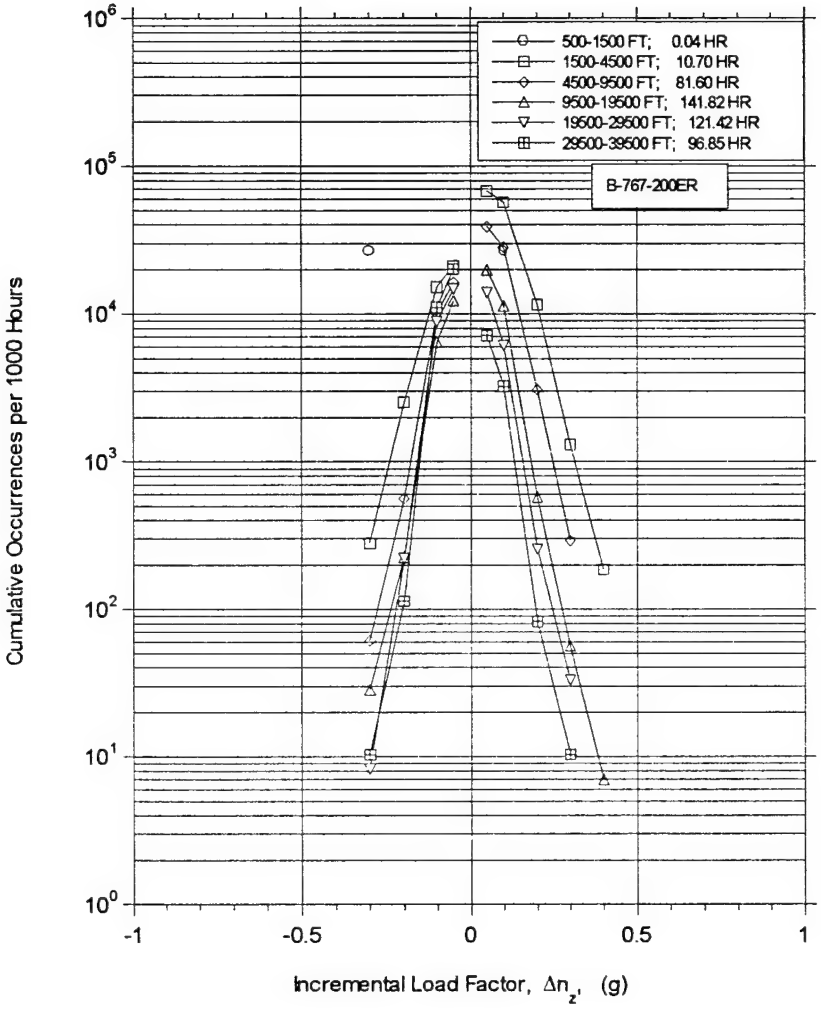

FIGURE A-48. CUMULATIVE OCCURRENCES OF INCREMENTAL MANEUVER LOAD FACTOR PER 1000 HOURS DURING DESCENT BY ALTITUDE

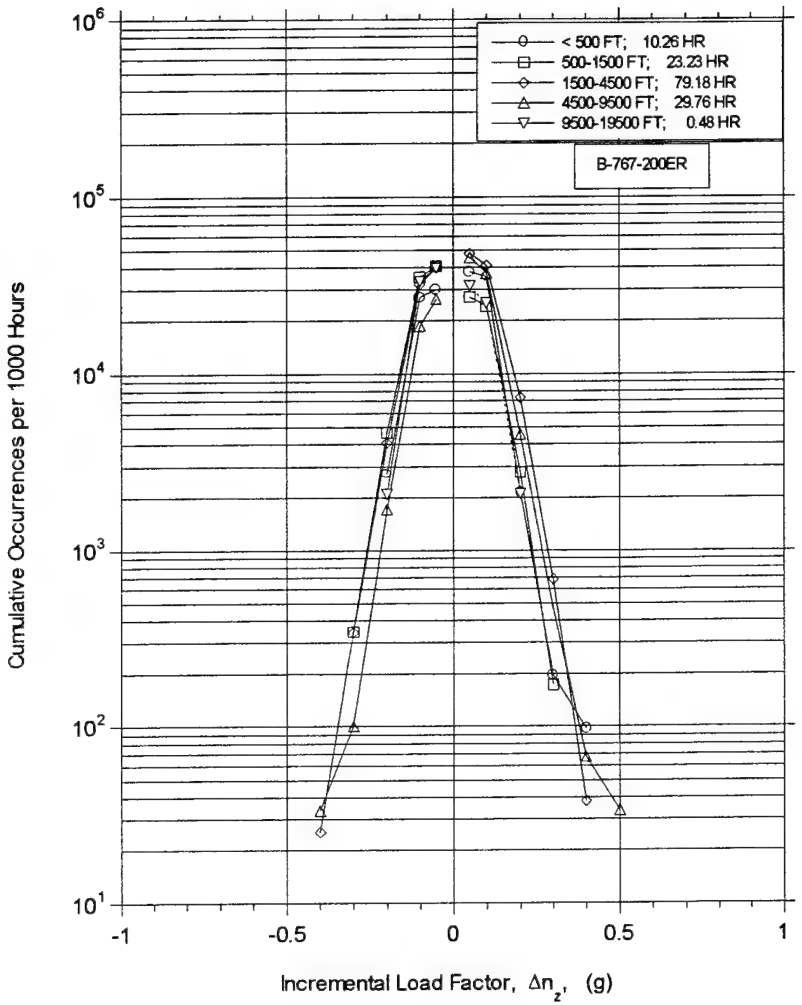

FIGURE A-49. CUMULATIVE OCCURRENCES OF INCREMENTAL MANEUVER LOAD FACTOR PER 1000 HOURS DURING APPROACH BY ALTITUDE

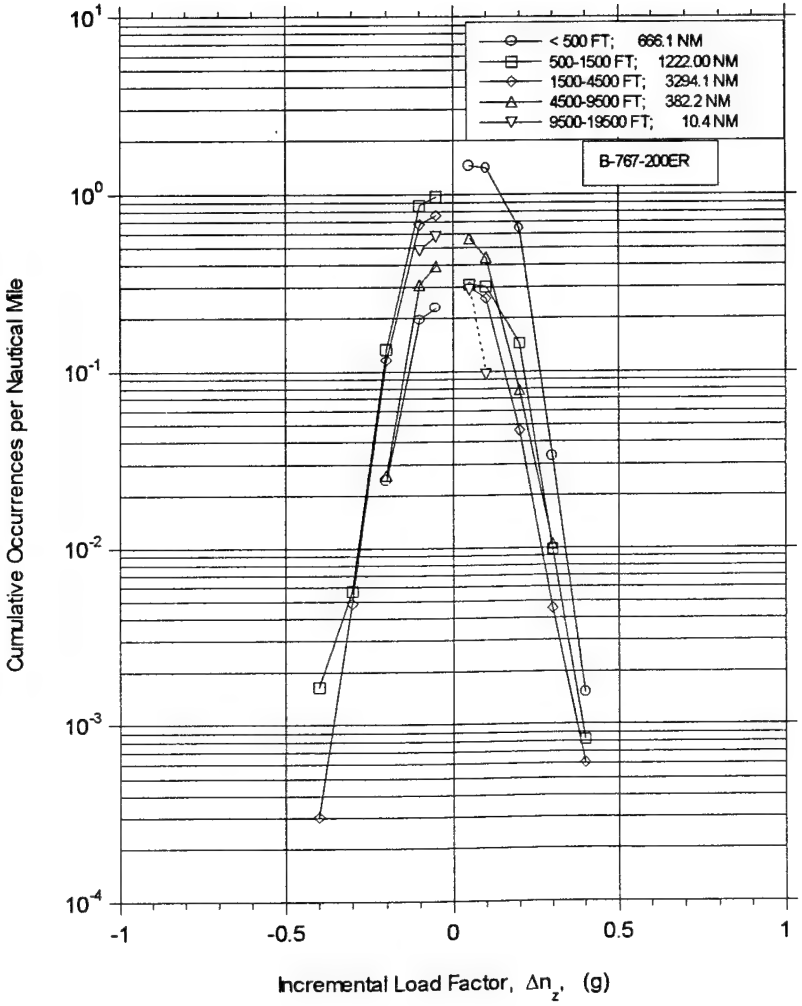

FIGURE A-50. CUMULATIVE OCCURRENCES OF INCREMENTAL MANEUVER LOAD FACTOR PER NAUTICAL MILE DURING DEPARTURE BY ALTITUDE

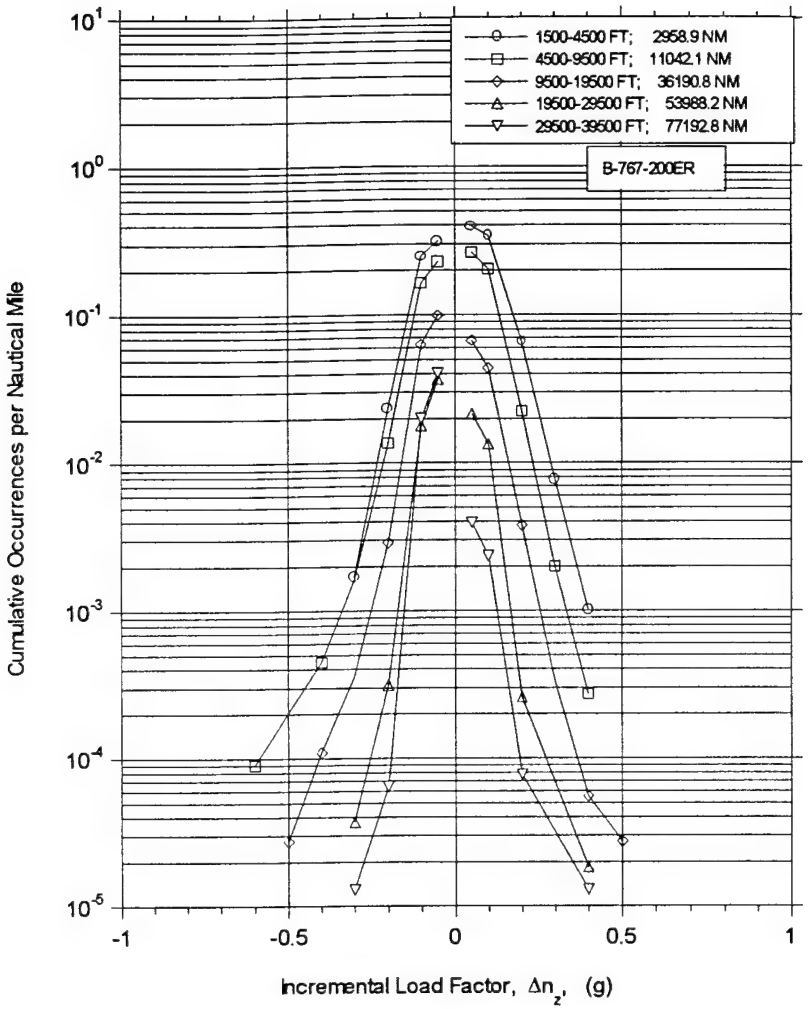

FIGURE A-51. CUMULATIVE OCCURRENCES OF INCREMENTAL MANEUVER LOAD FACTOR PER NAUTICAL MILE DURING CLIMB BY ALTITUDE

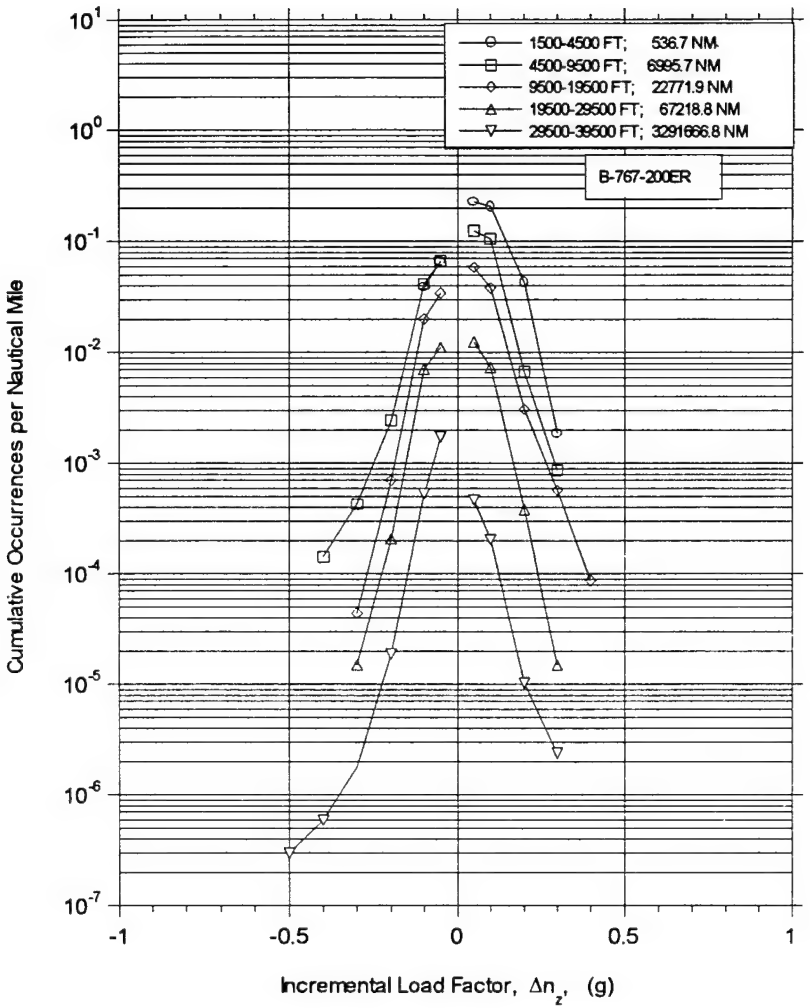

FIGURE A-52. CUMULATIVE OCCURRENCES OF INCREMENTAL MANEUVER LOAD FACTOR PER NAUTICAL MILE DURING CRUISE BY ALTITUDE

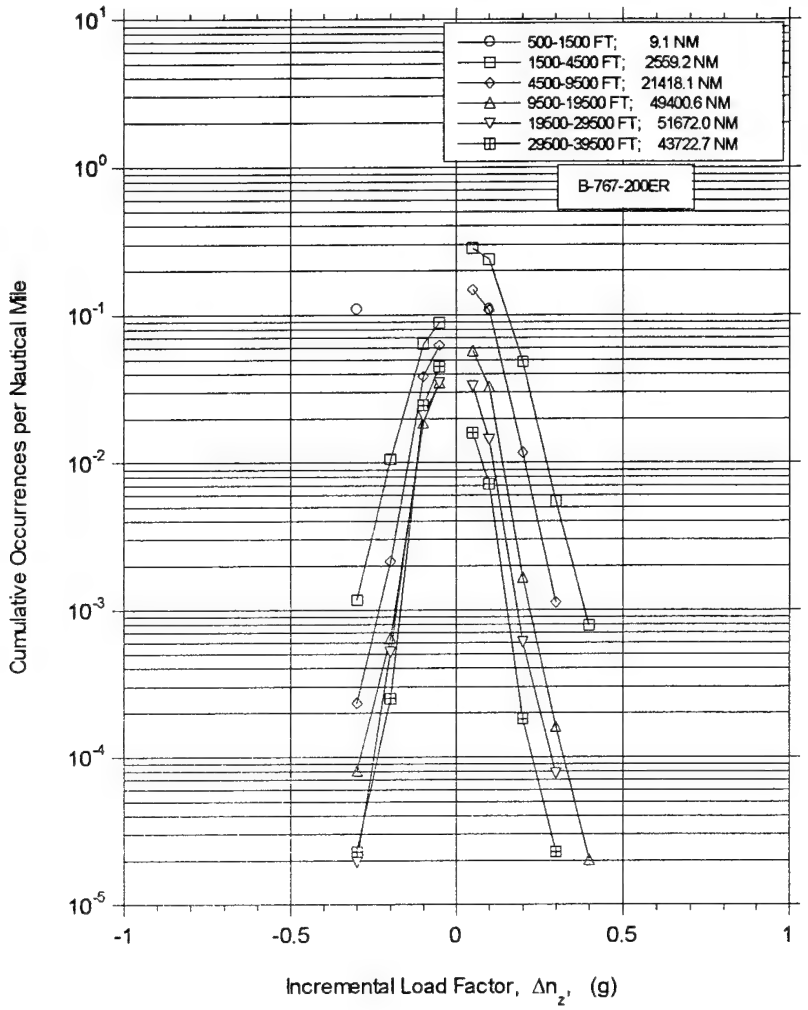

FIGURE A-53. CUMULATIVE OCCURRENCES OF INCREMENTAL MANEUVER LOAD FACTOR PER NAUTICAL MILE DURING DESCENT BY ALTITUDE

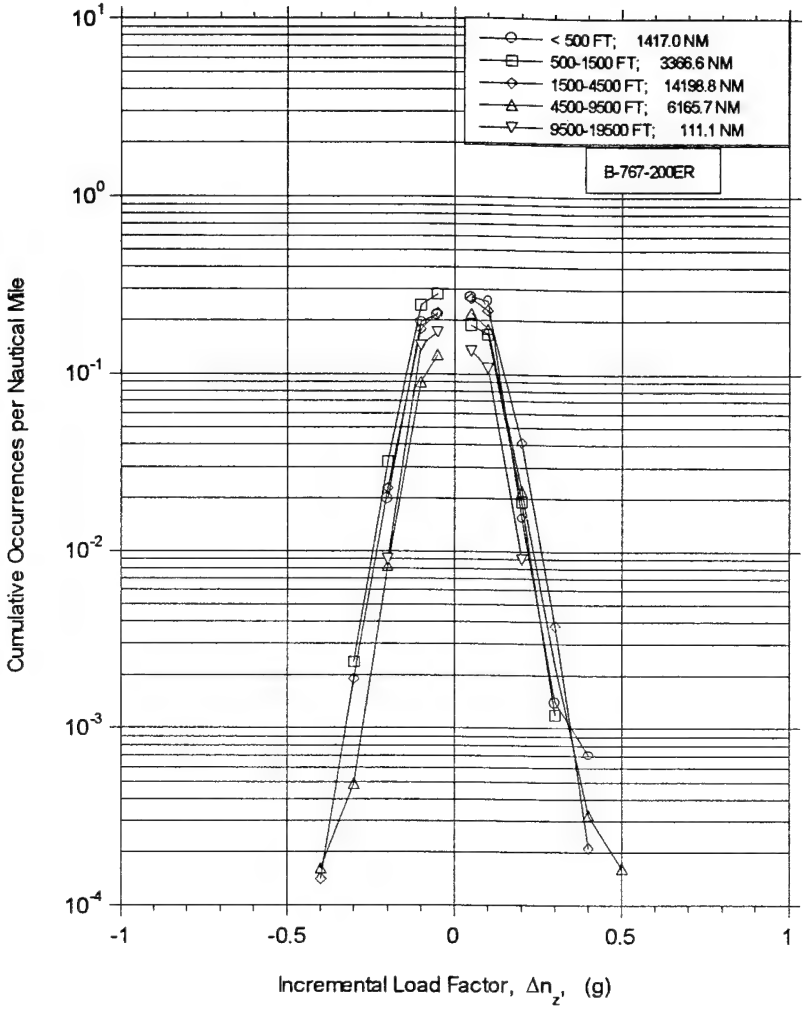

FIGURE A-54. CUMULATIVE OCCURRENCES OF INCREMENTAL MANEUVER LOAD FACTOR PER NAUTICAL MILE DURING APPROACH BY ALTITUDE

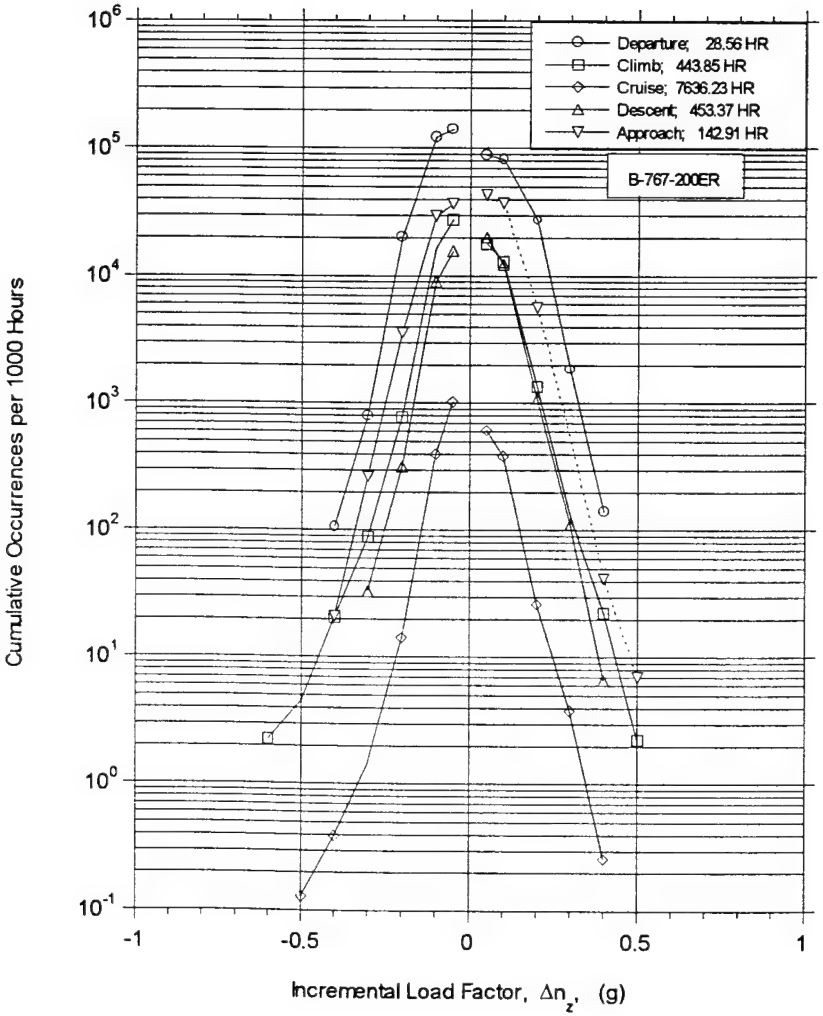

FIGURE A-55. CUMULATIVE OCCURRENCES OF INCREMENTAL MANEUVER LOAD FACTOR PER 1000 HOURS BY FLIGHT PHASE

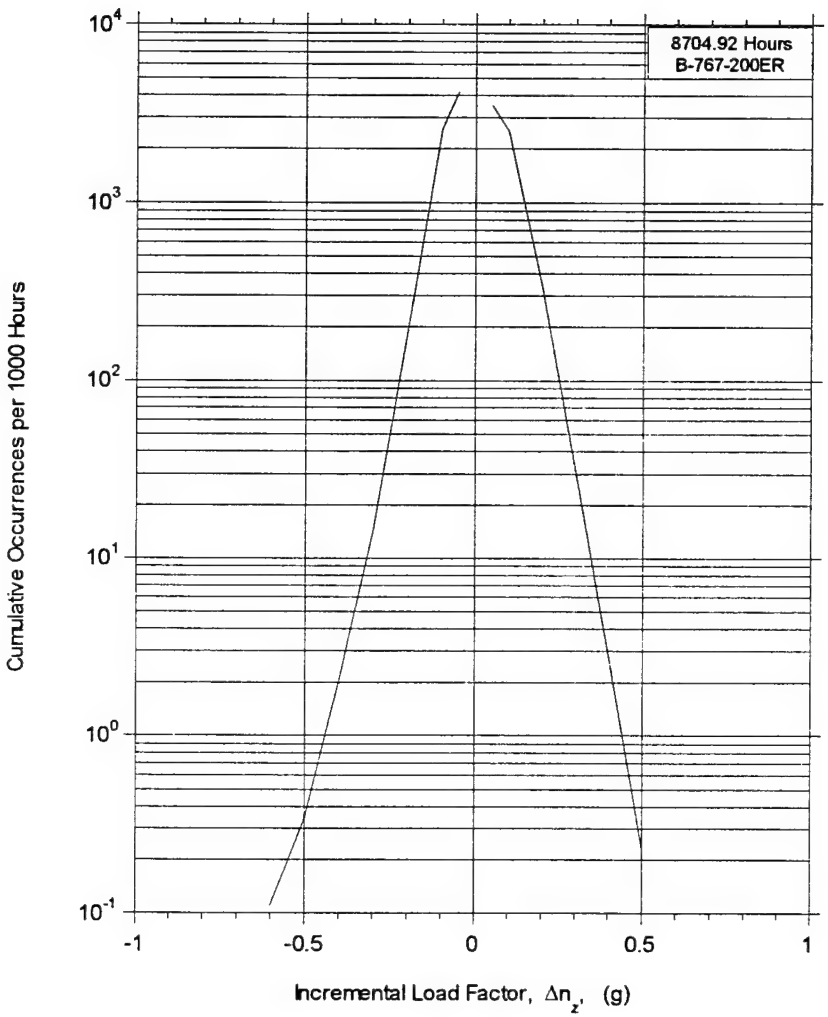

FIGURE A-56. CUMULATIVE OCCURRENCES OF INCREMENTAL MANEUVER LOAD FACTOR PER 1000 HOURS, COMBINED FLIGHT PHASES

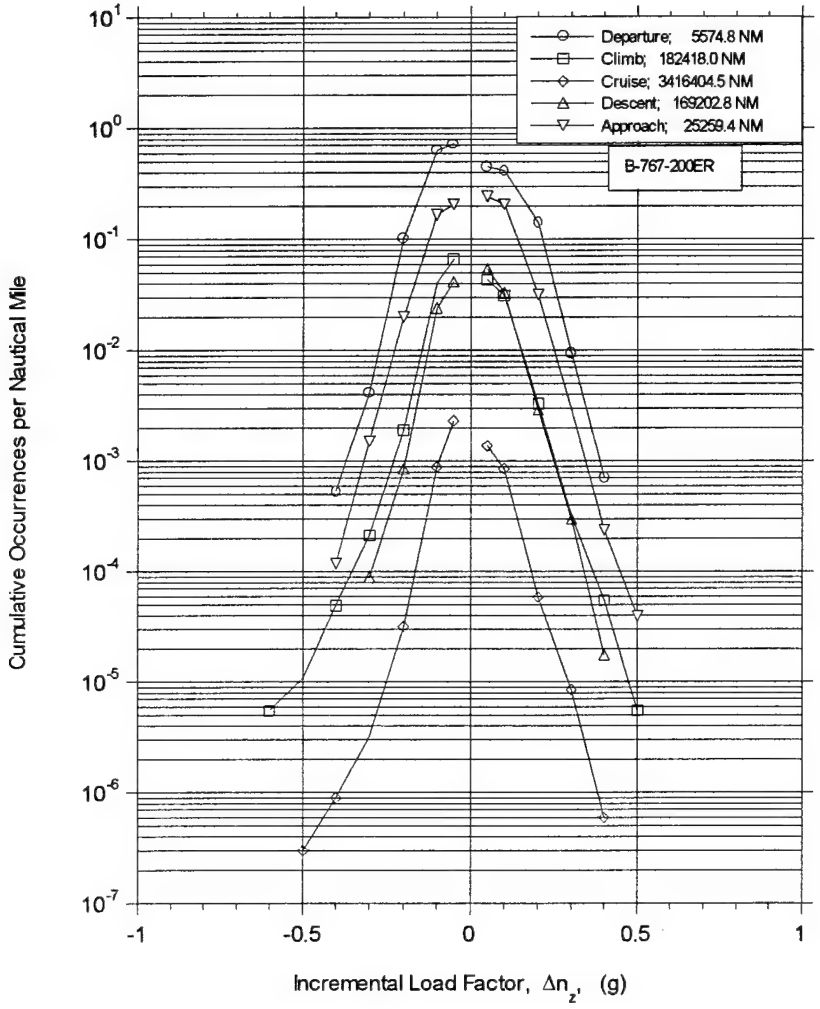

FIGURE A-57. CUMULATIVE OCCURRENCES OF INCREMENTAL MANEUVER LOAD FACTOR PER NAUTICAL MILE BY FLIGHT PHASE

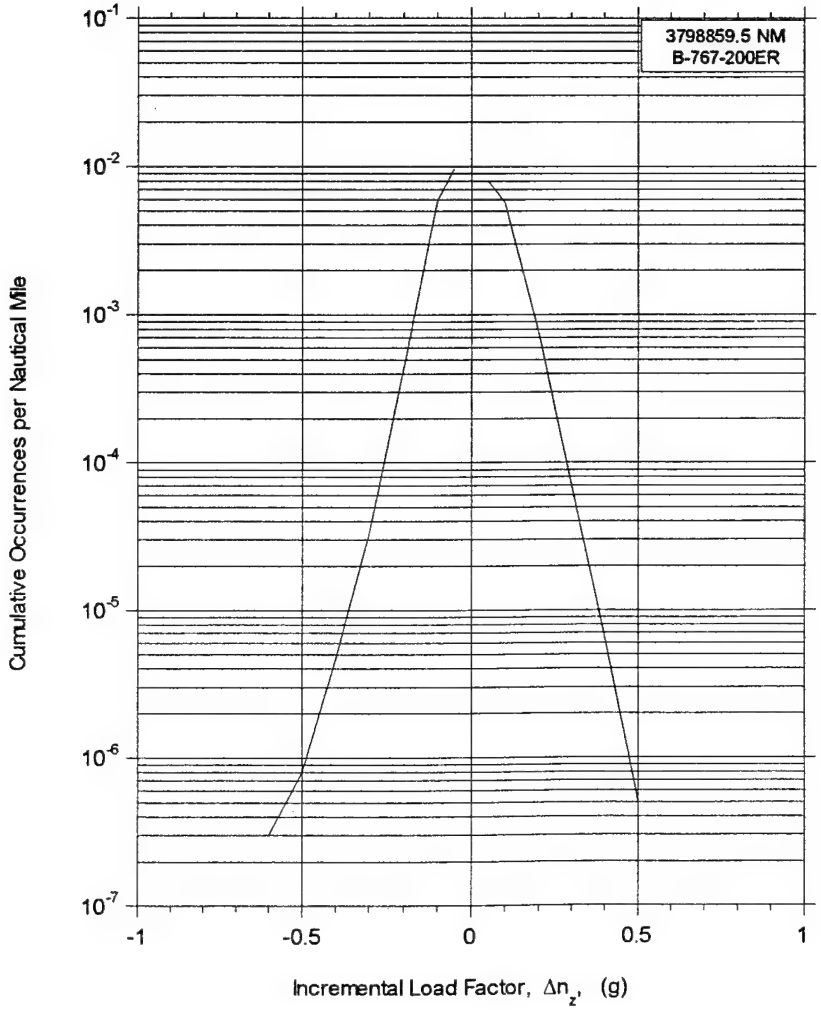

FIGURE A-58. CUMULATIVE OCCURRENCES OF INCREMENTAL MANEUVER LOAD FACTOR PER NAUTICAL MILE, COMBINED FLIGHT PHASES

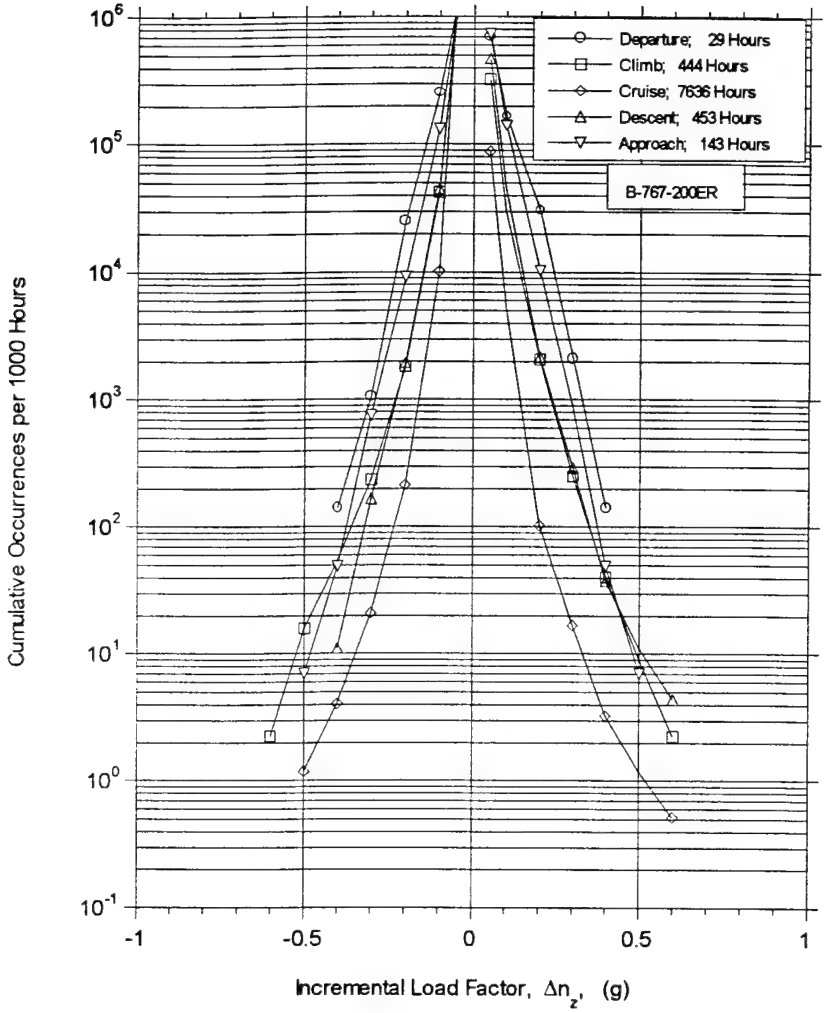

FIGURE A-59. CUMULATIVE OCCURRENCES OF COMBINED MANEUVER AND GUST INCREMENTAL LOAD FACTOR PER 1000 HOURS BY FLIGHT PHASE

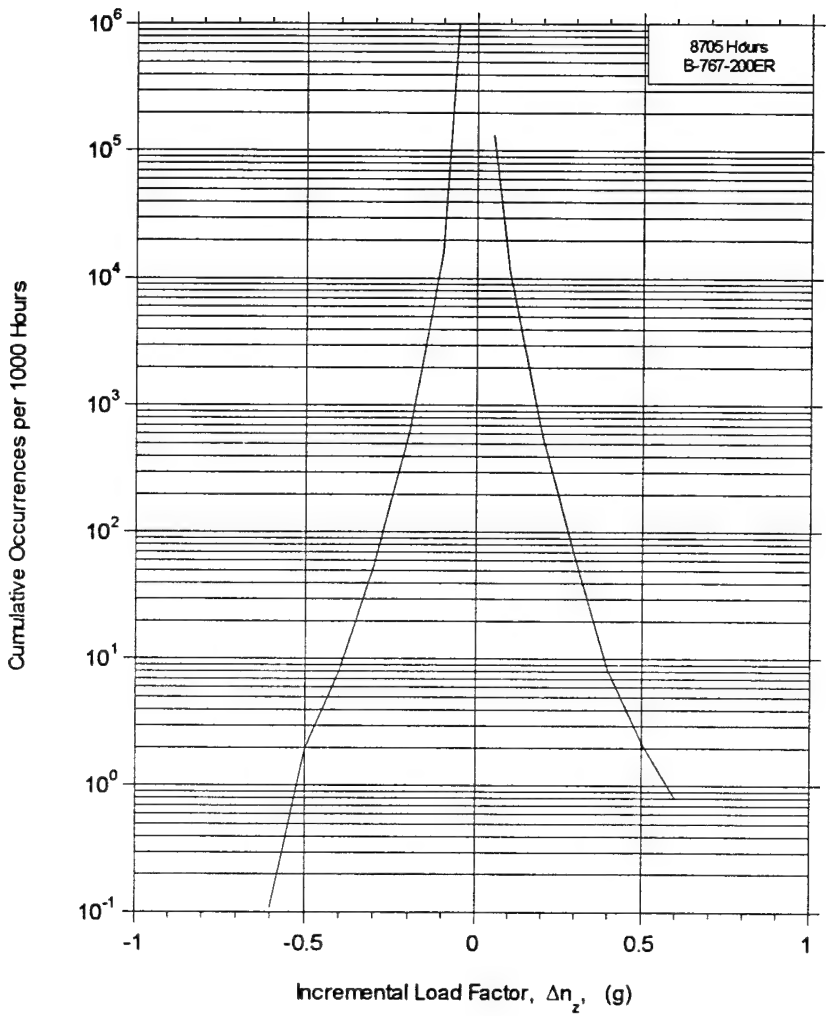

FIGURE A-60. CUMULATIVE OCCURRENCES OF INCREMENTAL VERTICAL LOAD FACTOR PER 1000 HOURS,COMBINED FLIGHT PHASES

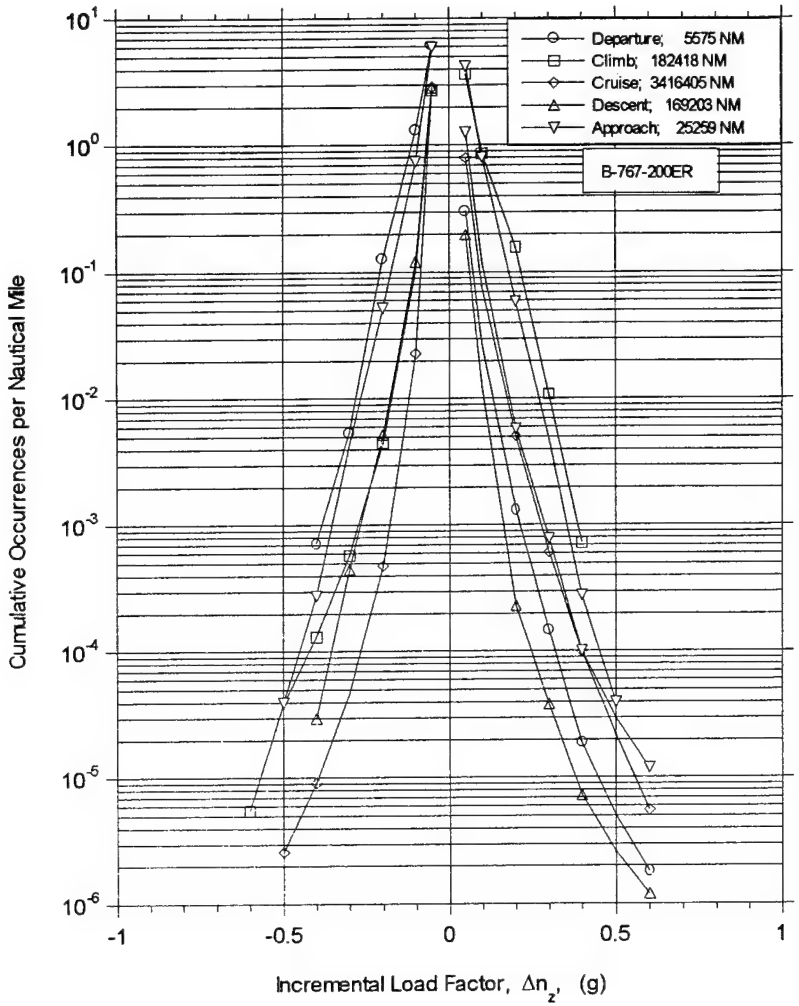

FIGURE A-61. CUMULATIVE OCCURRENCES OF INCREMENTAL VERTICAL LOAD FACTOR PER NAUTICAL MILE BY FLIGHT PHASE

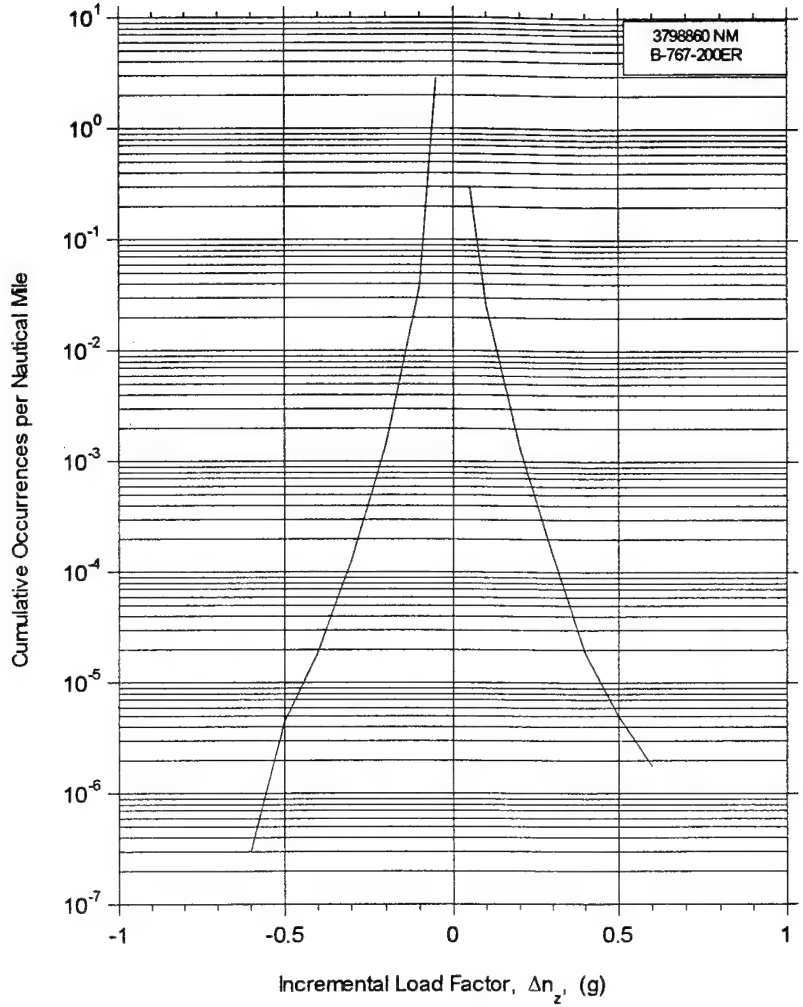

FIGURE A-62. CUMULATIVE OCCURRENCES OF INCREMENTAL VERTICAL LOAD FACTOR PER NAUTICAL MILE, COMBINED FLIGHT PHASES

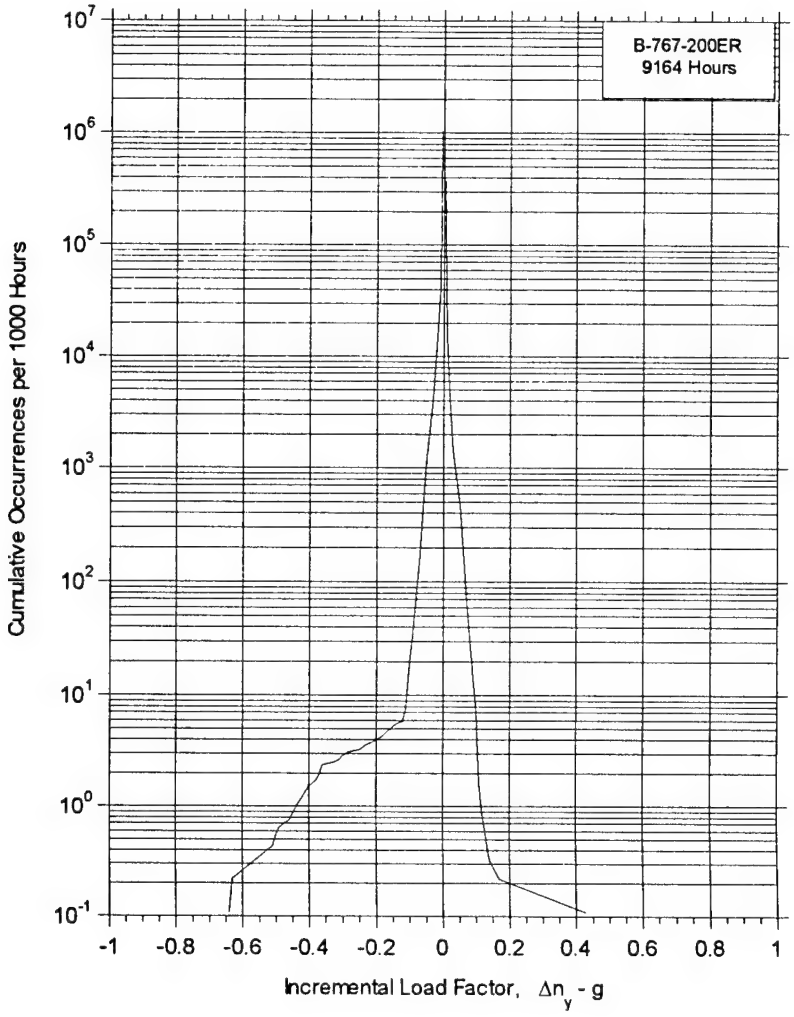

FIGURE A-63. CUMULATIVE OCCURRENCES OF LATERAL LOAD FACTOR PER 1000 HOURS, COMBINED FLIGHT PHASES

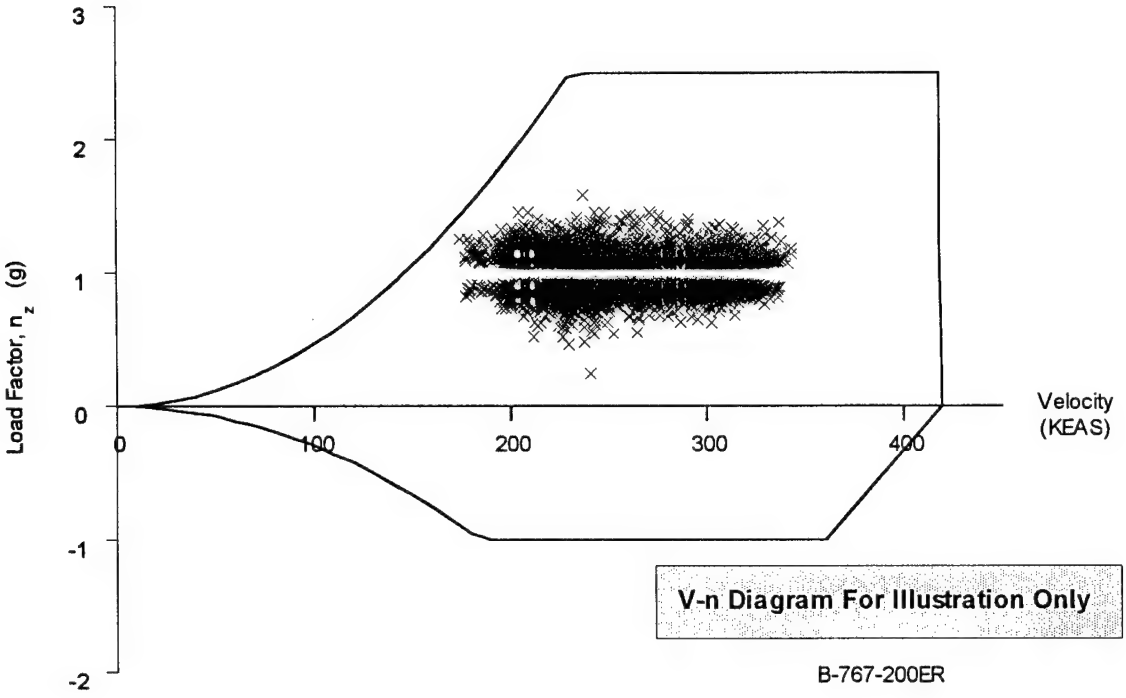

FIGURE A-64. COINCIDENT MANEUVER LOAD FACTOR AND SPEED VERSUS V-n DIAGRAM FOR FLAPS RETRACTED

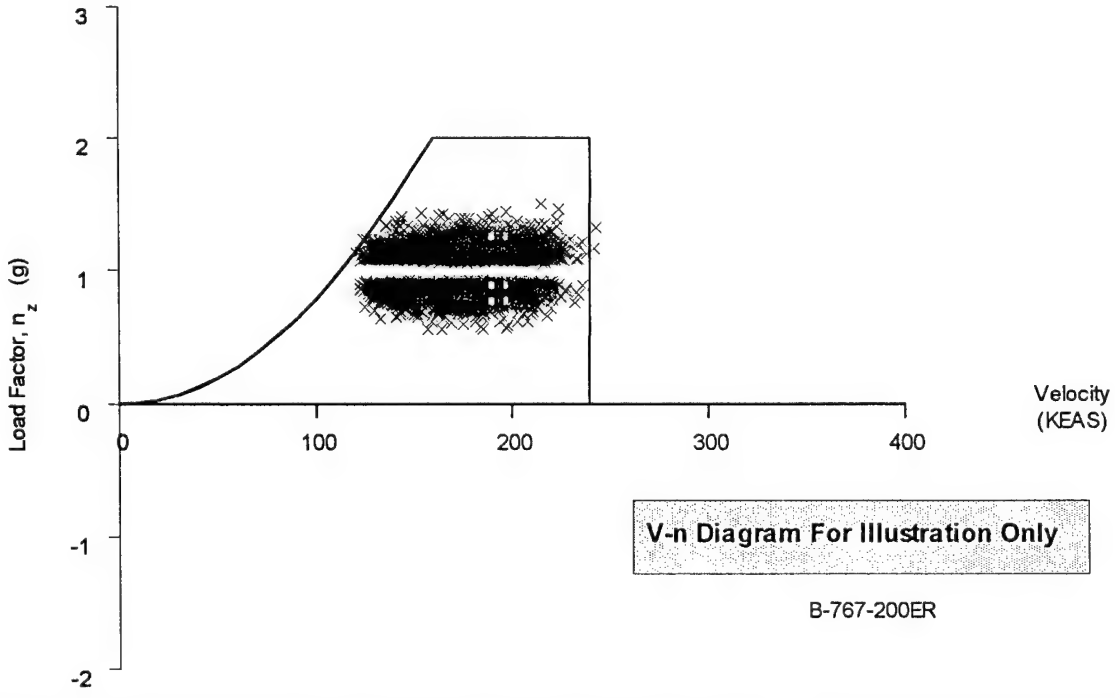

FIGURE A-65. COINCIDENT MANEUVER LOAD FACTOR AND SPEED VERSUS V-n DIAGRAM FOR FLAPS EXTENDED

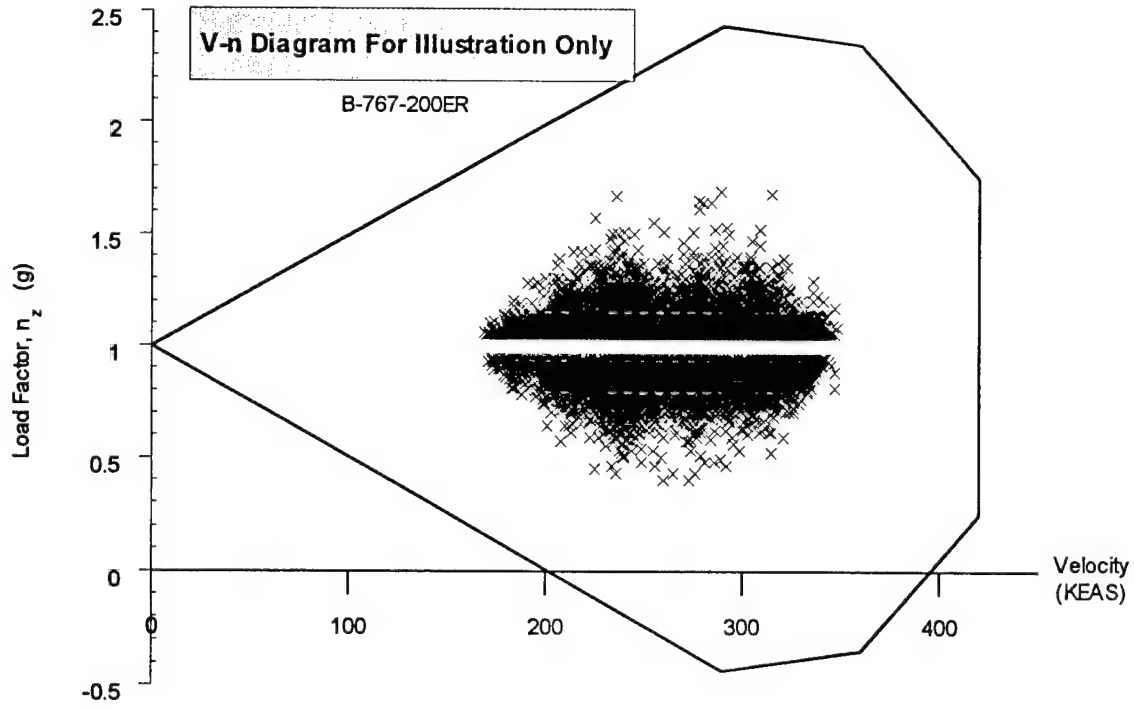

FIGURE A-66. COINCIDENT GUST LOAD FACTOR AND SPEED VERSUS V-n DIAGRAM FOR FLAPS RETRACTED

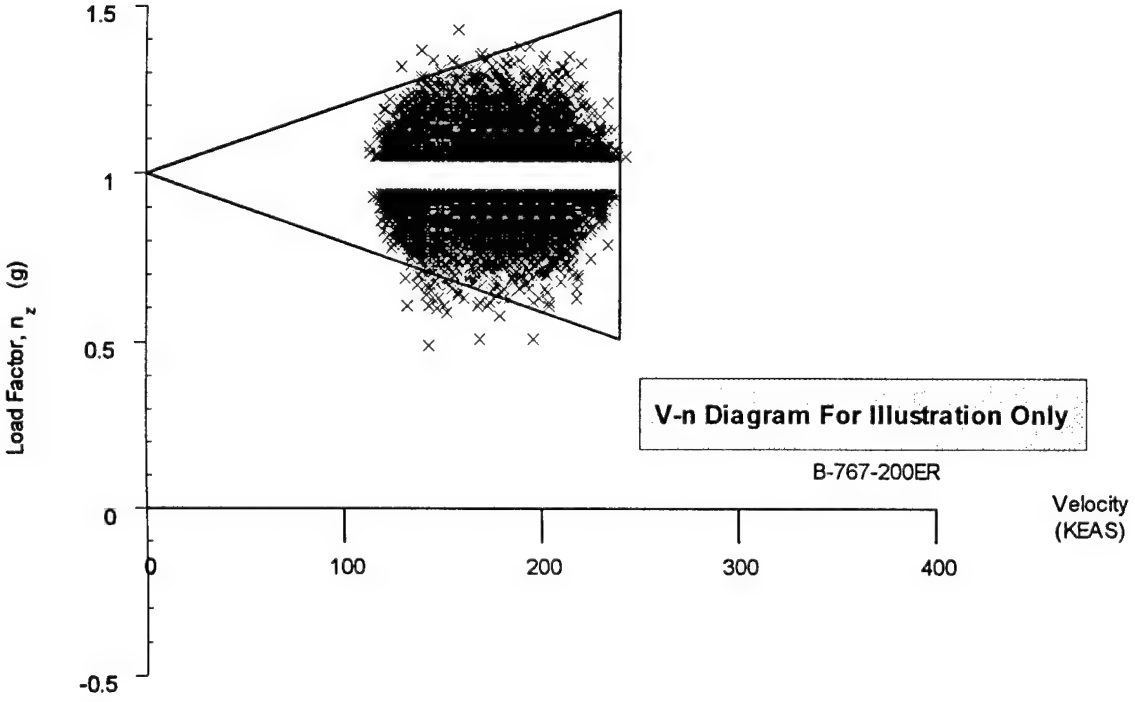

FIGURE A-67. COINCIDENT GUST LOAD FACTOR AND SPEED VERSUS V-n DIAGRAM FOR FLAPS EXTENDED

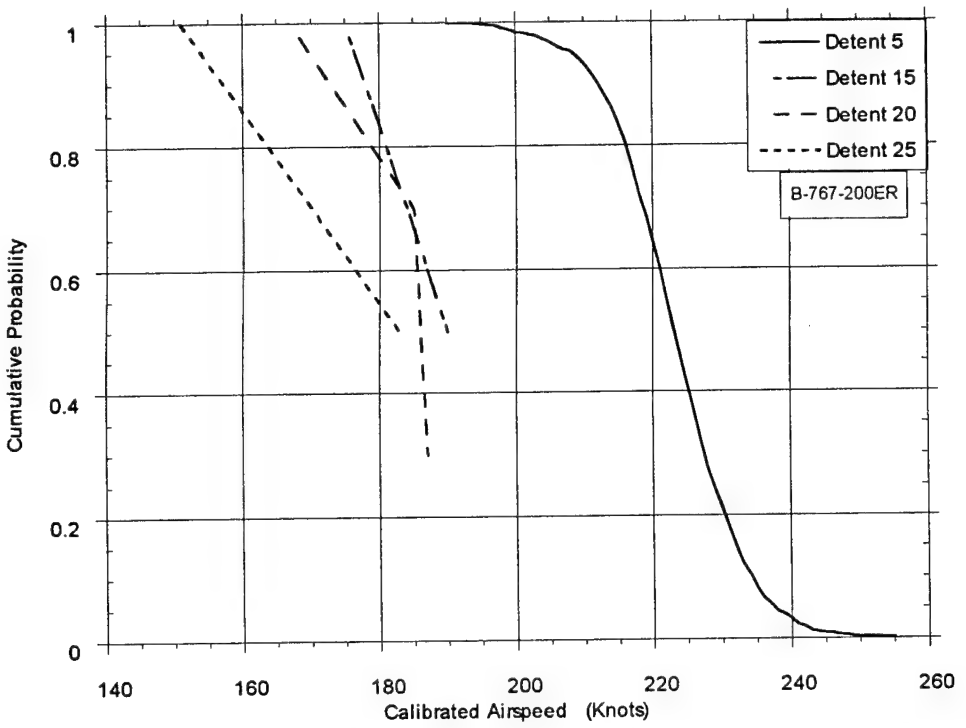

FIGURE A-68. CUMULATIVE PROBABILITY OF MAXIMUM AIRSPEED IN FLAP DETENT DURING DEPARTURE

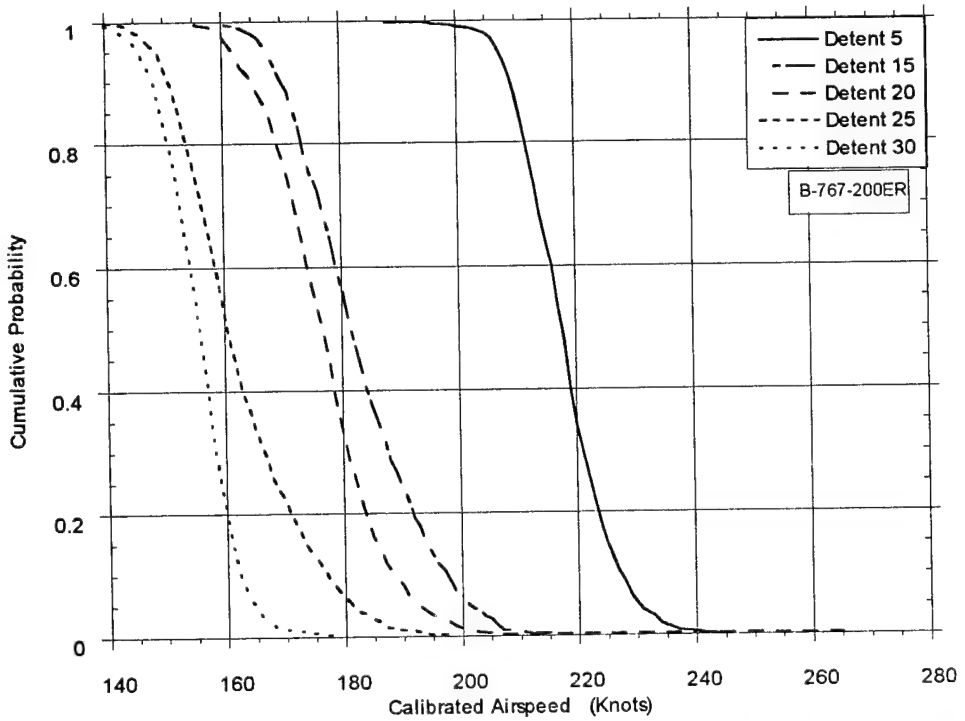

FIGURE A-69. CUMULATIVE PROBABILITY OF MAXIMUM AIRSPEED IN FLAP DETENT DURING APPROACH

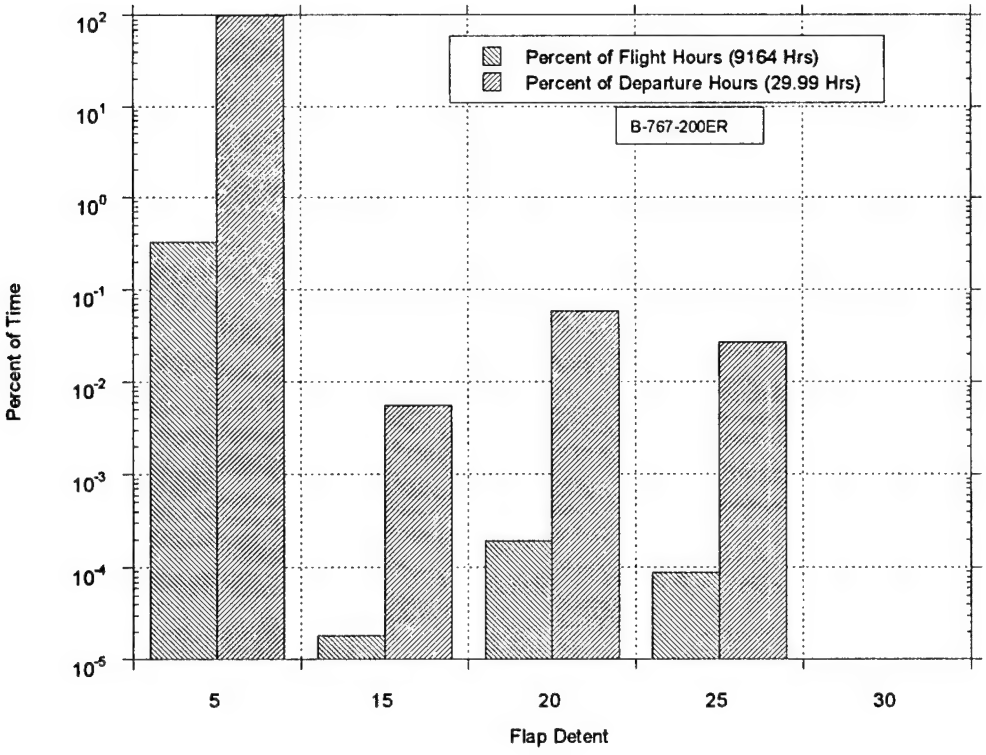

FIGURE A-70. PERCENT OF TIME IN FLAP DETENT DURING DEPARTURE

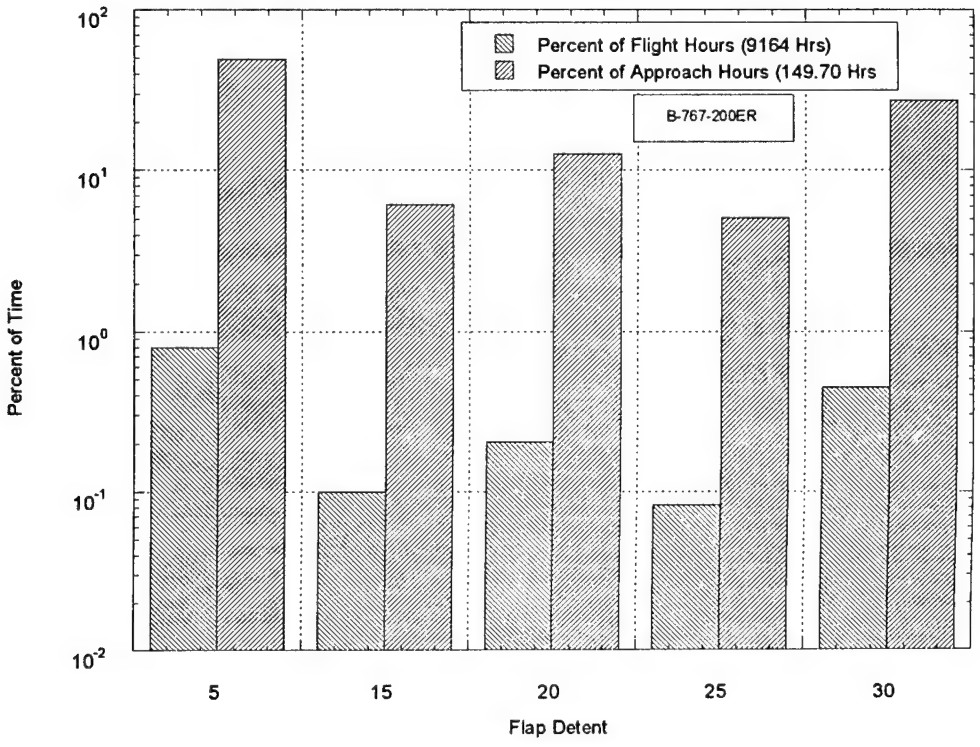

FIGURE A-71. PERCENT OF TIME IN FLAP DETENT DURING APPROACH

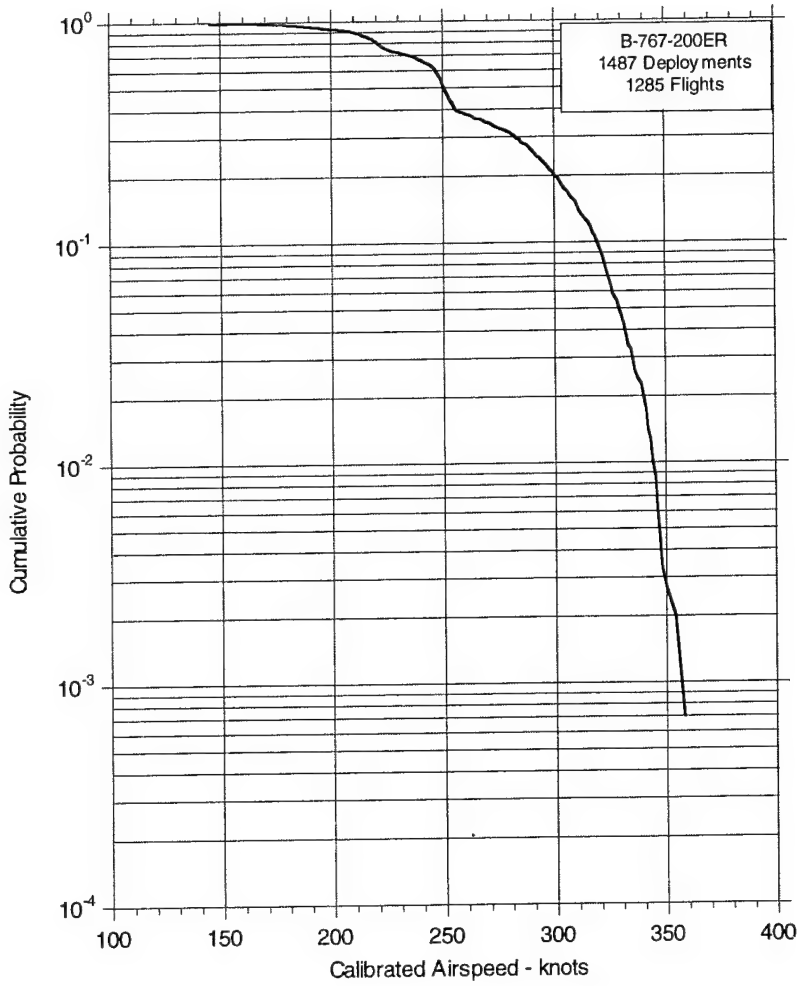

FIGURE A-72. CUMULATIVE PROBABILITY OF MAXIMUM SPEED DURING SPEED BRAKE DEPLOYMENT

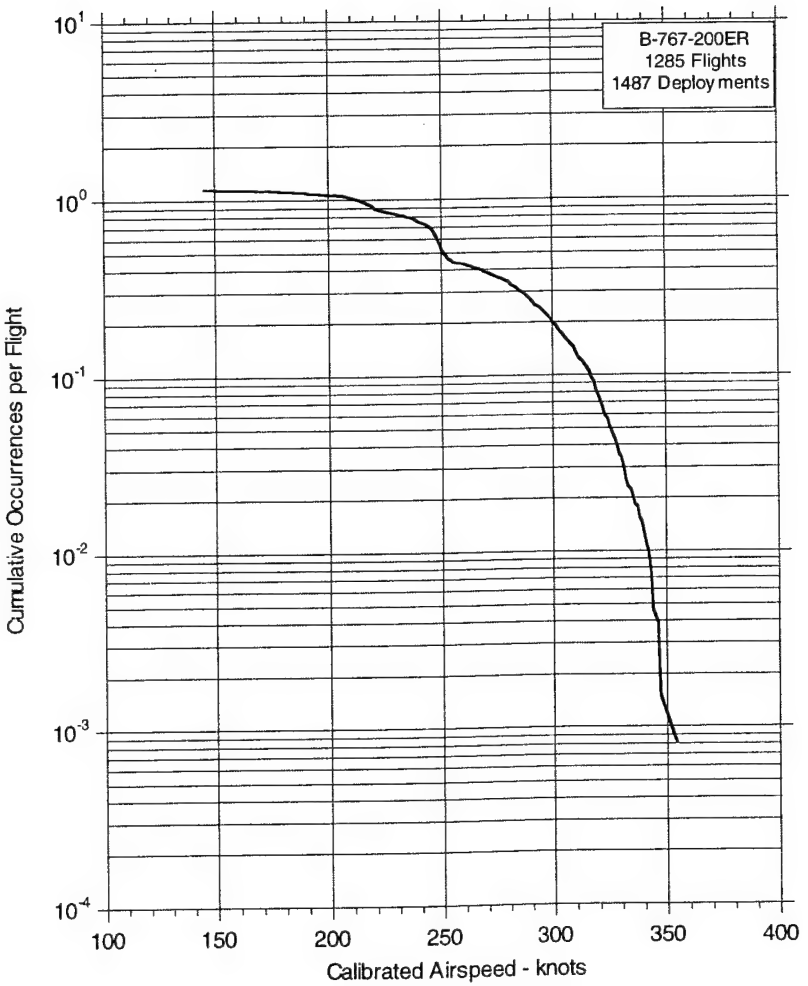

FIGURE A-73. CUMULATIVE FREQUENCY OF SPEED AT SPEED BRAKE DEPLOYMENT

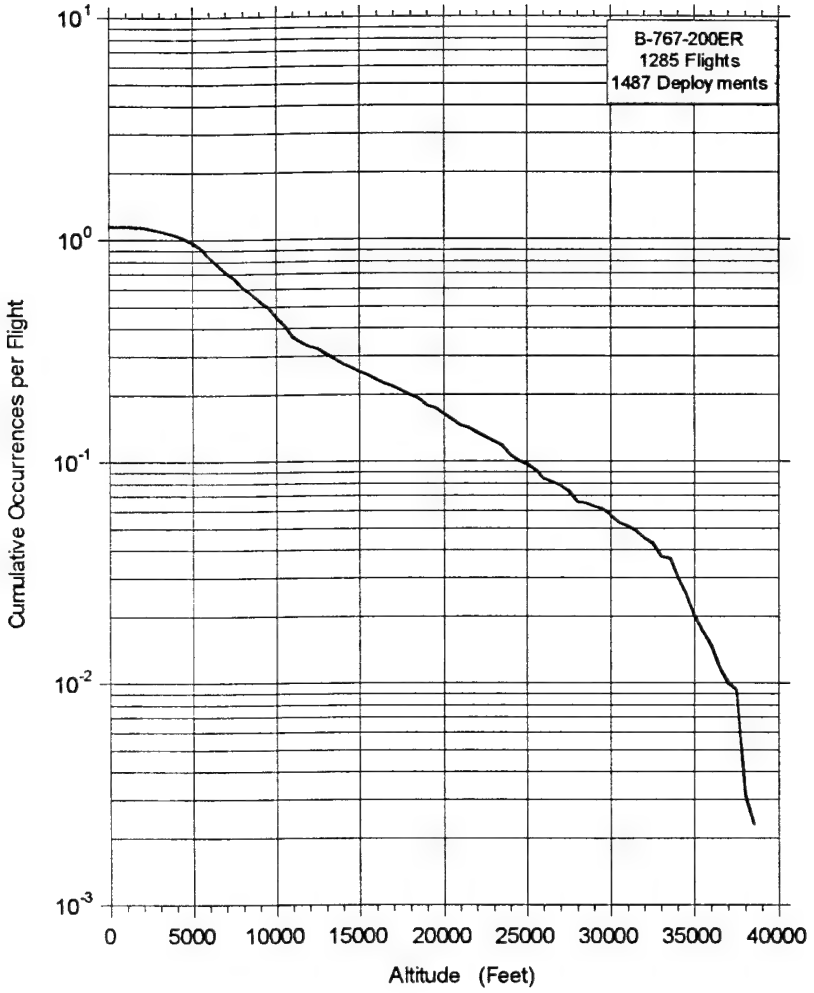

FIGURE A-74. CUMULATIVE FREQUENCY OF ALTITUDE AT SPEED BRAKE DEPLOYMENT

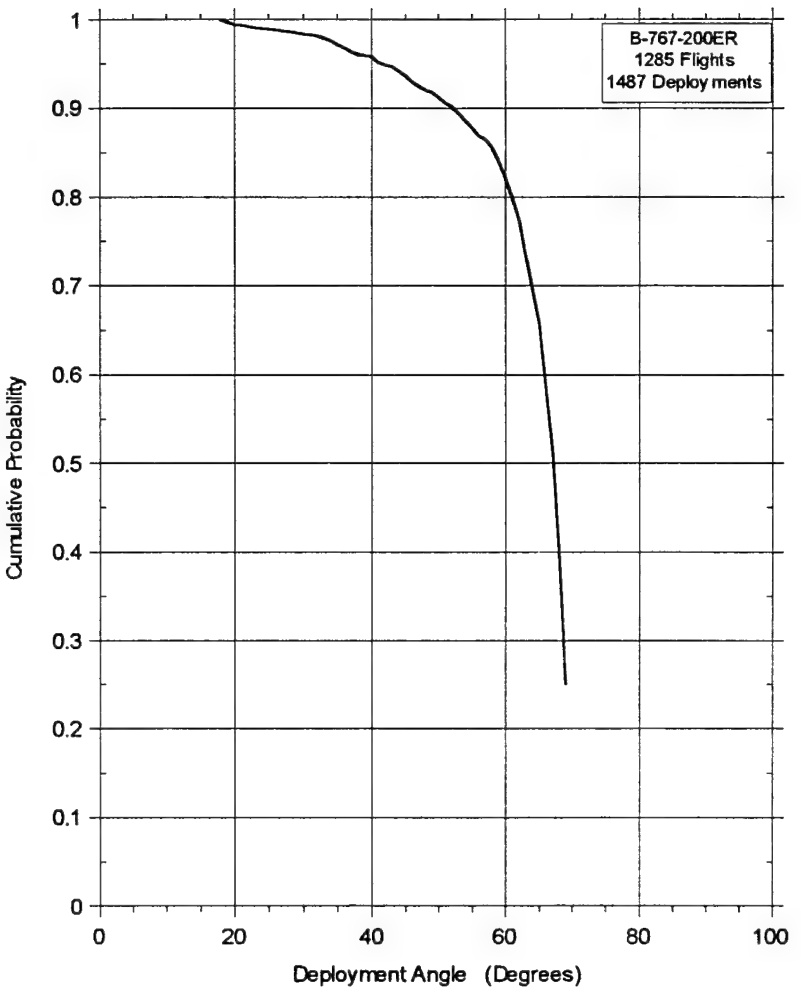

FIGURE A-75. CUMULATIVE PROBABILITY OF MAXIMUM DEPLOYMENT ANGLE DURING SPEED BRAKE DEPLOYMENT, FLAPS RETRACTED

Flap Detent Setting

Speed Brake Deflection (degrees)

B-767-200ER 1285 Flights	Detent 0	Detent 1	Detent 5	Detent 15	Detent 25	Detent 30
0.0	6.83436	0.04111	0.01056	0.01556	0.00500	0.05375
1.0	52.72786	0.23536	0.00000	0.00000	0.00000	0.00000
2.5	6500.56348	39.35472	1.67961	2.05758	0.48108	0.38314
5.0	2378.42798	37.67447	3.91967	3.86228	0.93189	1.59306
7.5	8.57142	0.77519	0.28814	0.36203	0.14333	0.77886
10.0	2.42903	3.65581	0.72142	2.73694	1.57733	8.95719
15.0	7.46325	7.94489	2.16028	9.37731	4.35844	28.68475
20.0	0.96047	0.43103	0.04897	0.07703	0.04603	0.15619
25.0	1.26039	0.21686	0.00897	0.01758	0.00092	0.00306
30.0	0.82139	0.11258	0.01769	0.01528	0.00139	0.00261
35.0	1.06039	0.08889	0.00389	0.02000	0.00092	0.00092
40.0	31.16986	5.09733	0.36358	0.24728	0.05258	0.00964

FIGURE A-76. CUMULATIVE FLIGHT HOURS FOR COINCIDENT SPEED BRAKE DEFLECTION AND FLAP HANDLE POSITION

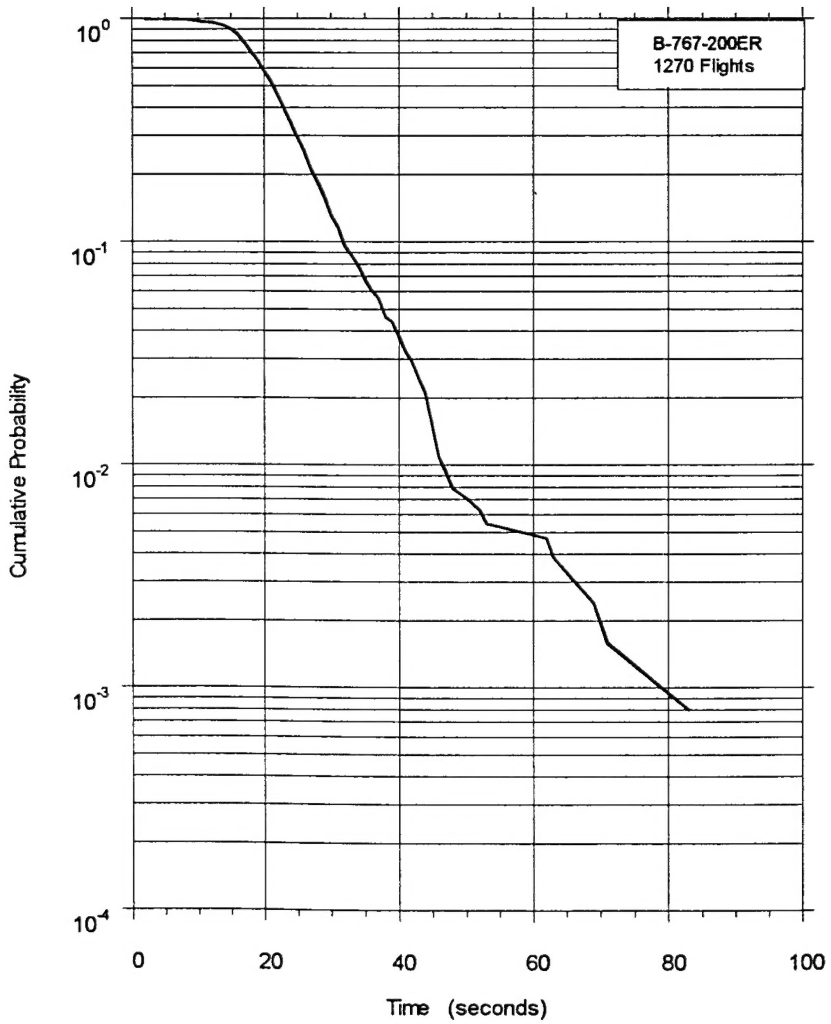

FIGURE A-77. CUMULATIVE PROBABILITY OF TIME WITH THRUST REVERSERS DEPLOYED

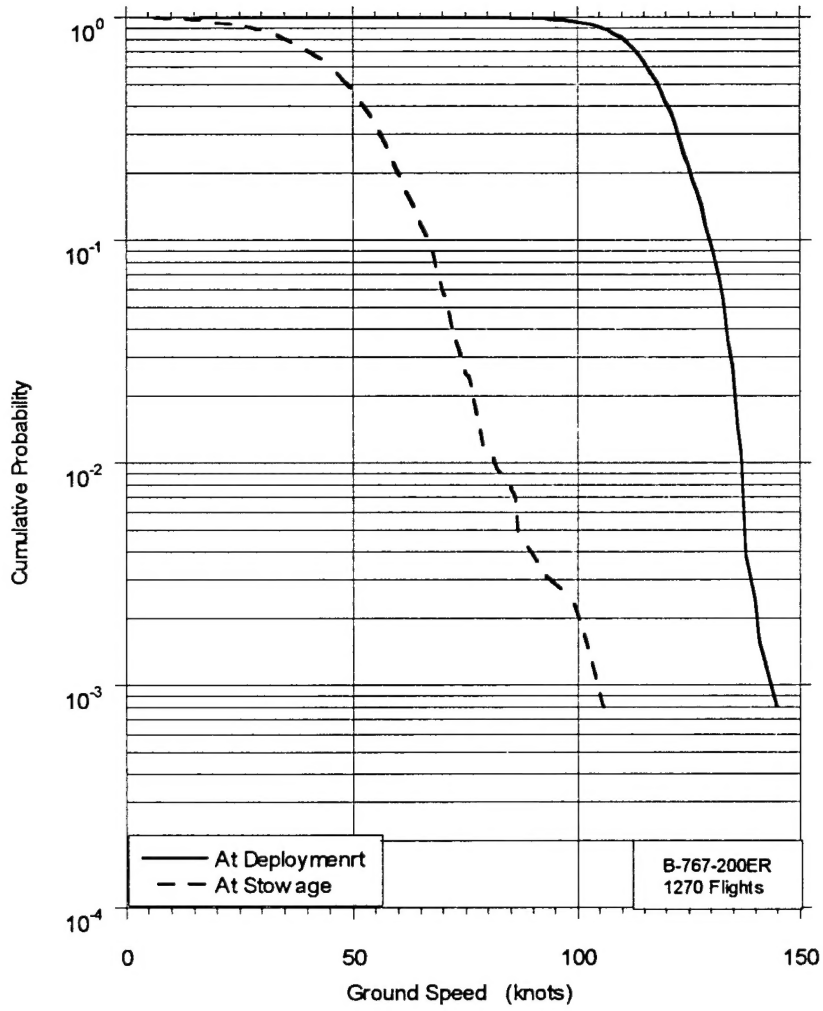

FIGURE A-78. CUMULATIVE PROBABILITY OF SPEED AT THRUST REVERSER DEPLOYMENT AND STOWAGE

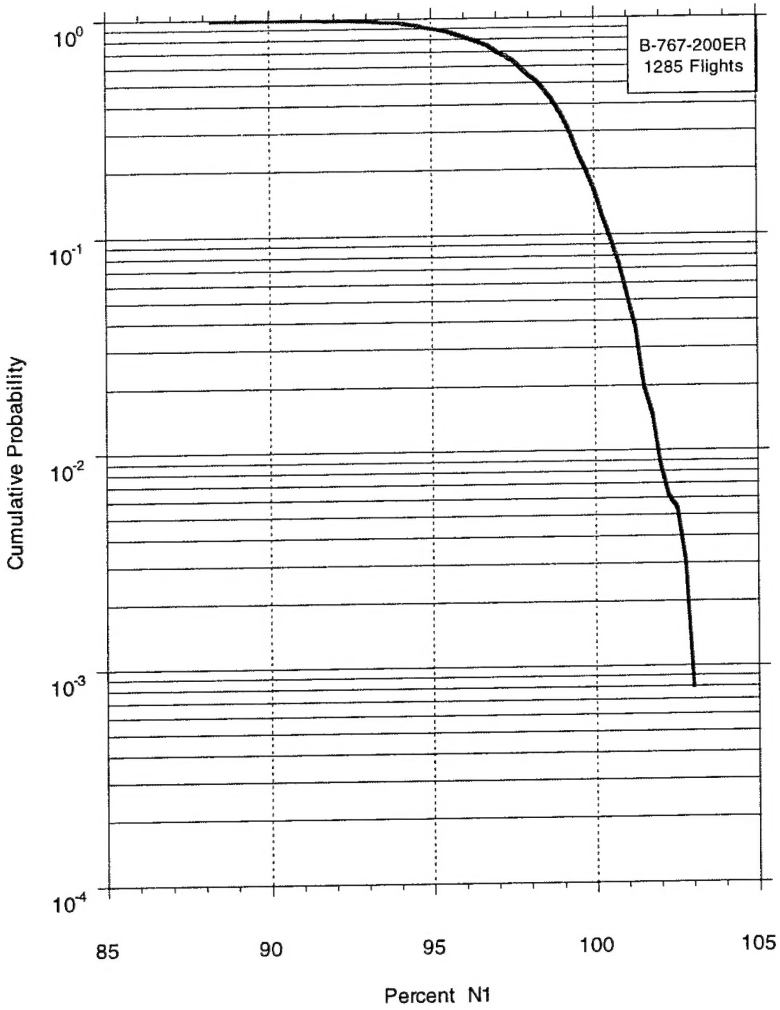

FIGURE A-79. CUMULATIVE PROBABILITY OF PERCENT OF N_1 AT TAKEOFF

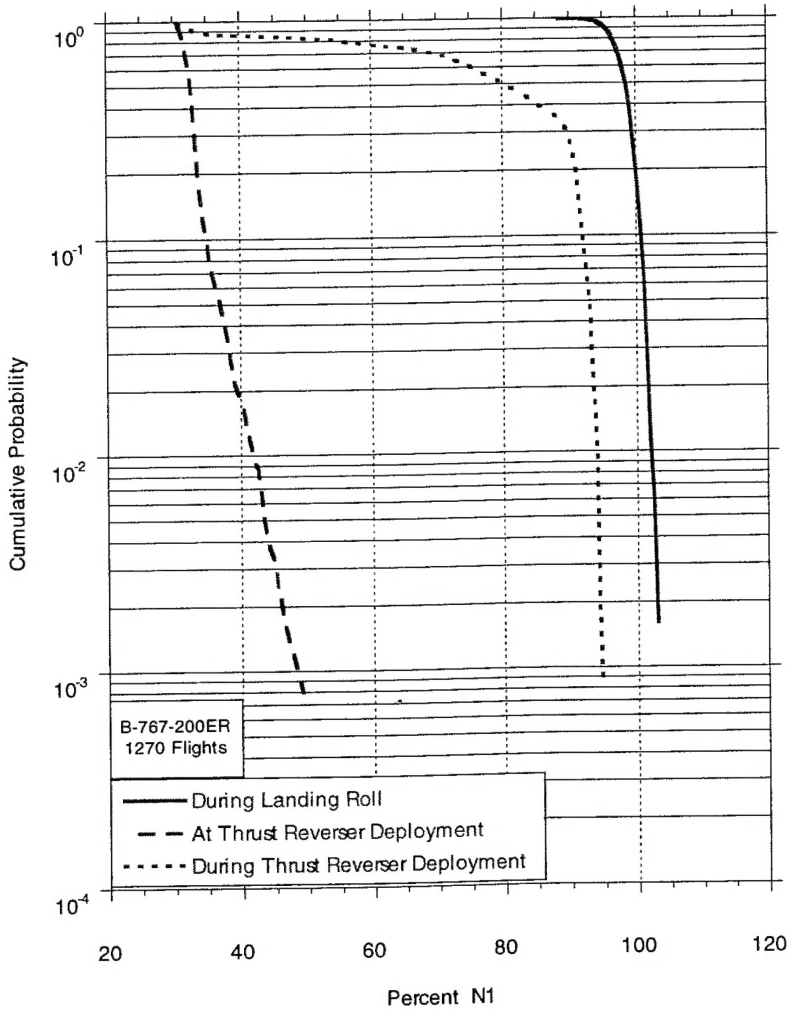

FIGURE A-80. CUMULATIVE PROBABILITY OF PERCENT OF N_1 DURING LANDING ROLL, AT THRUST REVERSER DEPLOYMENT, AND DURING THRUST REVERSER DEPLOYMENT

APPENDIX B—GREAT CIRCLE DISTANCE CALCULATION

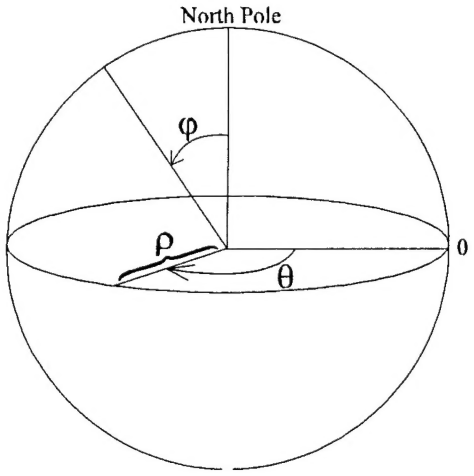

Given:

Latitude and Longitude of Departure and Destination Airports	ρ = distance from center φ = angle from North Pole θ = angle E/W of prime meridian

Procedure: (see sketch)

The standard mathematical system for spherical coordinates is shown, where three variables specify location: ρ, φ, and θ.

Let a = Great Circle Distance in angular measure.

Latitude is measured away from the Equator (0°) to the North Pole (+90°) and the South Pole (-90°); whereas in the standard spherical coordinate system, the North Pole, Equator, and South Pole lie at 0°, 90°, and 180°, respectively. Therefore,

$$\varphi = 90° - \text{latitude}$$

transforms latitude readings into equivalent angles (φ) in the standard spherical coordinate system.

Then

$$b = 90° - \text{Latitude}_{Dep}$$
$$c = 90° - \text{Latitude}_{Des}$$

where b and c are values of φ for the departure and destination locations, respectively.

Longitude is measured away from the prime meridian (0°). Longitudes to the east are positive and to the west negative. However, the standard spherical coordinate system measures its angles in the opposite direction. Therefore,

θ = - longitude

transforms longitude readings into equivalent angles (θ) in the standard spherical coordinate system.

Then

$$A = (-\text{Longitude}_{Des}) - (-\text{Longitude}_{Dep})$$
$$= \text{Longitude}_{Dep} - \text{Longitude}_{Des}$$

where A is the value of θ between the departure and destination locations.

The following equation, based on the spherical coordinate system, allows the computation of the Great Circle Distance, a. (Law of cosines for oblique spherical triangles)

$$\cos a = \cos b \cos c + \sin b \sin c \cos A$$

Substituting for b, c, and A from the above equalities,

$$\cos a = \cos (90° - \text{Lat}_{Dep}) \cos (90° - \text{Lat}_{Des}) + \sin (90° - \text{Lat}_{Dep}) \sin (90° - \text{Lat}_{Des}) \cos (\text{Lon}_{Dep} - \text{Lon}_{Des})$$

Since

$$\cos (90° - \text{Lat}_{Dep}) = \sin \text{Lat}_{Dep}$$
$$\cos (90° - \text{Lat}_{Des}) = \sin \text{Lat}_{Des}$$
$$\sin (90° - \text{Lat}_{Dep}) = \cos \text{Lat}_{Dep}$$
$$\sin (90° - \text{Lat}_{Des}) = \cos \text{Lat}_{Des}$$

by replacement one obtains

$$\cos a = \sin (\text{Lat}_{Dep}) \sin (\text{Lat}_{Des}) + \cos (\text{Lat}_{Dep}) \cos (\text{Lat}_{Des}) \cos (\text{Lon}_{Des} - \text{Lon}_{Dep})$$

Thus a, the angular measure of the great circle arc connecting the departure and destination locations, is obtained as

$$a = \cos^{-1} [\sin (\text{Lat}_{Dep}) \sin (\text{Lat}_{Des}) + \cos (\text{Lat}_{Dep}) \cos (\text{Lat}_{Des}) \cos (\text{Lon}_{Des} - \text{Lon}_{Dep})]$$

So, for a expressed in radians

$$GCD = a \text{ radians} \left(\frac{180 \text{ deg.}}{\pi \text{ radians}}\right)\left(\frac{60 \text{ min.}}{1 \text{ deg.}}\right)\left(\frac{1 \text{nm}}{1 \text{ min.}}\right) = \left(\frac{10800a}{\pi}\right) \text{ nm}$$

and for a expressed in degrees,

$$GCD = a \text{ degrees} \left(\frac{60 \text{ min.}}{1 \text{ deg.}}\right)\left(\frac{1 \text{ nm}}{1 \text{ min.}}\right) = 60a \text{ nm}$$